SYNCHRONIZATION OPTIMIZATION ON DUAL-AXIS SYSTEMS BY VARIABLE GAIN CROSS-COUPLED CONTROLLER

GÜRHAN BEKAR

MAY 2023

ÇANKAYA UNIVERSITY

GRADUATE SCHOOL OF NATURAL AND APPLIED SCIENCES

DEPARTMENT OF ELECTRICAL AND ELECTRONICS ENGINEERING
M.Sc. Thesis in
ELECTRICAL AND ELECTRONICS ENGINEERING

SYNCHRONIZATION OPTIMIZATION ON DUAL-AXIS SYSTEMS BY
VARIABLE GAIN CROSS-COUPLED CONTROLLER

GÜRHAN BEKAR

MAY 2023

ABSTRACT

SYNCHRONIZATION OPTIMIZATION ON DUAL-AXIS SYSTEMS BY VARIABLE GAIN CROSS-COUPLED CONTROLLER

BEKAR, Gürhan
M.Sc. in Electrical and Electronics Engineering

Supervisor: Assoc. Prof. Dr. Oğuzhan ÇİFDALÖZ
May 2023, 99 pages

Fast and accurate trajectory control is fundamental for modern machines such as CNC machinery, pick and place robots, path following unmanned vehicles and gantries. For one axis, satisfactory trajectory control can be accomplished easily. But for multi-axis systems, getting adequate trajectory control and low contour error can be tricky. Friction, inner or inner disturbances, gear backlash, servo lag can cause uncoordinated motion which will lead inter-axial uncoordinated motion and contour error. In many cases, lowering or controlling unwanted effects by individual control techniques cannot be enough to get required accuracy. Excelling coordinated motion requires a comprehensive and structural approach.

In this thesis, a two-axis system is introduced and different trajectories such as linear, circular, elliptic and parabolic trajectories are followed. Then proposed method is applied for eliminating contour error by variable gain cross-coupled controller. Control structure's block diagram and variable gain calculation steps are explained comprehensively. Finally, suggested structure is simulated under friction, inner disturbance and both friction and inner disturbance simultaneously. Results indicate proposed systems' efficiency to increase inter-axial coordination and decrease contour error.

Keywords: Cross-Coupled Controller, Contour Error, Uncoordinated Motion, Synchronization Optimization, Variable Gain.

ÖZET

ÇİFT EKSENLİ SİSTEMLERDE DEĞİŞKEN KAZANÇLI ÇAPRAZ-EŞLEŞMELİ KONTROLCÜ İLE SENKRONİZASYON OPTİMİZASYONU

BEKAR, Gürhan
Elektrik-Elektronik Mühendisliği Yüksek Lisans

Danışman: Doç. Dr. Öğr. Üyesi Oğuzhan ÇİFDALÖZ
Mayıs 2023, 99 sayfa

Günümüzde hızlı ve doğru hareket kontrolü; CNC tezgahları, al ve bırak robotlar, yörünge izleyen insansız hava araçları ve kızaklı makinalar gibi bir çok sistem için oldukça önemlidir. Tek eksen için istenilen düzeyde yörünge takibi kolaylıkla sağlanabilir. Ancak çok eksenli sistemlerde yeterli yörünge takibi ve düşük kontur hatasının elde edilmesi karmaşık olabilir. Sürtünme, dişli geri tepmesi ve servo gecikmeleri eksenlerin hareketlerinde koordinasyonsuzluğa sebep olur. Bu koordinasyonsuzluk eksenler arası senkronizasyonu bozarak kontur hatasına sebep olacaktır. Birçok durumda her bir eksen kontrolcüsünün ayrı ayrı tasarlanması istenmeyen etkilerin azaltılmasında ve harekette istenilen doğruluğun yakalanmasında etkili olamayacaktır.

Bu tezde iki eksenli bir sistem ele alınmış olup, düz çizgi, daire, elips ve parabol şeklinde yörüngeler izlenmiştir. Ardından kontur hatalarını elimine etmek için Değişken Kazançlı Çapraz-Eşleşmeli Kontrolcü tekniği uygulanmıştır. Değişken kazanç farklı yörünge tipleri için ayrı ayrı hesaplanarak kontrolcü yapısına entegre edilmiştir. Kontrol yapısını gösteren blok diyagramlar ve değişken kazanç hesapları detaylı bir şekilde açıklanmıştır. Son olarak önerilen yapı; sürtünme, dış gürültü ve her iki etmen aynı anda uygulanarak test edilmiştir. Simülasyon sonuçları önerilen yapının eksenler arası koordinasyonu artırdığına ve kontur hatasını düşürdüğüne işaret etmektedir.

Anahtar Kelimeler: Çapraz-Eşleşmeli Kontrolcü, Kontur Hatası, Koordine Olmayan Hareket, Senkronizasyon Optimizasyonu, Değişken Kazanç.

ACKNOWLEDGEMENT

I would like to express my sincere gratitude to Assoc. Prof. Dr. Oğuzhan ÇİFDALÖZ for his supervision, special guidance, suggestions, and encouragement during the development of this thesis.

It is a pleasure to express my special thanks to my dear wife Hilal for her valuable support. And my little daughters Ayça and Asya. You are my biggest source of motivation.

TABLE OF CONTENTS

LIST OF TABLE

LIST OF FIGURES

LIST OF SYMBOLS AND ABBREVIATIONS

CCC	:Cross-Coupled Controller
CNC	:Computerized Numerical Control
PD	:Proportional Derivative Controller
PI	:Proportional Integral Controller
PID	:Proportional Integral Derivative Controller
C_x, C_y	:Variable Gain of X and Y Axis Respectively
E_x, E_y	:Axial Error of X and Y Axis Respectively
ε	:Contour Error (Synchronization Error)
K_x, K_y	:Controller of X and Y Axis Respectively
P^*	:Desired Position
P_a	:Actual Position
P_x, P_y	:Plant of X and Y Axis Respectively
R	:Radius of the Desired Circle
R_x, R_y	:Coordinate of Position on Desired Contour
θ	:Degree Between X Axis and Desired Contour
V	:Required Feed Rate
V_x, V_y	:Required Feed Rate of X and Y Axis Respectively
W_x, W_y	:Prefilter of X and Y Axis Respectively
X_0, Y_0	:Coordinates of Desired Circle's Center
X_e, Y_e	:Coordinates of Desired Ellipse's Center
X_r, Y_r	:Command of X and Y Axis Respectively

CHAPTER I

INTRODUCTION

1.1   PROBLEM STATEMENT

In today's world fast and accurate motion is crucial for many applications in various sectors. There are many robust control techniques for precise control. Mostly these techniques are applied independently for each axis in multi-axis systems. These control mechanisms can be sufficient for many applications, but if precise path following is required or contour error is sensitive; individual axis control may not be enough. CNC machines, pick and place robots and path following unmanned vehicles are examples of precise path following applications.

Assuming it is necessary to follow a circular path, X and Y axes have to move simultaneously in order to follow a circular trajectory. If one of these axes will move slower or faster than it should be, resulted trajectory will be different from the desired one. As we can see from the Figure 1.1, the desired contour cannot be obtained due to the slow movement of the Y-Axis.
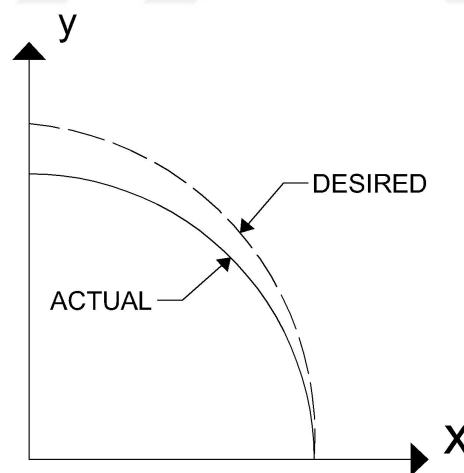
Figure 1.1: Uncoordinated Multi Axis Motion - 1.

While considering a simple line drawing situation, if Y-Axis starts late, the result will not be as desired. Figure 1.2 demonstrates this scenario.
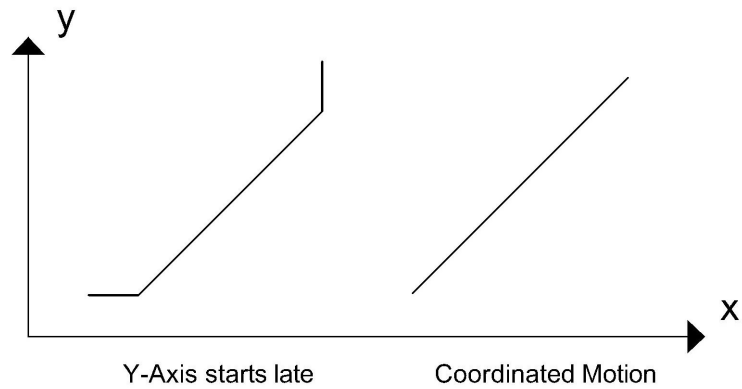
Figure 1.2: Uncoordinated Multi Axis Motion - 2.

The root cause of lack of coordination must be searched in individual axes. Gear backlash, servo lag, friction are the most common causes of individual axis error. And this lack of coordination causes contour error. Contour errors cannot be reduced by individual axis control approach. It requires more comprehensive control strategy.

There are various methods to compensate contour errors such as:

• Cross coupled controller

• Adaptive coupling control

• Sliding mode controller

• Leader-following structures

In this thesis, Cross-Coupled Controller (CCC) is examined as a conceptual approach and during the studies, first, a controller was designed for each axis. In this phase, all of the parameters were same and there were no friction or disturbance, so desired contour can be obtained easily.

Then, high level friction was applied for X-Axis. Thus, X-Axis could move much more slower than it should be and contour deviation occurred. To compensate the deviation, a CCC was proposed and designed CCC was applied for different contours and results were examined comprehensively.

Later on, sinusoidal inner disturbance was applied to X-Axis instead of friction, as a result of the inner disturbance, actual contour deviated from the desired contour. Proposed CCC was tested for this case and results were examined in detail.

Finally both friction and inner disturbance were applied simultaneously to X-Axis and assessment of the purposed structure was fulfilled.

1.2   LITERATURE SURVEY

First CCC introduced by Sarachik et al. in 1957 [1]. This system had non-symmetrical master-slave structure. Y-Axis follows X-Axis. When error occurs, proposed system slows down the motion in one dimension and speeds up in another. In 1980 Koren suggested a symmetrical CCC structure [2]. Koren designed a CCC whose input was calculated according to each axis' error. Output of CCC was added or extracted from each axis' input command. In this paper, compensation technique was suggested as a whole system. Koren suggested more developed approach in another paper [3]. To deal with low effectiveness of conventional CCC with nonlinear contour error, Koren suggested variable gain CCC. For different contours variable gain was calculated and significant improvement was obtained.

In later years, many studies were carried out on CCC structure. For example, in 1999 Yeh et. al. emphasized the CCC's efficiency on synchronization in his studies [4]. For further improvement, theoretical analysis and systematic design methodologies were studied. Yeh at. al. designed CCC by contouring error transfer function instead of common PID structure and tested the method under different operating conditions. The results proved proposed structure's robustness and effectiveness to overcome synchronization error. In 2002 Shih et al. introduced a novel approach for CCC that directly compensate the reference position for both axes [5]. Major benefit of the design was applicability into any axial tracking problem. Individual axis controller was proportional and CCC was PI type. Simulation and experimental results showed the proposed structure's efficiency. Another CCC study was made by Liu et al. [6]. The goal of this work was asymptotic convergence of tacking and best transient performance under affordable control efforts. To achieve these goals adaptive CCC was used. Although it did not solve the problem with synchronization, suggested structure improved tracking performance and coordination between axes.

Master-slave control structure was used widely to overcome synchronization problems. Tsai et al. suggested a master-slave structure for gantry axes' synchronization and considered 2 axes and 3 servo motor system [7]. In this system, one motor controls vertical axis and the other two motors controlled parallel Y-Axis. Parallel moving motors' coordination was important for coordinated motion. For synchronization compensation repetitive control was used. Two axes' output were used as compensation controller's input. And output of compensator was added or extracted from each axis' input command.

Another study related to CCC in the literature belongs to Xiao et al. In this study, they suggested a CCC methodology with optimal control architecture and synchronization control was solved by Linear Quadratic Gaussian optimal control

structure [8]. Then, Riccatti Difference Equation was solved. After the initial steps synchronization control strategy and system's stability were generated and analyzed. Simulation and experiments were applied on permanent magnet linear motors. And Sun et. al. suggested a model-free CCC and used PD controller for it [9]. This controller was proven to accomplish asymptotic convergence to zero of position and synchronization error. Also saturation function was added to CCC. It was claimed that proposed system is easy to implement. In the conclusion, proposed system's effectiveness was unfolded. Sun et al. saw contour error problem as a motion synchronization [10]. Thus, Sun et al. porposed synchronization error as a differential position error between adjacent axes and used CCC approach with saturation control and feedback/feedforward control. Sun et al. accomplished asymptotic convergence of synchronization and position errors. As an experiment a CNC machine tool was used and effectiveness of proposed structure was demonstrated. In 2012 Byun et al. proposed CCC with disturbance observer to decrease synchronization error due to skew disturbance [11]. Byun et al. suggested disturbance observer to minimize mismatched dynamics between the real and modeled plant. Also rejected instantly disturbance. They used a PD controller for CCC. Experiment results indicated that suggested structure is more effective compared to CCC without disturbance observer to reduce synchronization error. Also Xiao et. al. suggested PID based CCC structure [12]. In order to show proposed control strategies effectiveness, uncoupled controller was compared with cross coupled controller. In simulation and experiments, proposed structure had adequate performance to compensate synchronization errors.

In 2006 Xiao et. al. suggested that synchronization problem is not fully addressed [13]. Proposed methodology was adding coupling and synchronization factors to synchronization error by new quadratic performance index. This index was utilized to minimize tracking and synchronization errors. Suggested methodology was applied to two axes permanent magnet linear motors. Effectiveness of new structure was proved by experiments.

Dual inverted pendulum is well studied for many different problems thanks to its simple setup, instability and non-linearity. In 2007 Tsai et al. discussed inverted pendulum's synchronization [14]. Two linear servomotor were used to control the pendulum. A robust synchronization control scheme was proposed to compensate pendulum's balancing and synchronous tracking control. Experimental results indicated low synchronization error.

On the other hand, Lin et al. proposed digital signal processor based on cross-coupled sliding mode control for dual linear servo motor system [15]. Dynamic model of the system contained uncertainty, outer disturbances and nonlinear friction. These unwanted parameters led low accurate tracking. Proposed structure was implemented to

dual-axes gantry system and results indicated validity of the proposed solution.

Lead the following is another approach to solve synchronization error. In 2013 Wu et al. suggested distributed synchronization structure with flocking control [16]. PID controller was used for synchronization controller. The simulation results indicated designed systems' effectiveness and robustness. Asymptotic convergence to zero was accomplished for tracking and synchronization error.

In 2014 Blaka suggested time-optimal trajectory generation for multi-axis time synchronization for uncoordinated motion [17]. The generator used 3 integrators for generating motion variables. As a parameter, Jerk was reduced first for each axis except the slowest one. Main benefit of the proposed structure was no initial/final state limitation.

Chen et al. taken the studies on CCC one step further [18]. Chen et al. adopted synchronous error transfer function matrix and H_∞. In order to develop the novel system, synchronous error was defined. Then H_∞ was used as CCC. Suggested structure was applicable to multi-axis systems and decreased synchronous error. He et. al. suggested CCC structure for compensation of dual-motor system's load disturbance at motor start and network related in-coordination [19]. Network controlled dual-motor system was modeled by MATLAB Truetime toolbox. In the suggested structure CCC input was derived from each axis' output and CCC input was extracted from motors' input. He et. al.'s approach was unique on its' CCC structure. Experiment results showed suggested structure's effectiveness. In 2017 Zhong et al. suggested CCC structure to compensate friction compensation in multi-axis servo system [20]. Proposed technique was designed for four-axis servo system. Adaptive-fuzzy was proposed for independent axis control and global sliding mode controller for CCC. Designed structure showed effectivity against uncertainties and nonlinear friction. Also guaranteed asymptotic convergence to zero for all axes.

Li et al., another name working on this subject, analyzed H-type gantry system's mechanical coupling between the two axes and proposed an adaptive robust controller for synchronization [21]. In their study, dynamic thrust allocation decreased the effect of load disturbances. Experimental results indicated good tracking performance and adequate synchronization.

Sliding mode controller is another proposed structure for synchronization problem. In 2020 Yao et. al. suggested sliding mode control and active disturbance rejection control for multi-axis synchronization [22]. Cascade sliding mode control was proposed and active disturbance rejection control was derived. For tuning of controller parameters, space-time scaling method was used. Suggested structure was experimented on coating conveyor mechanism.

5

<div align="center">

CHAPTER II

CONTROL STRUCTURE

</div>

2.1 CONTROL STRUCTURE FOR REFERENCE CONDITIONS

2.1.1 Plant

In this thesis a conceptual design is suggested for synchronization problem of dual-axis systems. Thus, generic integrator is used as a plant. If required, suggested CCC structure can be used for more complicated plants.

$$P = \frac{1}{s} \tag{II.1}$$

2.1.2 Controller Design for Individual Axis

PI type controller is chosen for individual axis control.

$$K = k_p + \frac{k_i}{s} = \frac{k_p s + k_i}{s} = \frac{k_p \left(s + \frac{k_i}{k_p}\right)}{s} \tag{II.2}$$

Thus,

$$PK = \left(\frac{1}{s}\right)\left(\frac{k_p \left(s + \frac{k_i}{k_p}\right)}{s}\right) = \frac{k_p \left(s + \frac{k_i}{k_p}\right)}{s^2} \tag{II.3}$$

Closed loop complementary sensitivity transfer function is

$$T = \frac{PK}{1 + PK} = \frac{\frac{k_p \left(s + \frac{k_i}{k_p}\right)}{s^2}}{1 + \frac{k_p \left(s + \frac{k_i}{k_p}\right)}{s^2}} \tag{II.4}$$

$$T = \frac{k_p \left(s + \frac{k_i}{k_p}\right)}{s^2 + k_p \left(s + \frac{k_i}{k_p}\right)} \tag{II.5}$$

Prefilter is,

$$W = \frac{k_i / k_p}{s + k_i / k_p} \tag{II.6}$$

Thus,

$$TW = \left(\frac{k_p \left(s + \frac{k_i}{k_p} \right)}{s^2 + k_p \left(s + \frac{k_i}{k_p} \right)} \right) \left(\frac{k_i/k_p}{s + k_i/k_p} \right) \qquad (\text{II}.7)$$

$$TW = \frac{k_i}{s^2 + k_p s + k_i} \qquad (\text{II}.8)$$

As a design parameter overshoot is chosen $\leq 4.3\%$

$$0.043 = exp\left(\frac{-\zeta\pi}{\sqrt{1 - \zeta^2}} \right) \qquad (\text{II}.9)$$

Take *ln* function of both sides

$$ln(0.043) = ln\left(exp\left(\frac{-\zeta\pi}{\sqrt{1 - \zeta^2}} \right) \right) \qquad (\text{II}.10)$$

Multiply by $(-1/\pi)$ both sides

$$-\pi = \frac{-\zeta\pi}{\sqrt{1 - \zeta^2}} \qquad (\text{II}.11)$$

$$\sqrt{1 - \zeta^2} = \zeta \qquad (\text{II}.12)$$

Take square of both sides

$$1 - \zeta^2 = \zeta^2 \qquad (\text{II}.13)$$

$$\zeta = \frac{1}{\sqrt{2}} = 0.707 \qquad (\text{II}.14)$$

As a design parameter settling time is determined equal to 0.5s

$$t_s = 5\tau = 0.5 \qquad (\text{II}.15)$$

$$\tau = 0.1 \qquad (\text{II}.16)$$

Relationship between τ and w_n is,

$$\tau = \frac{1}{\zeta w_n} \qquad (\text{II}.17)$$

$\tau = 1/\sqrt{2}$ thus,

$$w_n = 10\sqrt{2} \tag{II.18}$$

Standard second order system transfer function is,

$$T_2 = \frac{w_n^2}{s^2 + 2\zeta w_n s + w_n^2} \tag{II.19}$$

Controller expression was given in (II.8). Thus,

$$\frac{k_i}{s^2 + k_p s + k_i} = \frac{w_n^2}{s^2 + 2\zeta w_n s + w_n^2} \tag{II.20}$$

Thus,

$$k_i = w_n^2 = (10\sqrt{2})^2 = 200 \tag{II.21}$$

$$k_p = 2\zeta w_n = 2\left(\frac{1}{2}\right)(10\sqrt{2}) = 20 \tag{II.22}$$

Thus,

$$K = \frac{20s + 200}{s} \tag{II.23}$$

$$W = \frac{10}{s + 10} \tag{II.24}$$

Block diagram of dual-axis system is given in Figure 2.1.
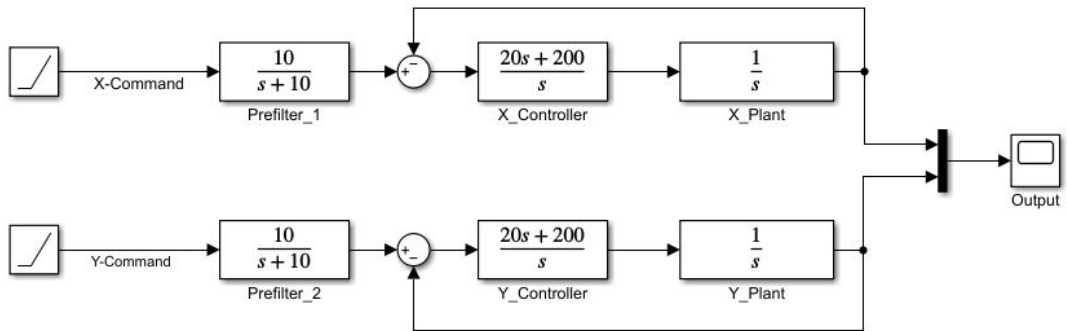
Figure 2.1: Block Diagram of Dual-Axis System.

2.2 EVALUATION OF DESIGNED CONTROL STRUCTURE

Evaluation of designed control structure is done by inspecting frequency responses of open loop transfer function, complementary sensitivity, sensitivity and controller's sensitivity.

Open loop transfer function's frequency response is given in Figure 2.2. Open loop bandwidth is 30 rad/s. And it has 0 rad/s gain margin and 65.5 rad/s phase margin.
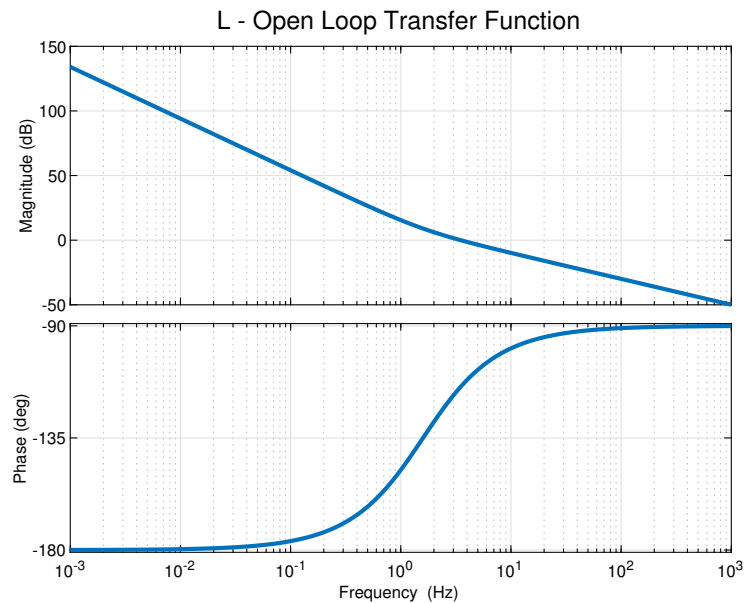
Figure 2.2: Frequency Response of Open Loop Transfer Function.

Complementary sensitivity transfer function's frequency response is given in Figure 2.3. It has 30 rad/s bandwidth. As expected in low frequencies, designed control structure gives exact command and in high frequencies controller, efficiency is decreasing.
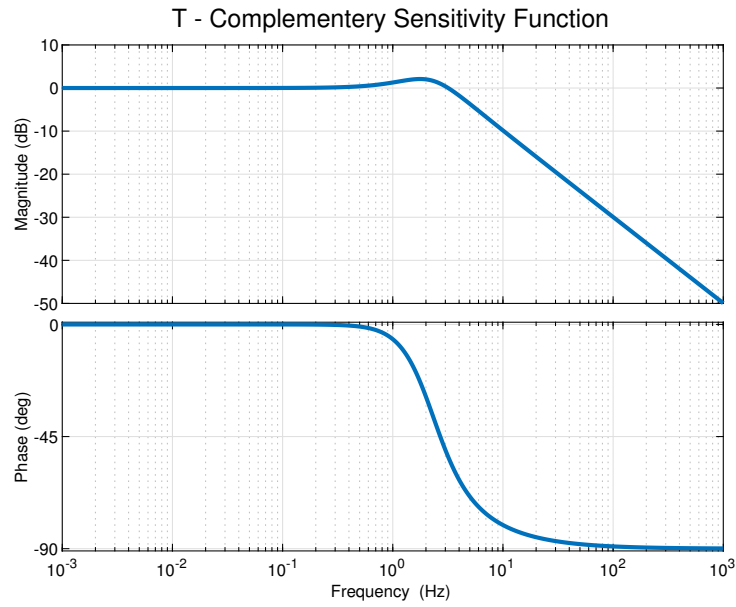
Figure 2.3: Frequency Response of Complementary Sensitivity.

Sensitivity transfer function's frequency response is in Figure 2.4. In low frequencies good error rejection is obtained but in high frequencies error is not rejecting.
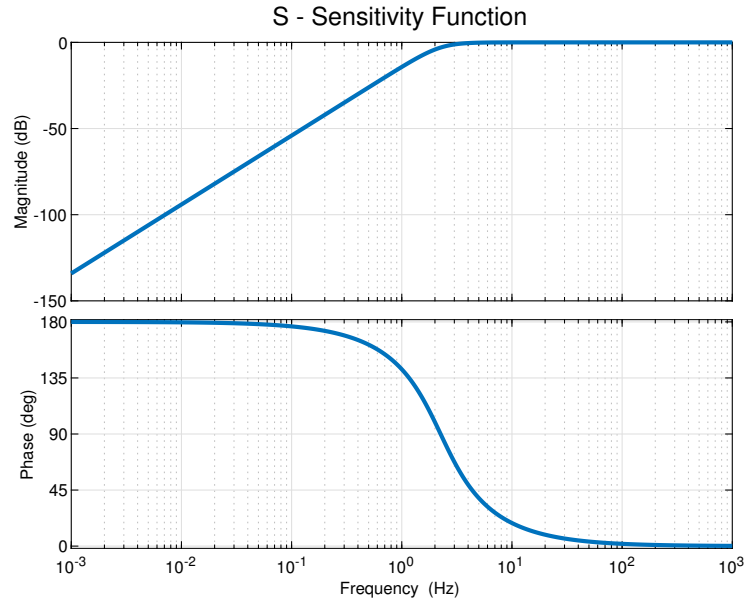
Figure 2.4: Frequency Response of System Sensitivity.

Controller sensitivity transfer function's frequency response is in Figure 2.5. As expected in low frequencies, the figure is like an integrator and in high frequencies, the figure is like a gain.
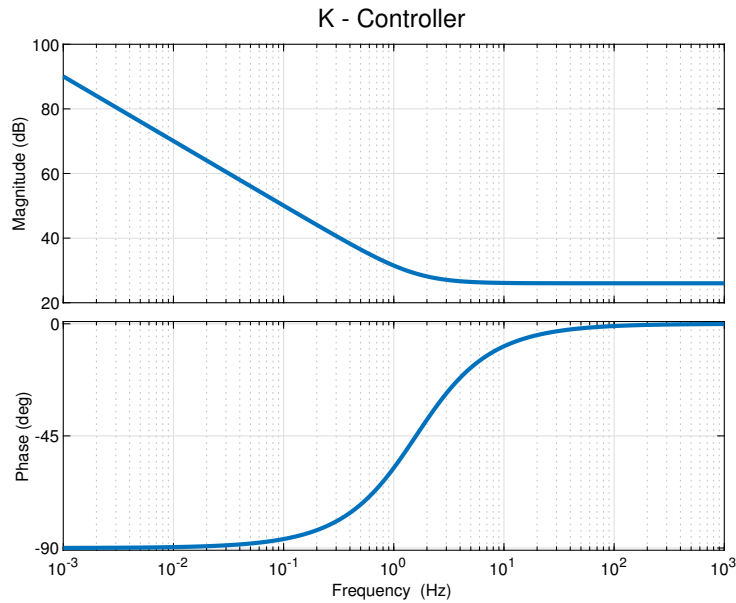
Figure 2.5: Frequency Response of Controller Sensitivity.

2.3 TRAJECTORY FOLLOWING WITH REFERENCE CONDITIONS

Assessment of proposed controller system will be simulated under various conditions. But it is needed to reference trajectories to compare proposed CCC structure's output. In this chapter; line, circle, ellipse and parabola is drawn under reference conditions.

2.3.1 Drawing Line with Reference Conditions

Design parameters are given below:

$$P_x = P_y = \frac{1}{s} \tag{II.25}$$

$$K_x = K_y = \frac{20s + 200}{s} \tag{II.26}$$

$$W_x = W_y = \frac{10}{s + 10} \tag{II.27}$$

Inputs are ramp input:

$$X_r = 3 \tag{II.28}$$

$$Y_r = 1 \tag{II.29}$$

Final graph is given in Figure 2.6:
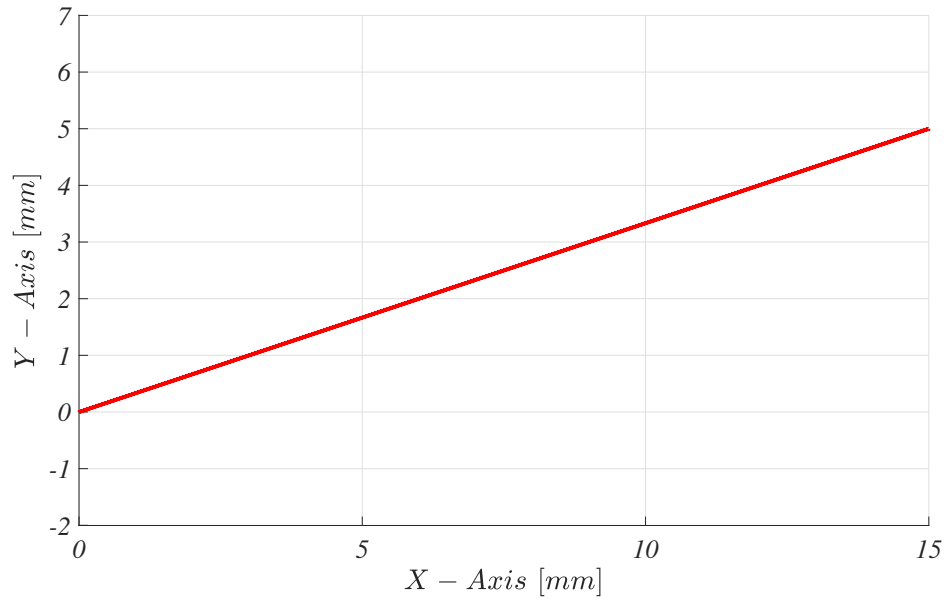
Figure 2.6: Drawing Line with Reference Conditions.

2.3.2 Drawing Circle with Reference Conditions

Design parameters are given below:

$$P_x = P_y = \frac{1}{s} \tag{II.30}$$

$$K_x = K_y = \frac{20s + 200}{s} \tag{II.31}$$

$$W_x = W_y = \frac{10}{s + 10} \tag{II.32}$$

Inputs are given below:

$$X_r = \sin(\theta) \tag{II.33}$$

Amplitude of $\sin(\theta)$ is 50 and initial phase is 0.

$$Y_r = \cos(\theta) \tag{II.34}$$

Amplitude of $\cos(\theta)$ is 50 and initial phase is $-\pi/2$.
Final graph is given in Figure 2.7:
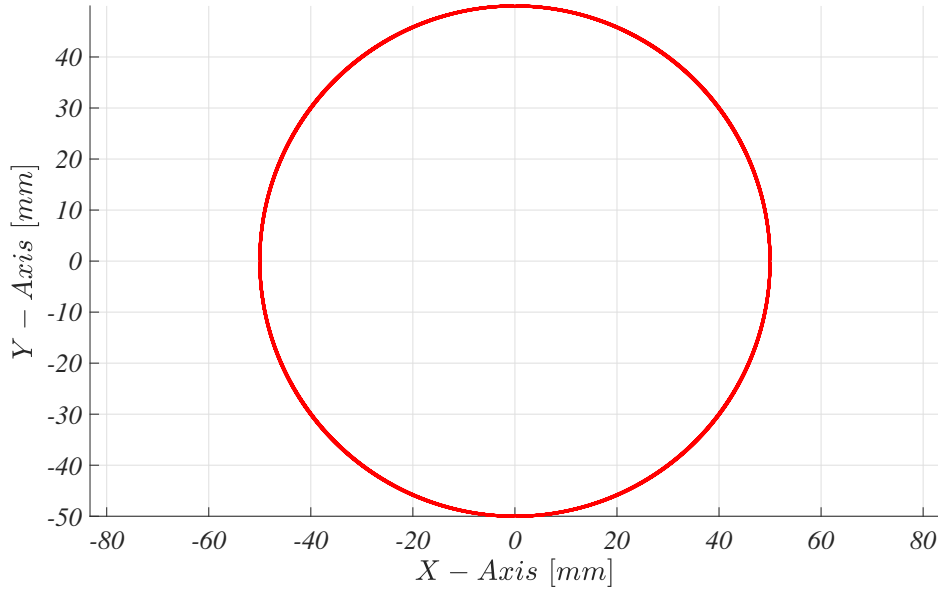
Figure 2.7: Drawing Circle with Reference Conditions.

2.3.3 Drawing Ellipse with Reference Conditions

Design parameters are given below:

$$P_x = P_y = \frac{1}{s} \tag{II.35}$$

$$K_x = K_y = \frac{20s + 200}{s} \tag{II.36}$$

$$W_x = W_y = \frac{10}{s + 10} \tag{II.37}$$

Inputs are given below:

$$X_r = \sin(\theta) \tag{II.38}$$

Amplitude of $\sin(\theta)$ is 10 and initial phase is 0.

$$Y_r = \cos(\theta) \tag{II.39}$$

Amplitude of $\cos(\theta)$ is 5 and initial phase is $-\pi/2$.

Final graph is given in Figure 2.8:
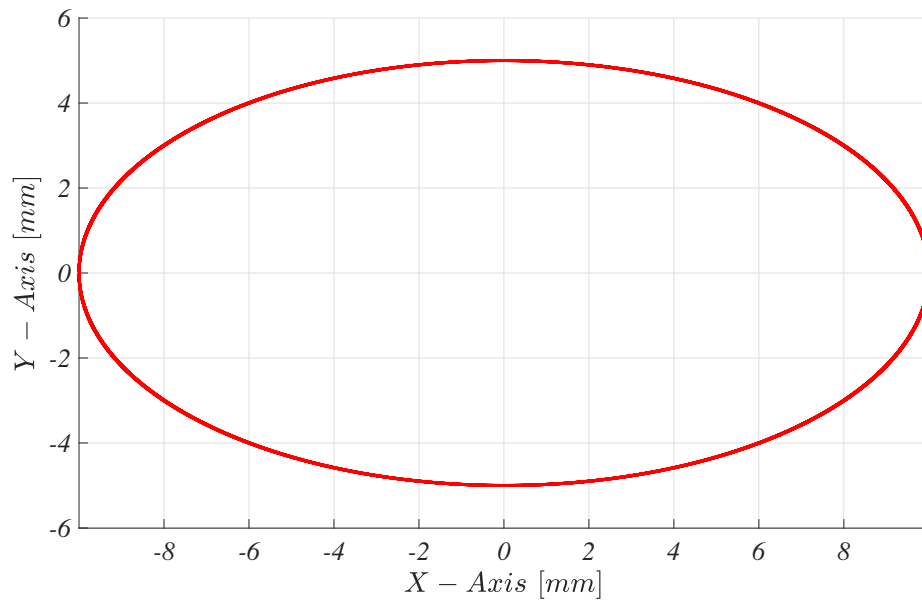
Figure 2.8: Drawing Ellipse with Reference Conditions.

2.3.4 Drawing Parabola with Reference Conditions

Design parameters are given below:

$$P_x = P_y = \frac{1}{s} \tag{II.40}$$

$$K_x = K_y = \frac{20s + 200}{s} \tag{II.41}$$

$$W_x = W_y = \frac{10}{s + 10} \tag{II.42}$$

Inputs of X-Axis is ramp input:

$$X_r = 1 \tag{II.43}$$

$$Y_r = 0.1(X_r)^2 \tag{II.44}$$

Final graph is given in Figure 2.9 :
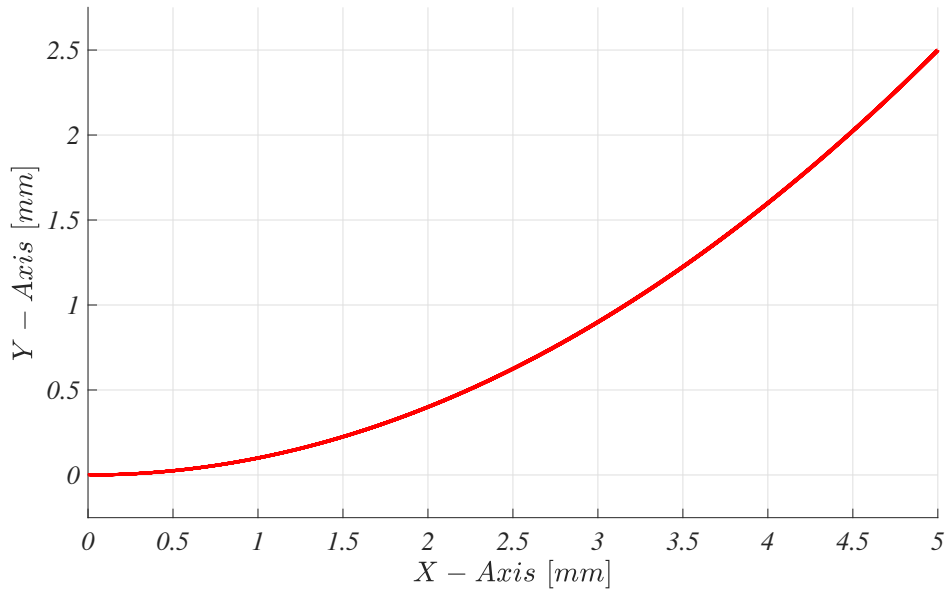
Figure 2.9: Drawing Parabola with Reference Conditions.

2.4 CROSS-COUPLED CONTROLLER DESIGN

Conventional approach to overcome synchronization problem is to control each axis separately. Even so designed controller may not be enough to accomplish required precise trajectory. Because only one axis' uncoordinated motion will lead contour error. Link is needed between two axes. Cross-Coupled Controller (CCC) makes it possible to react not only to command input but also each axis' mis-aligned motion.

The goal of the CCC is to eliminate contour error rather than position error. To get this goal CCC has three main processes:

1) Calculating contour error:

Contour error can be expressed as difference between axial position errors.

$$\varepsilon = -E_x C_x + E_y C_y \qquad \text{(II.45)}$$

Detail calculations of C_x and C_y are given in Section 2.5.

2) Controller for contour error:

In this thesis, proportional type controller is proposed. But more sophisticated controllers can also be used as CCC.

3) Injecting contour error to individual axis' command:

Add or extract CCC's output into individual axial output. One point must be emphasized, while calculating contour error, X-Aaxis' axial error is extracted from Y-Axis' axial error. Thus, output of CCC is added to Y-Axis and extracted from X-Axis.

15

The logic of this step is to accelerate straggly axis and decelerate front-runner axis.

There are many ways to establish CCC. One of them is direct feedforwarding. Basic feedforward CCC block diagram can be seen in Figure 2.10. Error of each axis is calculating separately. Axial error is input of controllers and CCC structure. By extracting axial error from each other, synchronization error is obtained as in Equation II.45. After controller of CCC, calculated synchronization error is injected into each axis with opposite sign.
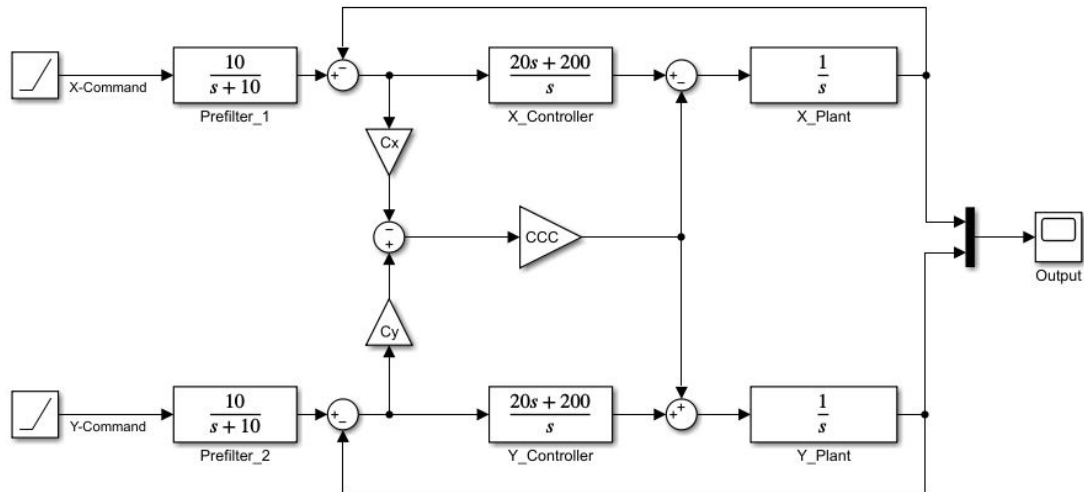
Figure 2.10: Block Diagram of Basic CCC Structure.

This solution decreases linear contour errors efficiently and successfully. But major drawback is low efficiency for nonlinear contours [3]. Thus, variable gain CCC is suggested to improve nonlinear contour performance. Variable gain CCC block diagram can be seen in Figure 2.11.

Major differences are variable gain calculation for different trajectories and using calculated gains for CCC's output. Calculating variable gains are given in Section 2.5. As basic CCC structure, axial error is calculated by extracting axial errors from each other and injecting each axis with opposite sign. But, in this case injecting output is multiplied by variable gain.
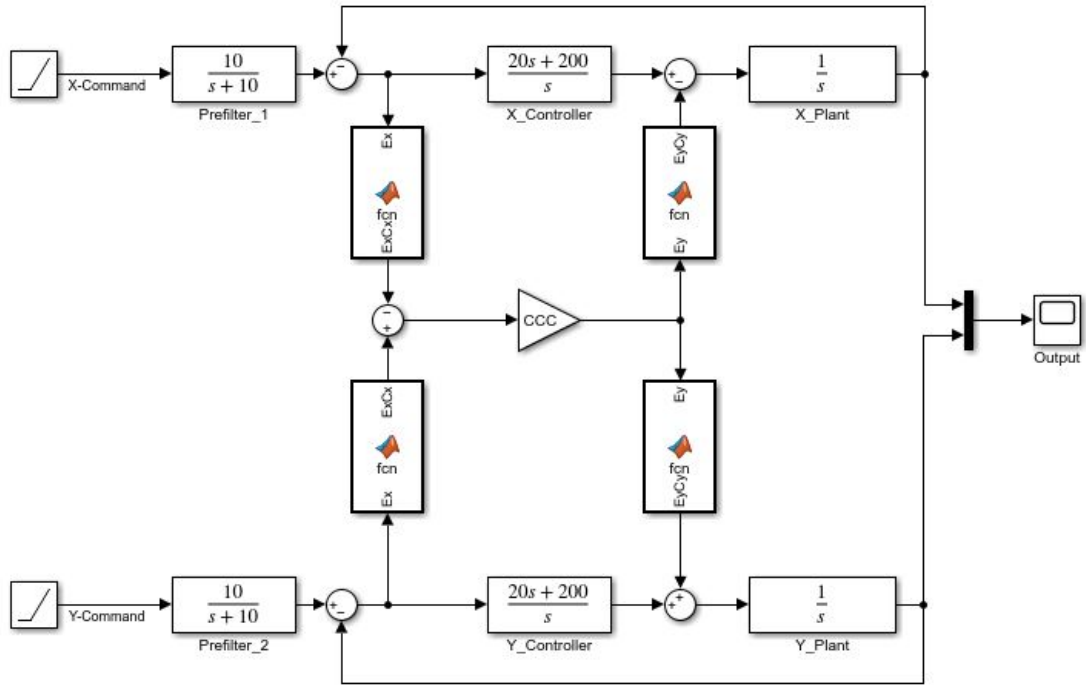
Figure 2.11: Block Diagram of CCC Structure with Variable Gain.

2.5 CALCULATING VARIABLE GAINS

2.5.1 Variable Gain for Linear Contour

For linear trajectories, contour error is the minimum distance between actual position (P_a) and desired contour which can be seen in Figure 2.12.

$$\varepsilon = -E_x \sin(\theta) + E_y \cos(\theta) \tag{II.46}$$

Where ε is contour error and E_x and E_y are axial position error for X and Y axes respectively.

From Figure 2.12 $\sin(\theta)$ and $\sin(\theta)$ can be calculated as:

$$\sin(\theta) = \frac{V_y}{V} \tag{II.47}$$

$$\cos(\theta) = \frac{V_x}{V} \tag{II.48}$$

Where V is required feed rate and V_x and V_y are axial feed rate for X and Y axes respectively. It is obtained by substituting Equation II.47 and Equation II.48 into Equation II.46.

$$\varepsilon = \frac{-E_x V_y + E_y V_x}{V} \tag{II.49}$$
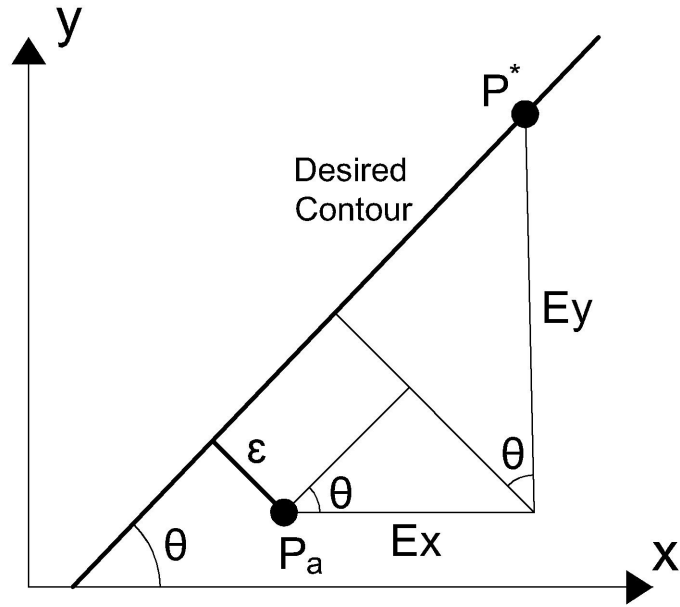
Figure 2.12: Error Model for Linear Contour.

From equation II.45 it can be obtained:

$$C_x = \frac{V_y}{V} \tag{II.50}$$

and

$$C_y = \frac{V_x}{V} \tag{II.51}$$

2.5.2 Variable Gain for Circular Contour

In circular contours, contour error is difference between distance from actual position to the center of the circle and center of the circle. Thus,

$$\varepsilon = \sqrt{(P_x - x_0)^2 + (P_y - y_0)^2} - R \tag{II.52}$$

Where P_x and P_y are actual position of the axes. x_0 and y_0 is center of the desired circle's center.
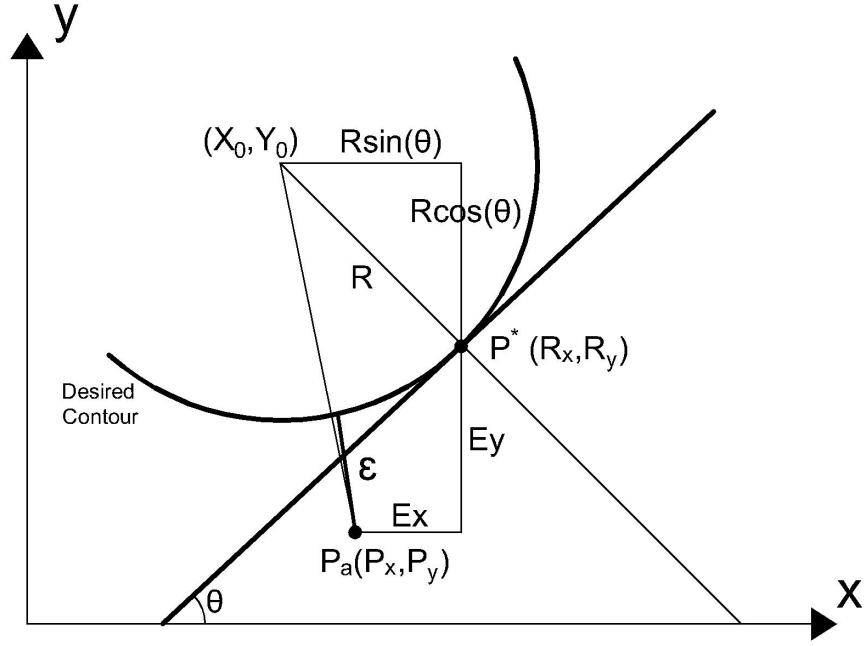
Figure 2.13: Error Model for Circular Contour.

From Figure 2.13 below expression can be calculated.

$$P_x = R_x - E_x \tag{II.53}$$

$$P_x = x_0 + R\sin(\theta) - E_x \tag{II.54}$$

And,

$$P_y = R_y - E_y \tag{II.55}$$

$$P_y = y_0 + R\cos(\theta) - E_y \tag{II.56}$$

It is obtained by substituting Equation II.54 and Equation II.56 into Equation II.52.

$$\varepsilon = \sqrt{(R\sin(\theta) - E_x)^2 + (-R\cos(\theta) - E_y)^2} - R \tag{II.57}$$

Apply Taylor series expansion into Equation II.57

$$\varepsilon = -E_x\left(\sin\theta - \frac{E_x}{2R}\right) + E_y\left(\cos\theta + \frac{E_y}{2R}\right) + Order\left(\frac{\varepsilon^2}{R}\right) \tag{II.58}$$

Contour error is much smaller than axial error and axial error is much smaller

than R. Thus,

$$\varepsilon = -E_x \left(\sin\theta - \frac{E_x}{2R} \right) + E_y \left(\cos\theta + \frac{E_y}{2R} \right) \tag{II.59}$$

From Equation II.45 it can be obtained:

$$C_x = \left(\sin\theta - \frac{E_x}{2R} \right) \tag{II.60}$$

and

$$C_y = \left(\cos\theta + \frac{E_y}{2R} \right) \tag{II.61}$$

2.5.3   Variable Gain for Elliptic Contour

For the ease of calculation, contour error of elliptic trajectory can be derived from circular trajectory. In Figure 2.14 there are one ellipse and 3 circles. The big circle is the biggest circle that can be tangent on two points of the ellipse. The small one is the biggest circle that can be fit into the ellipse. The dashed one represents the instantaneous circle that can be derived from the actual location on the ellipse. The contour error for an elliptic contour can be calculated by these two circles.

$$R_e = aR_a + bR_b \tag{II.62}$$

Where

$$a = \sin^2(\theta) \tag{II.63}$$

$$b = \cos^2(\theta) \tag{II.64}$$

20
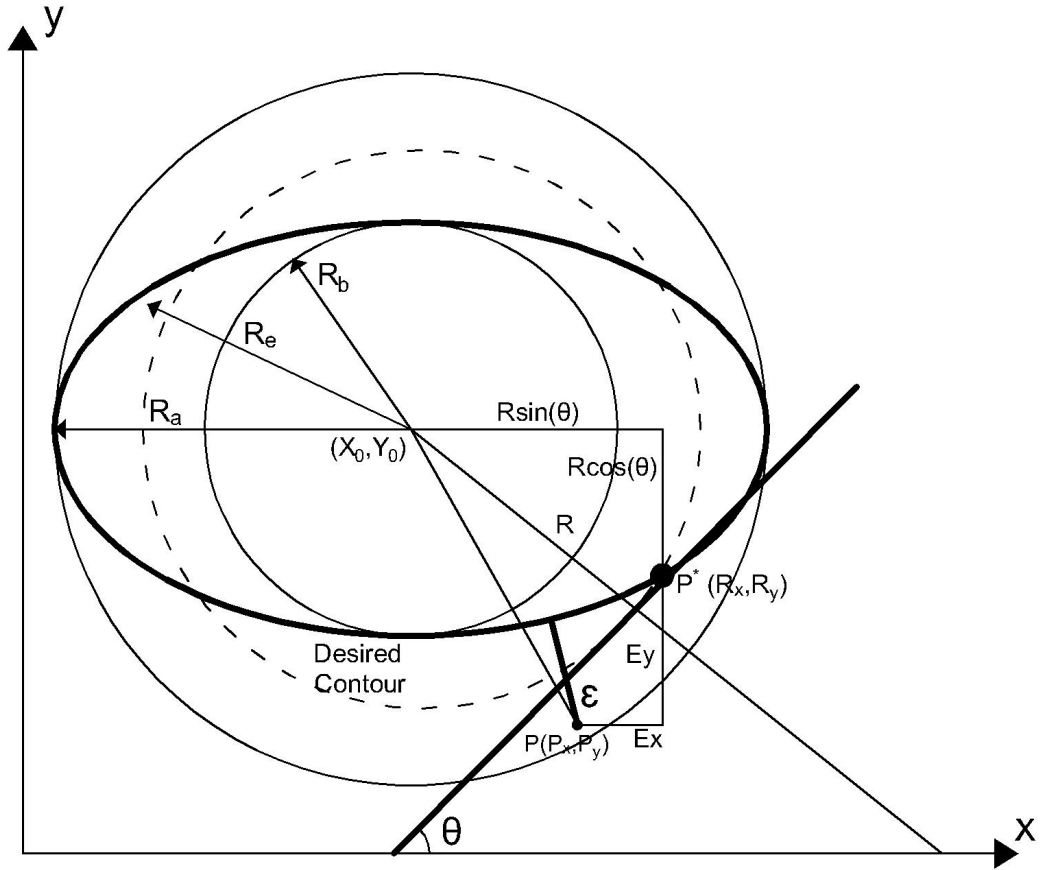
Figure 2.14: Error Model for Elliptic Contour.

The contour error for the elliptic contour is the difference between the distance from actual location to the center of the circle and the radius of the circle

$$\varepsilon = \sqrt{(P_x - x_e)^2 + (P_y - y_e)^2} - R_e \qquad (\text{II.65})$$

The actual position can be represented by the axial errors and the reference position.

$$P_x = R_x - E_x \qquad (\text{II.66})$$

$$P_x = R_e \sin(\theta) + x_e - E_x \qquad (\text{II.67})$$

And,

$$P_y = R_y - E_y \qquad (\text{II.68})$$

$$P_y = -R_e \sin(\theta) + x_e - E_x \qquad (\text{II.69})$$

21

It is obtained by substituting Equation II.67 and Equation II.69 into Equation II.65.

$$\varepsilon = \sqrt{(R_e \sin(\theta) - E_x)^2 + (-R_e \cos(\theta) - E_y)^2} - R_e \qquad \text{(II.70)}$$

Because Equation II.70 is difficult to implement in real-time control system, a simplification is proposed. By expanding the error in Equation II.70 by Taylor series expansion it is obtained,

$$\varepsilon = -E_x \left(\sin \theta - \frac{E_x}{2R_e} \right) + E_y \left(\cos \theta + \frac{E_y}{2R_e} \right) + Order \left(\frac{\varepsilon^2}{R_e} \right) \qquad \text{(II.71)}$$

If the contour error is much smaller than the axial errors and the axial errors are much smaller than the radius of the circle, the high-order term can be neglected and the contour error can be approximated by,

$$\varepsilon = -E_x C_x + E_y C_y \qquad \text{(II.72)}$$

Where

$$C_x = \sin \theta - \left(\frac{E_x}{2R_e} \right) \qquad \text{(II.73)}$$

$$C_y = \cos \theta - \left(\frac{E_y}{2R_e} \right) \qquad \text{(II.74)}$$

2.5.4 Variable Gain for Parabolic Contour

A non-circular contour can be approximated as a circle [3]. If the instantaneous radius of the curvature is much bigger than the axial error, the contour error can be expressed as,

$$\varepsilon = \sqrt{(P_x - x_0)^2 + (P_y - y_0)^2} - R \qquad \text{(II.75)}$$

Where R is the radius of the circle and (x_0, y_0) is the center of the circle. The actual position can be represented by the axial errors and the reference position.
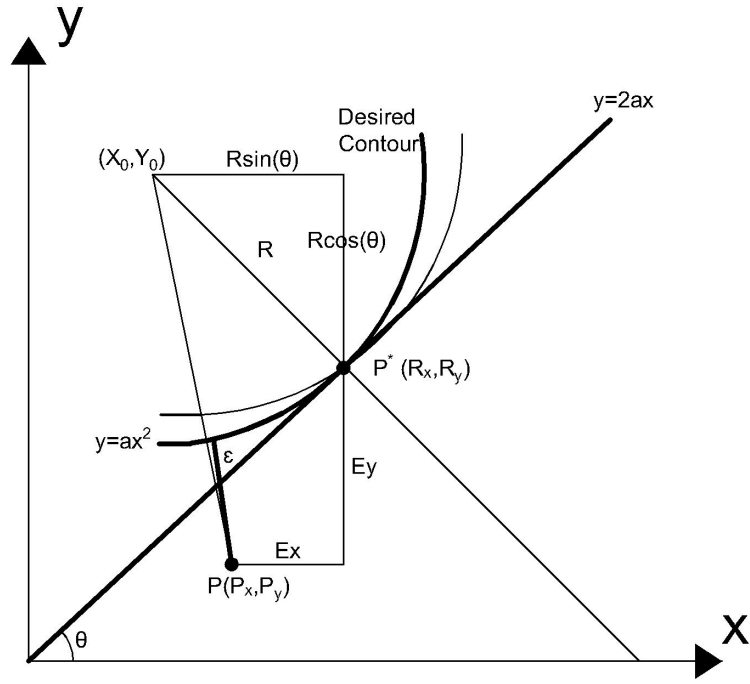
Figure 2.15: Error Model for Parabolic Contour.

$$P_x = R_x - E_x \qquad\qquad (\text{II}.76)$$

$$P_x = x_0 + R\sin(\theta) - E_x \qquad\qquad (\text{II}.77)$$

And,

$$P_y = R_y - E_y \qquad\qquad (\text{II}.78)$$

$$P_y = y_0 + R\cos(\theta) - E_y \qquad\qquad (\text{II}.79)$$

We obtain by substituting Equation II.77 and Equation II.79 into Equation II.80.

$$\varepsilon = \sqrt{(R\sin(\theta) - E_x)^2 + (-R\cos(\theta) - E_y)^2} - R \qquad\qquad (\text{II}.80)$$

Expanding the error in equation by Taylor series expansion

$$\varepsilon = -E_x\left(\sin\theta - \frac{E_x}{2R}\right) + E_y\left(\cos\theta + \frac{E_y}{2R}\right) + Order\left(\frac{\varepsilon^2}{R}\right) \qquad\qquad (\text{II}.81)$$

If the contour error is much smaller than the axial errors and the axial errors are much smaller than the radius of the circle, the high-order term can be neglected and the contour error can be approximated by,

$$\varepsilon = -E_x C_x + E_y C_y \tag{II.82}$$

Where

$$C_x = \sin\theta - \left(\frac{E_x}{2R_e}\right) \tag{II.83}$$

$$C_y = \cos\theta - \left(\frac{E_y}{2R_e}\right) \tag{II.84}$$

But R must be calculated for every point on the parabolic curve. In order to find R we need $sin(\theta)$ and $cos(\theta)$. From Figure 2.15 below expression can be obtained [3].

$$\sin(\theta) = \frac{2ax}{\sqrt{1 + (2ax)^2}} \tag{II.85}$$

$$\cos(\theta) = \frac{1}{\sqrt{1 + (2ax)^2}} \tag{II.86}$$

$$R = \frac{1}{2a}[1 + (2ax)^2]^{1.5} \tag{II.87}$$

CHAPTER III

SIMULATION RESULTS

Effectiveness of the proposed structure is examined with simulations under the effects of friction, inner disturbance and both of them simultaneously. These unwanted effects only applied to one axis to cause contour error. Intentionally friction and inner disturbance values are determined extremely high in order to see contour error clearly.

3.1   CCC STRUCTURE UNDER FRICTION

Friction is only applied to X-Axis. Plant of X-Axis is

$$P = \frac{1}{s + 25} \tag{III.1}$$

3.1.1   Drawing Line under Friction

Block diagram of the simulation structure is given in Figure 3.1. Friction is only applied to the X-Axis and CCC is P type with magnitude of 10000.

Figure 3.1: Block Diagram of Line Drawing under Friction.

Comparison of the reference line and simulation results are given in Figure 3.2 and Figure 3.3.
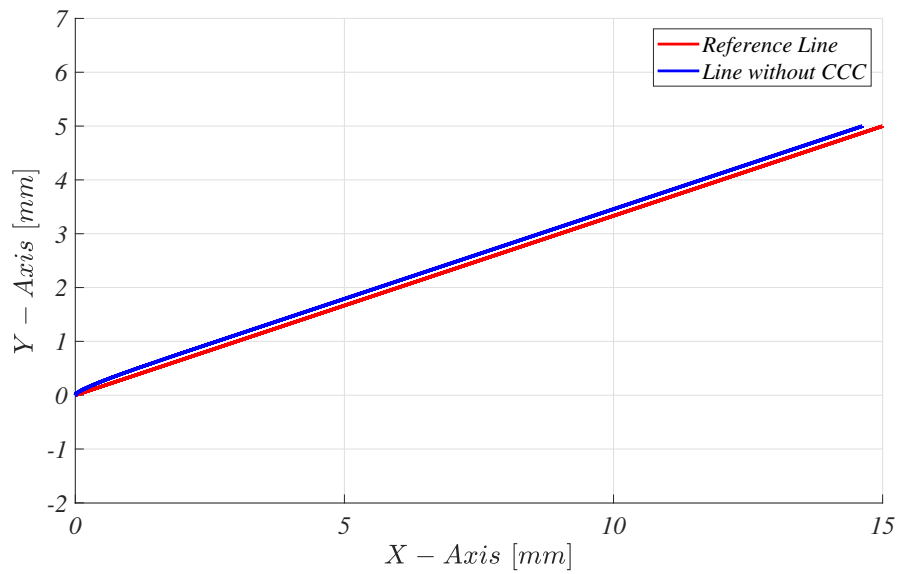
Figure 3.2: Drawing Line without CCC under Friction.

Without coupling, X-Axis move much slower than Y-Axis and uncoordinated motion is occurred which is obvious in Figure 3.2. Thus desired trajectory could not be achieved.
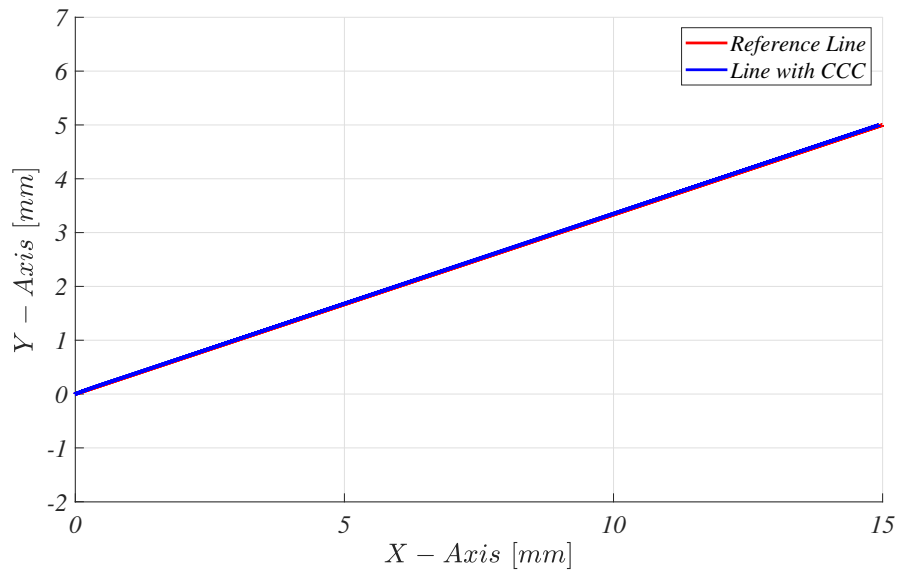
Figure 3.3: Drawing Line with CCC under Friction.

Thanks to CCC structure a significant improvement on contour error is achieved which can be seen in Figure 3.3. Duration of this simulation is 5 seconds.
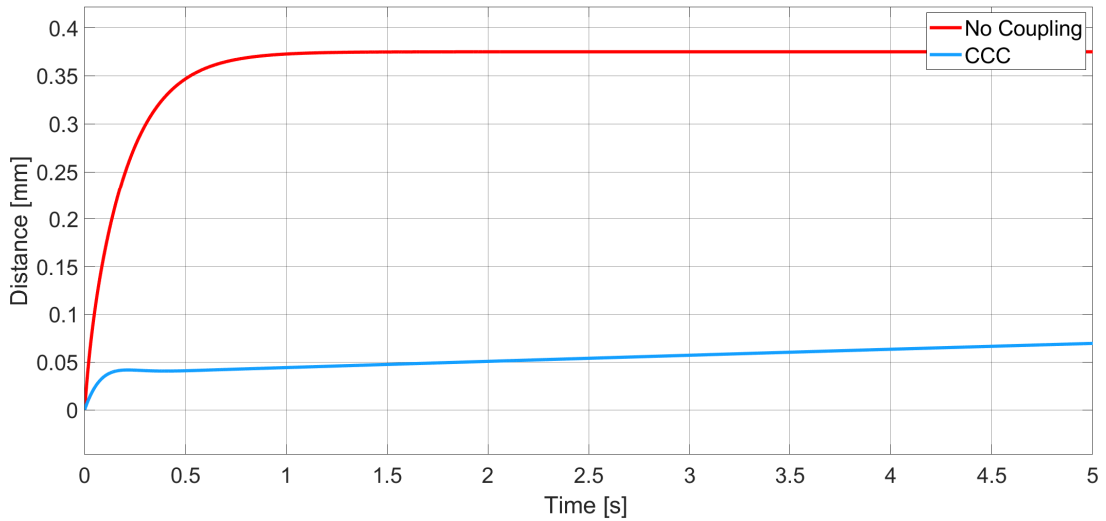
Figure 3.4: Drawing Line under Friction - Error of X-Axis.

High friction slows down X-Axis but CCC increases command according to the contour error. As a result, good command following is achieved for X-Axis in spite of high friction. Error is decreased from 0.375 to 0.05.
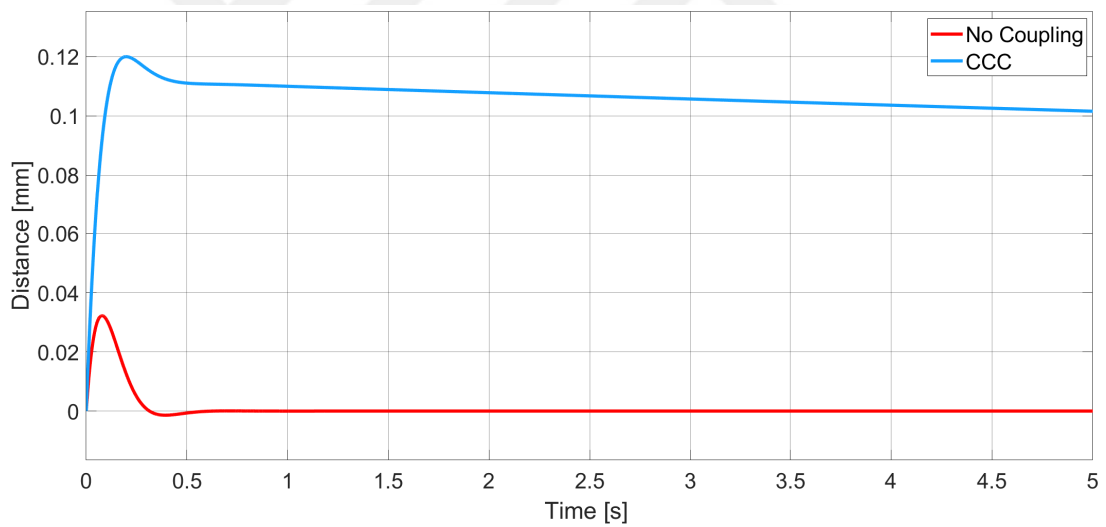
Figure 3.5: Drawing Line under Friction - Error of Y-Axis.

Y-Axis has no friction. But it is clear that Y-Axis is slower than its command. CCC compensation causes this deviation in order to increase synchronization performance.

Table 3.1: Drawing Line under Friction without Coupling.

Time	X Command	X Error	Y Command	Y Error	Syn. Error
0,000	0,000	0,000	0,000	0,000	0,000
0,250	0,750	0,277	0,245	0,005	-0,261
0,500	1,500	0,347	0,501	-0,001	-0,329
0,750	2,250	0,367	0,750	0,000	-0,348
1,000	3,000	0,373	1,000	0,000	-0,354
1,250	3,750	0,374	1,250	0,000	-0,355
1,500	4,500	0,375	1,500	0,000	-0,356
1,750	5,250	0,375	1,750	0,000	-0,356
2,000	6,000	0,375	2,000	0,000	-0,356
2,250	6,750	0,375	2,250	0,000	-0,356
2,500	7,500	0,375	2,500	0,000	-0,356
2,750	8,250	0,375	2,750	0,000	-0,356
3,000	9,000	0,375	3,000	0,000	-0,356
3,250	9,750	0,375	3,250	0,000	-0,356
3,500	10,500	0,375	3,500	0,000	-0,356
3,750	11,250	0,375	3,750	0,000	-0,356
4,000	12,000	0,375	4,000	0,000	-0,356
4,250	12,750	0,375	4,250	0,000	-0,356
4,500	13,500	0,375	4,500	0,000	-0,356
4,750	14,250	0,375	4,750	0,000	-0,356
5,000	15,000	0,375	5,000	0,000	-0,356

In Table 3.1 and Table 3.2, each axis' command, axial error and synchronization error is given with and without CCC. Synchronization error is calculated according to

$$\varepsilon = -E_x C_x + E_y C_y$$

In Table 3.1 stable contour error can be seen clearly due to the friction in X-Axis. But Y-Axis has no error. Because of the difference between axes, synchronization error is occurred.

Table 3.2: Drawing Line under Friction with Coupling.

Time	X Command	X Error	Y Command	Y Error	Syn. Error
0,000	0,000	0,000	0,000	0,000	0,000
0,251	0,752	0,042	0,132	0,118	-0,002
0,501	1,502	0,041	0,390	0,111	-0,004
0,751	2,252	0,043	0,640	0,111	-0,005
1,001	3,002	0,044	0,891	0,110	-0,007
1,251	3,752	0,046	1,141	0,109	-0,009
1,501	4,502	0,048	1,392	0,109	-0,011
1,751	5,252	0,049	1,642	0,108	-0,012
2,001	6,002	0,051	1,893	0,108	-0,014
2,251	6,752	0,052	2,143	0,107	-0,016
2,501	7,502	0,054	2,394	0,107	-0,017
2,751	8,252	0,056	2,644	0,106	-0,019
3,001	9,002	0,057	2,895	0,106	-0,021
3,251	9,752	0,059	3,146	0,105	-0,022
3,501	10,502	0,060	3,396	0,105	-0,024
3,751	11,252	0,062	3,647	0,104	-0,026
4,001	12,002	0,063	3,897	0,104	-0,027
4,251	12,752	0,065	4,148	0,103	-0,029
4,501	13,502	0,066	4,398	0,103	-0,031
4,751	14,252	0,068	4,649	0,102	-0,032
5,000	15,000	0,070	4,898	0,102	-0,034

After compensation by CCC, synchronization error is reduced significantly which can be seen in Table 3.2. Error of X-Axis is reduced and Y-Axis is increased. Error in X-Axis is decreased and increased in Y-Axis. Thanks to the CCC structure synchronization error is dramatically reduced.

3.1.2 Drawing Circle under Friction

Block diagram of the simulation structure is given in Figure 3.6. Friction is only applied to the X-Axis and CCC is P type with magnitude of 10000.

Figure 3.6: Block Diagram of Circle Drawing under Friction.

Comparison of the reference circle and simulation results are given in Figure 3.7 and Figure 3.8.
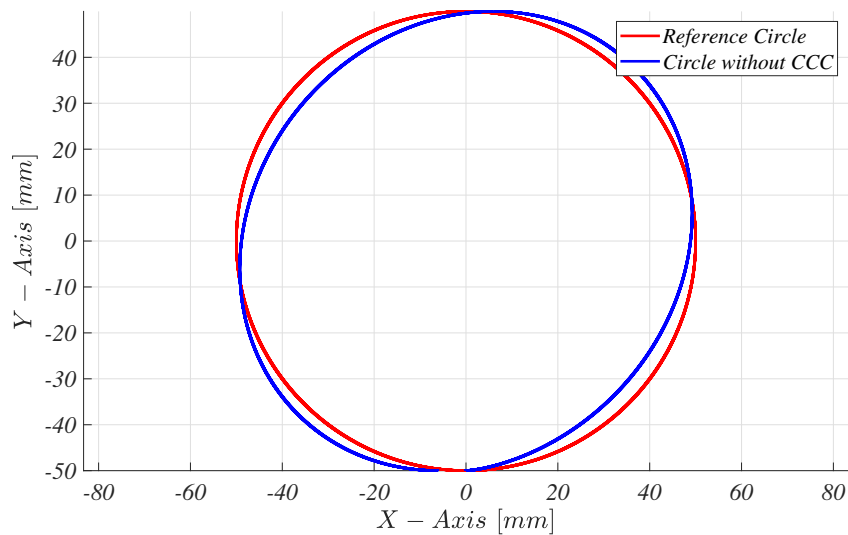
Figure 3.7: Drawing Circle under Friction without CCC.

Uncoordinated motion causes contour error on circular trajectory. Serious deviation is occurred between desired and actual contours.
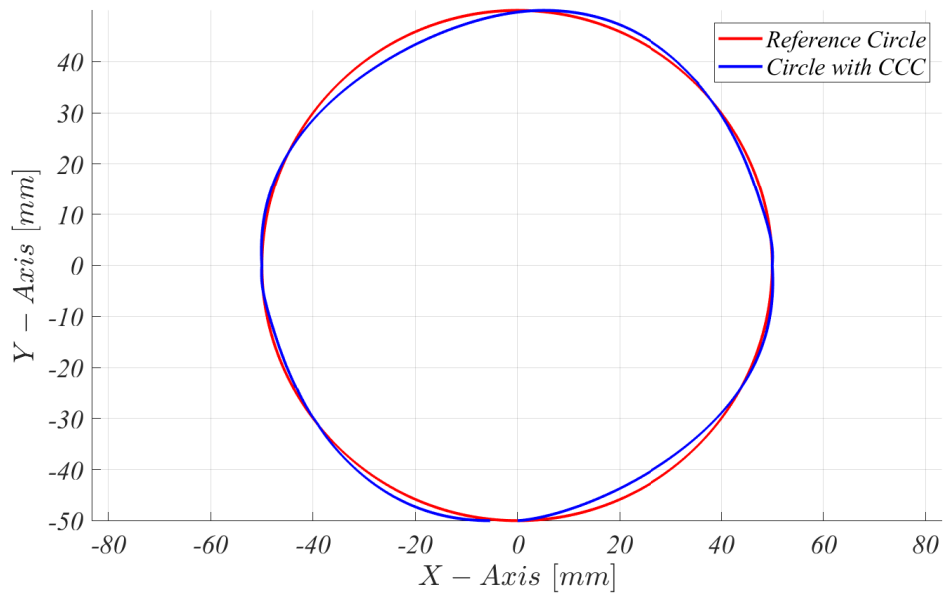
Figure 3.8: Drawing Circle under Friction with CCC.

CCC successfully compensates synchronization error and actual trajectory is much more like a circle. Duration of this simulation is 2π seconds.
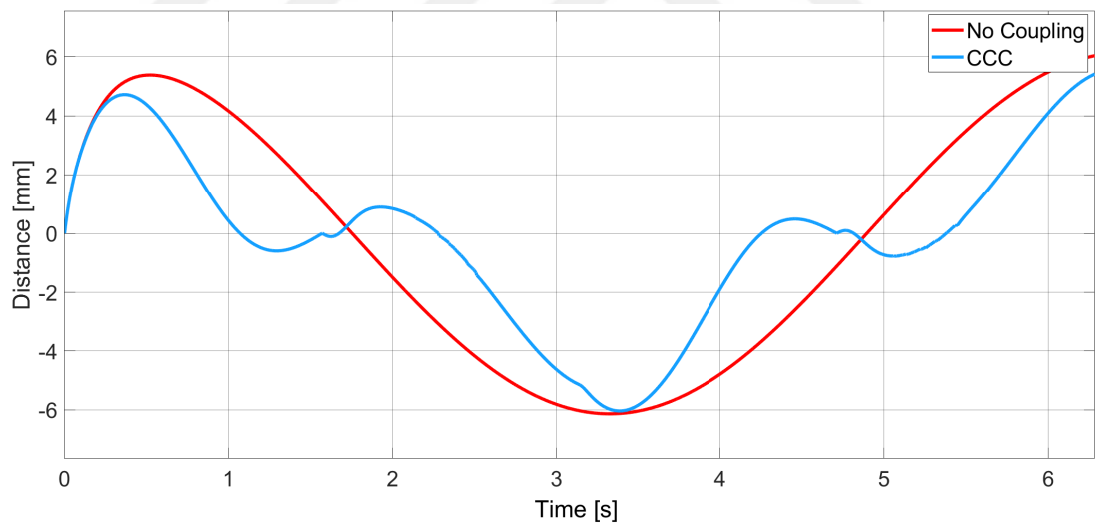
Figure 3.9: Drawing Circle under Friction - Error of X-Axis.

Error of X-Axis is smaller with CCC compared to no-coupling version. Almost zero error is achieved in X-Axis.
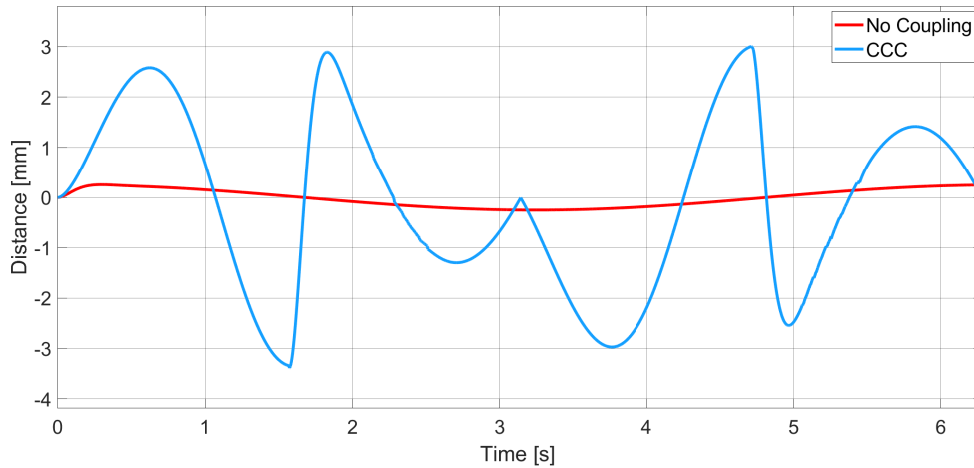
Figure 3.10: Drawing Circle under Friction - Error of Y-Axis.

In Y-Axis, different case is occurred. Without coupling there is almost no error. With CCC, in order to compensate contour error, Y-Axis' command is manipulated which lead to higher error.

Table 3.3: Drawing Circle under Friction without Coupling.

Time	X Command	X Error	Y Command	Y Error	Syn. Error
0	0,000	0,000	-50,000	0,000	0,000
$\pi/8$	19,148	5,226	-46,435	0,246	-88,419
$\pi/4$	35,341	4,943	-35,563	0,194	-167,609
$3\pi/8$	46,192	3,320	-19,257	0,118	-151,004
$\pi/2$	50,000	1,109	-0,015	0,025	-55,434
$5\pi/8$	46,203	-1,277	19,183	-0,072	57,654
$3\pi/4$	35,362	-3,476	35,507	-0,158	117,461
$7\pi/8$	19,129	-5,146	46,416	-0,220	88,522
π	-0,020	-6,030	50,249	-0,249	-11,951
$9\pi/8$	-19,490	-5,986	46,284	-0,239	106,038
$5\pi/4$	-35,356	-5,050	35,549	-0,194	171,967
$11\pi/8$	-46,200	-3,334	19,238	-0,118	151,861
$3\pi/2$	-50,000	-1,115	0,045	-0,025	55,743
$13\pi/8$	-46,196	1,279	-19,202	0,072	-57,707
$7\pi/4$	-35,348	3,478	-35,521	0,158	-117,234
$15\pi/8$	-19,157	5,144	-46,405	0,220	-88,100
2π	0,000	6,030	-50,249	0,249	12,801

Without CCC high error in X-Axis is occurred. Maximum 6.03 error is observed. But in Y-axis, relatively less error is occurred. Quite high synchronization error can be observed in Table 3.3.

Table 3.4: Drawing Circle under Friction with Coupling.

Time	X Command	X Error	Y Command	Y Error	Syn. Error
0,000	0,000	0,000	-50,000	0,000	0,000
$\pi/8$	19,157	4,700	-48,128	1,944	0,000
$\pi/4$	35,344	2,218	-37,580	2,213	-0,001
$3\pi/8$	46,195	-0,443	-18,059	-1,071	-0,001
$\pi/2$	50,000	0,001	3,379	-3,363	-0,001
$5\pi/8$	46,199	0,885	16,987	2,136	-0,001
$3\pi/4$	35,361	-0,455	35,806	-0,456	-0,002
$7\pi/8$	19,118	-3,090	47,482	-1,281	0,000
π	-0,054	-5,162	50,011	-0,011	0,000
$9\pi/8$	-19,125	-5,700	48,566	-2,368	0,000
$5\pi/4$	-35,361	-2,588	37,942	-2,593	0,001
$11\pi/8$	-46,201	0,277	18,447	0,669	0,001
$3\pi/2$	-50,000	0,003	-2,990	3,006	0,001
$13\pi/8$	-46,177	-0,759	-17,346	-1,830	0,001
$7\pi/4$	-35,339	0,640	-36,012	0,639	0,001
$15\pi/8$	-19,148	3,344	-47,572	1,384	0,000
2π	0,000	5,407	-49,994	-0,006	0,000

Significant synchronization error decrease is obtained by proposed structure which can be seen in Table 3.4. In this table less X-Axis error and more Y-Axis error can be observed.

3.1.3 Drawing Ellipse under Friction

Block diagram of the simulation structure is given in Figure 3.11. Friction is only applied to the X-Axis and CCC is P type with magnitude of 10000.
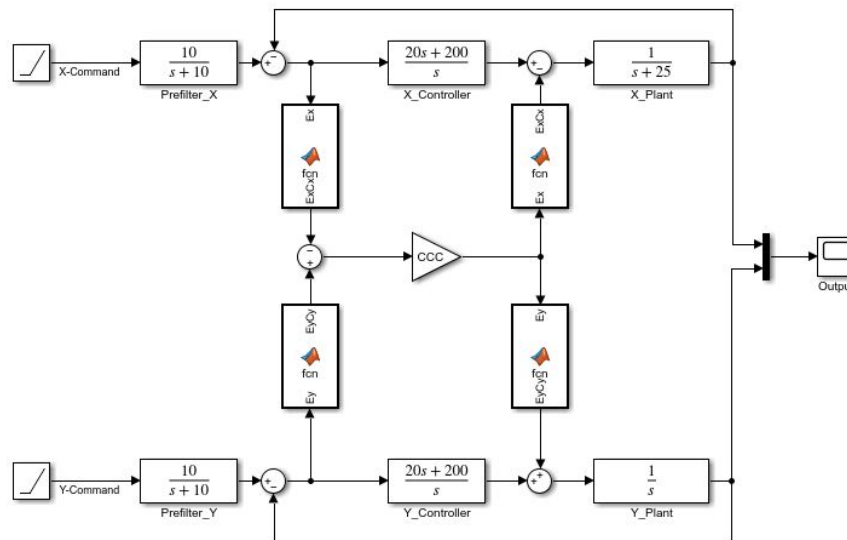

Figure 3.11: Block Diagram of Ellipse Drawing under Friction.

Comparison of the reference ellipse and simulation results are given in Figure 3.12 and Figure 3.13.
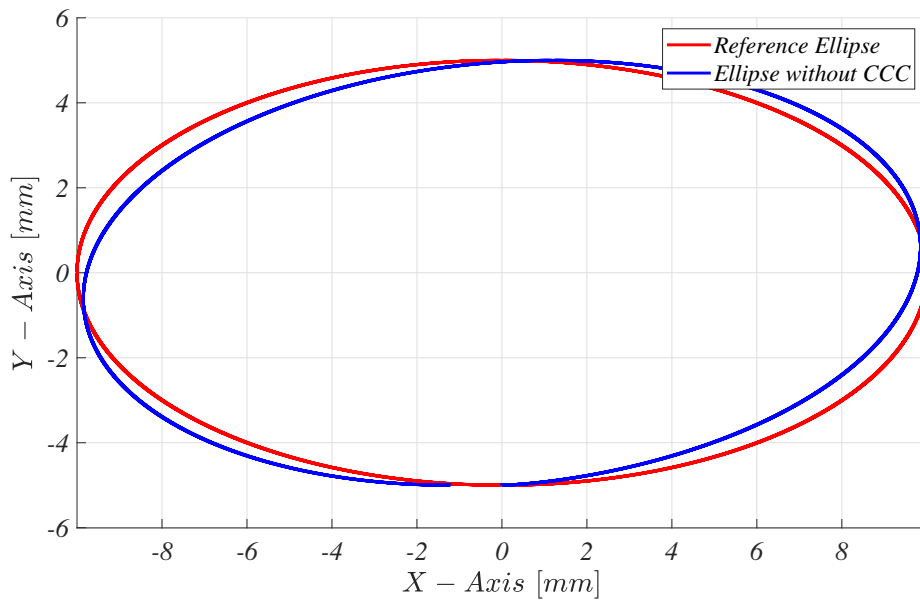
Figure 3.12: Drawing Ellipse under Friction without CCC.

Friction causes contour error which can be seen in Figure 3.15.
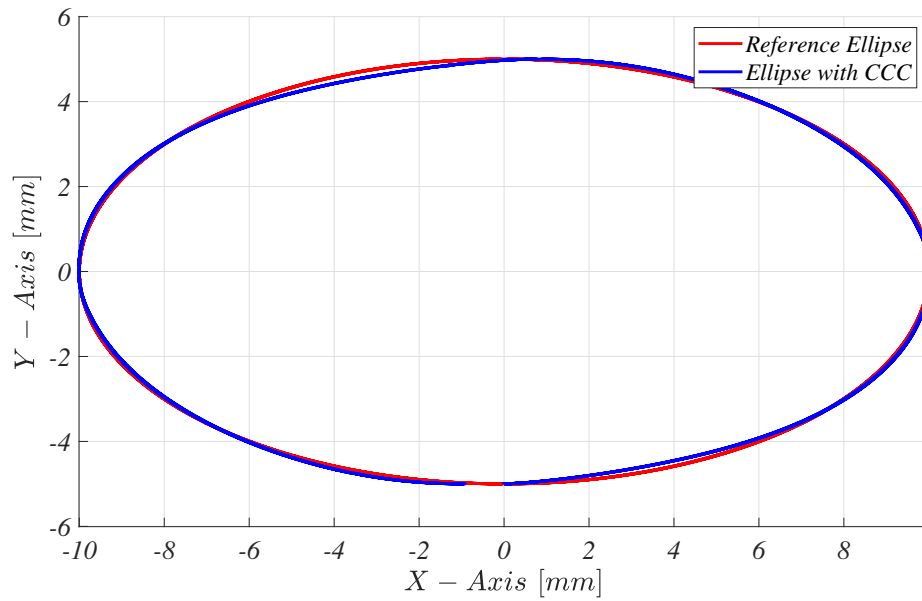
Figure 3.13: Drawing Ellipse under Friction with CCC.

After CCC is applied almost desired elliptic contour is achieved. Duration of this simulation is 2π seconds.
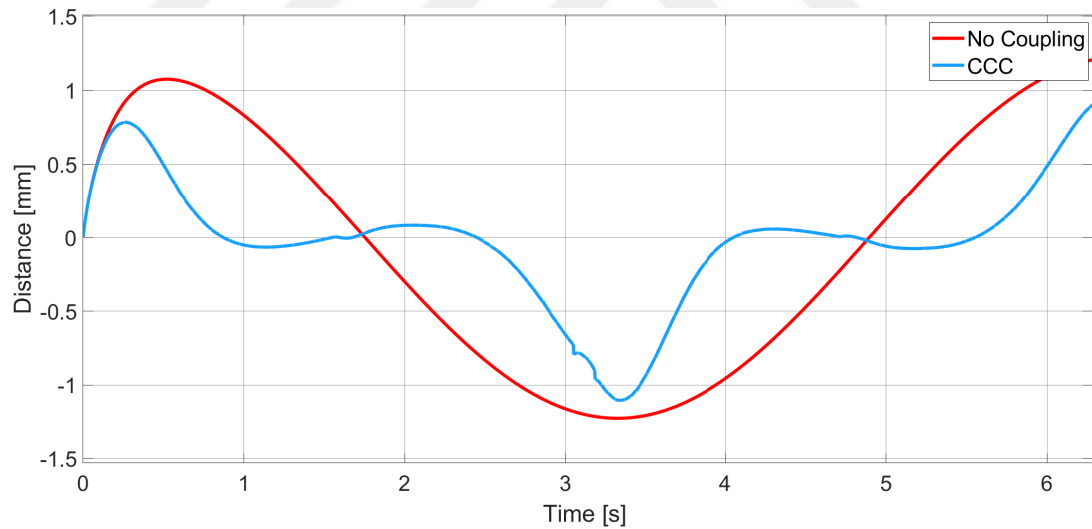
Figure 3.14: Drawing Ellipse under Friction - Error of X-Axis.

Circular and elliptic trajectories are similar. So similar error graphics are obtained. Due to CCC's compensation, error of X-Axis is reduced.
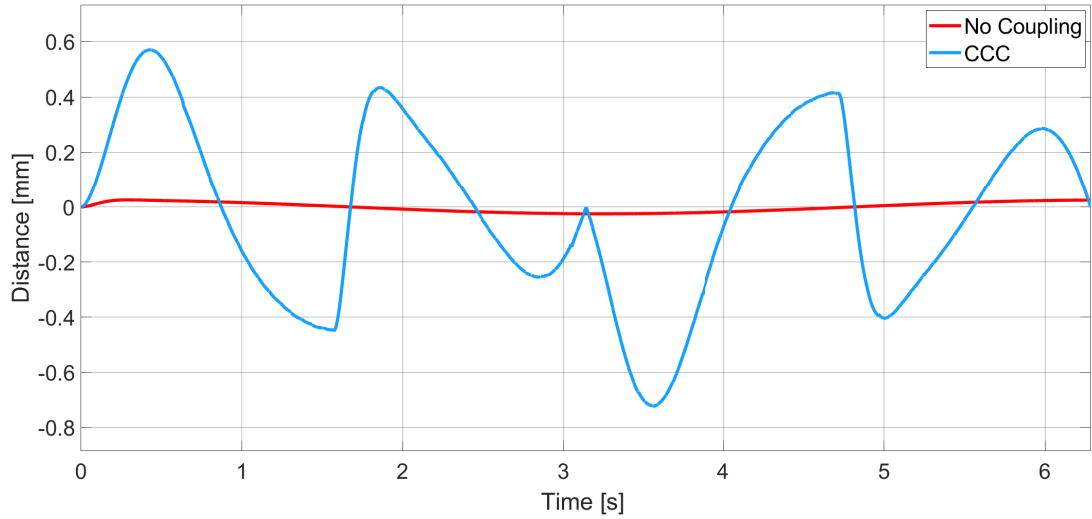
Figure 3.15: Drawing Ellipse under Friction - Error of Y-Axis.

Error of Y-Axis is decreased. CCC increased Y-Axis error to compensate the synchronization error. Error in Y-axis is increased significantly which can be seen in Fig 3.15.

Table 3.5: Drawing Ellipse under Friction without Coupling.

Time	X Command	X Error	Y Command	Y Error	Syn. Error
0,000	0,000	0,000	-5,000	0,000	0,000
$\pi/8$	3,830	1,045	-4,643	0,025	-3,887
$\pi/4$	7,068	0,989	-3,556	0,019	-6,919
$3\pi/8$	9,238	0,664	-1,926	0,012	-6,112
$\pi/2$	10,000	0,222	-0,001	0,002	-2,172
$5\pi/8$	9,241	-0,255	1,918	-0,007	2,347
$3\pi/4$	7,072	-0,695	3,551	-0,016	4,862
$7\pi/8$	3,826	-1,029	4,642	-0,022	3,838
π	-0,004	-1,206	5,025	-0,025	-0,114
$9\pi/8$	-3,824	-1,199	4,644	-0,024	4,479
$5\pi/4$	-7,071	-1,010	3,555	-0,019	7,075
$11\pi/8$	-9,240	-0,667	1,924	-0,012	6,138
$3\pi/2$	-10,000	-0,223	0,004	-0,003	2,268
$13\pi/8$	-9,239	0,256	-1,920	0,007	-2,350
$7\pi/4$	-7,070	0,696	-3,552	0,016	-4,862
$15\pi/8$	-3,831	1,029	-4,640	0,022	-3,838
2π	0,000	1,206	-5,025	0,025	0,130

Quite high error in X-Axis and relatively low error in Y-Axis can be seen in Table 3.5. Because of the un-coordinated motion high synchronization error is occurred.

Table 3.6: Drawing Ellipse under Friction with Coupling.

Time	X Command	X Error	Y Command	Y Error	Syn. Error
0,000	0,000	0,000	-5,000	0,000	0,000
π**/8**	3,833	0,680	-5,182	0,563	-0,001
π**/4**	7,073	0,066	-3,665	0,131	-0,001
3π**/8**	9,240	-0,064	-1,600	-0,313	-0,002
π**/2**	10,000	0,005	0,448	-0,447	-0,002
5π**/8**	9,237	0,079	1,536	0,379	-0,002
3π**/4**	7,069	0,040	3,456	0,080	-0,001
7π**/8**	3,817	-0,282	4,855	-0,233	-0,001
π	-0,004	-0,833	5,001	-0,001	0,000
9π**/8**	-3,828	-0,867	5,338	-0,719	0,000
5π**/4**	-7,077	-0,100	3,733	-0,201	0,001
11π**/8**	-9,242	0,058	1,631	0,278	0,002
3π**/2**	-10,000	0,005	-0,421	0,419	0,002
13π**/8**	-9,237	-0,072	-1,564	-0,351	0,002
7π**/4**	-7,064	-0,023	-3,494	-0,045	0,001
15π**/8**	-3,827	0,320	-4,884	0,265	0,001
2π	0,000	0,903	-4,999	-0,001	0,000

High performance is obtained when drawing ellipse with CCC. And it can be seen in comparison of Table 3.5 and Table 3.6. Almost zero synchronization error is achieved.

3.1.4 Drawing Parabola under Friction

Block diagram of the simulation structure is given in Figure 3.16. Friction is only applied to the X-Axis and CCC is P type with magnitude of 1000.
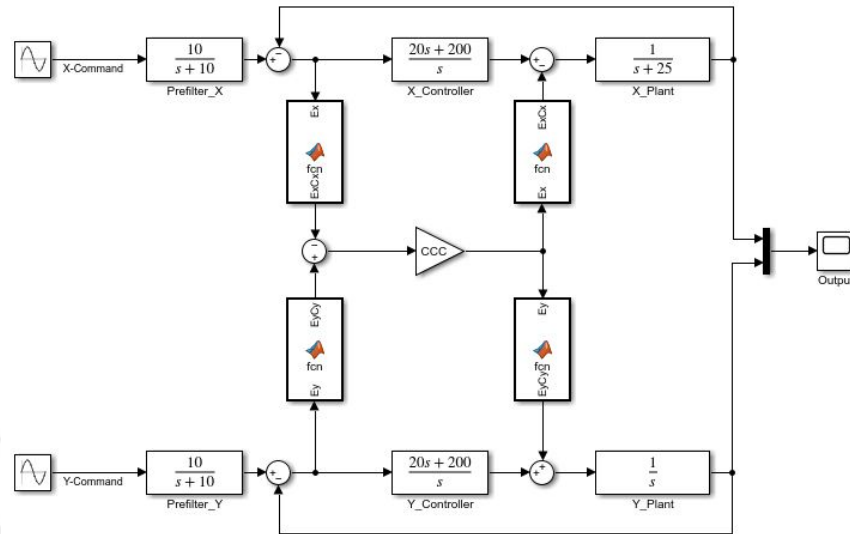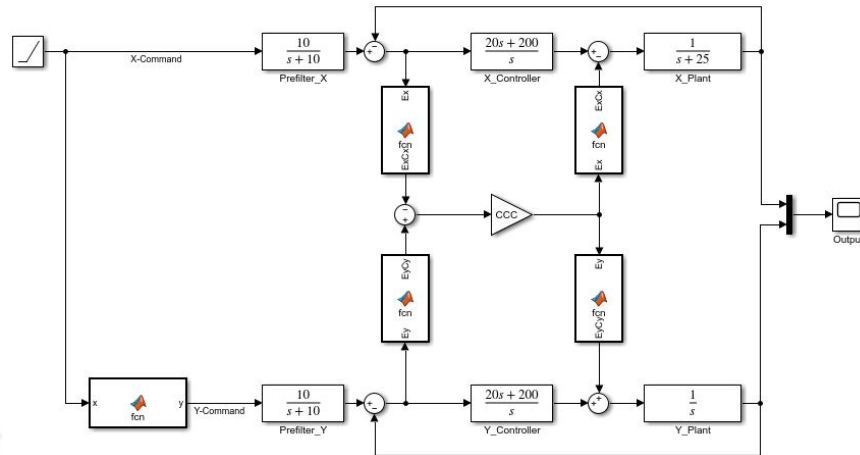

Figure 3.16: Block Diagram of Parabola Drawing under Friction.

Comparison of the reference parabola and simulation results are given in Figure 3.17 and Figure 3.18.
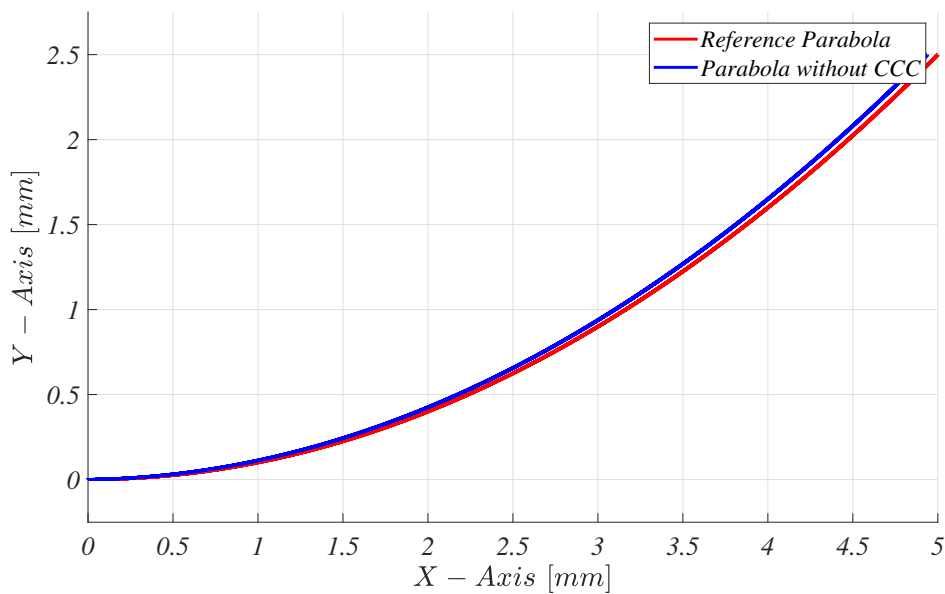
Figure 3.17: Drawing Parabola under Friction without CCC.

Effect of friction can be seen in Figure 3.17. Error is increased with time.
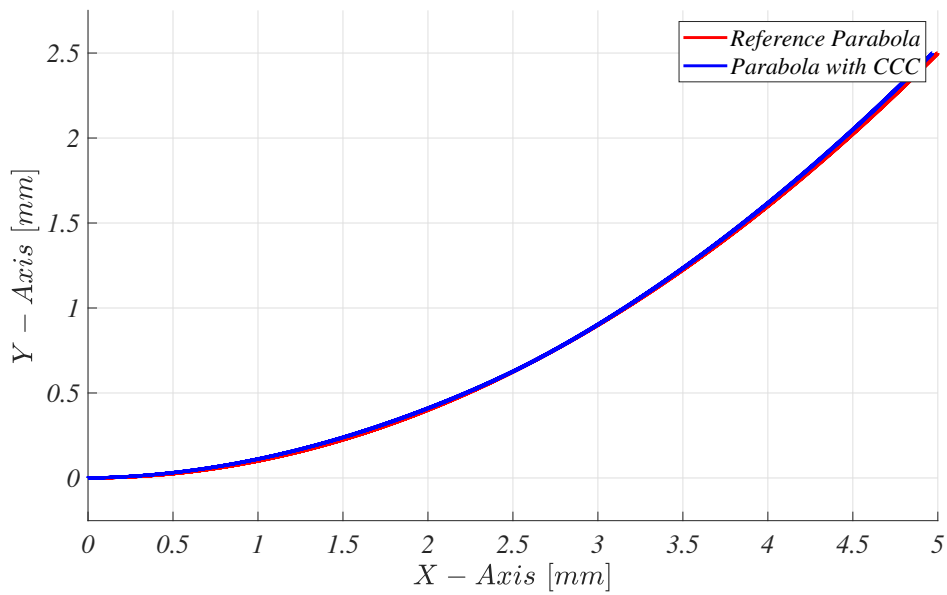
Figure 3.18: Drawing Parabola under Friction with CCC.

Despite of the high friction, satisfactory contour error compensation is obtained. Duration of this simulation is 5 seconds.
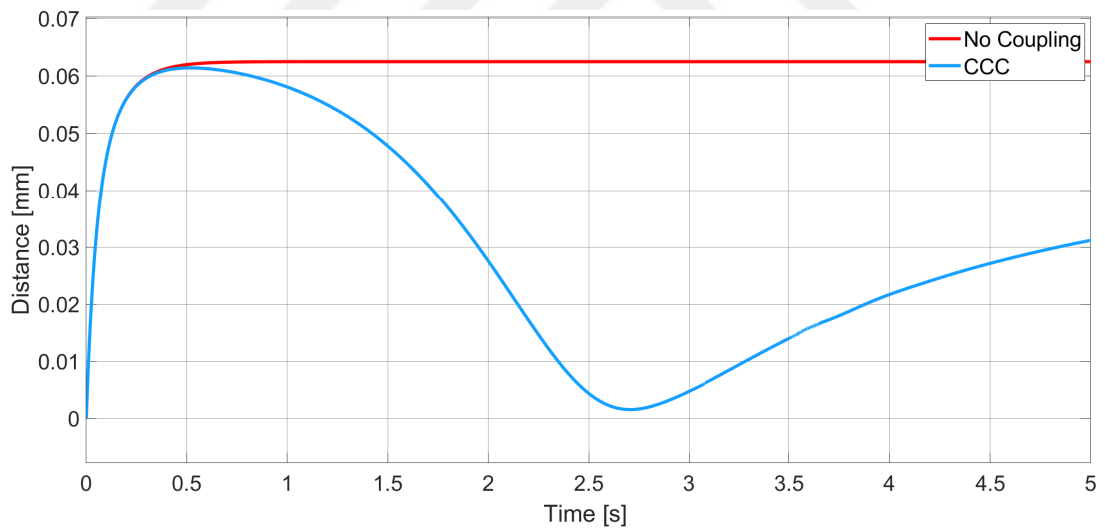
Figure 3.19: Drawing Parabola under Friction - Error of X-Axis.

In X-Axis, constant error is occurred without coupling because of the friction. But in CCC structure, much smaller error is occurred which can be seen in Figure 3.19. But increasing error tendency is also obvious which indicate decreasing synchronization performance.
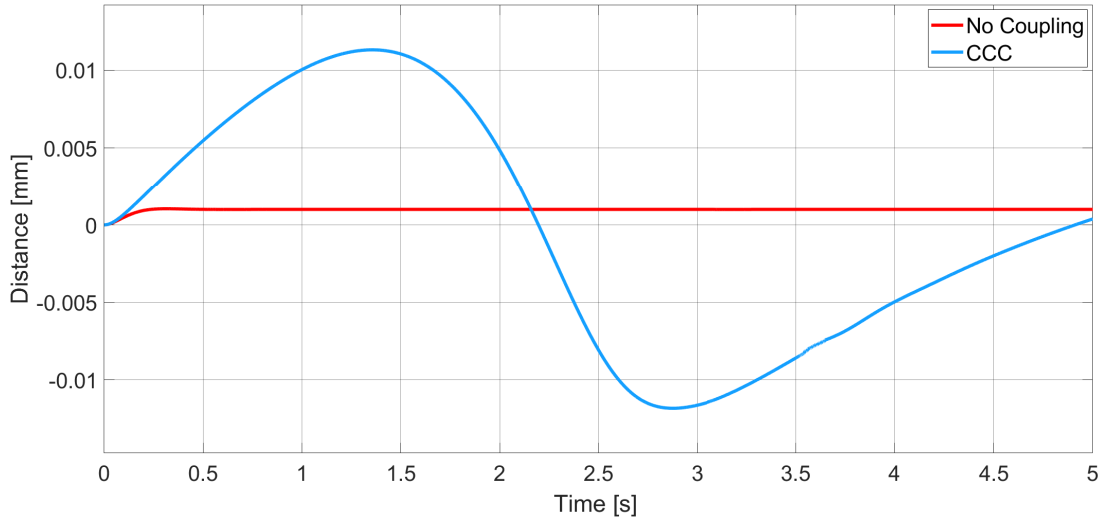
Figure 3.20: Drawing Parabola under Friction - Error of Y-Axis.

In Y-Axis, error is deviated according to contour error which can be seen in Figure 3.20.

Table 3.7: Drawing Parabola under Friction without Coupling.

Time	X Command	X Error	Y Command	Y Error	Syn. Error
0,000	0,000	0,000	0,000	0,000	0,000
0,250	0,250	0,058	0,005	0,001	-0,002
0,500	0,500	0,062	0,024	0,001	-0,005
0,750	0,750	0,062	0,055	0,001	-0,008
1,000	1,000	0,062	0,099	0,001	-0,011
1,250	1,250	0,062	0,155	0,001	-0,014
1,500	1,500	0,062	0,224	0,001	-0,017
1,750	1,750	0,062	0,305	0,001	-0,019
2,000	2,000	0,062	0,399	0,001	-0,022
2,250	2,250	0,062	0,505	0,001	-0,024
2,500	2,500	0,062	0,624	0,001	-0,027
2,750	2,750	0,062	0,755	0,001	-0,029
3,000	3,000	0,062	0,899	0,001	-0,031
3,250	3,250	0,062	1,055	0,001	-0,033
3,500	3,500	0,062	1,224	0,001	-0,035
3,750	3,750	0,062	1,405	0,001	-0,036
4,000	4,000	0,062	1,599	0,001	-0,038
4,250	4,250	0,063	1,805	0,001	-0,040
4,500	4,500	0,063	2,024	0,001	-0,041
4,750	4,750	0,063	2,255	0,001	-0,042
5,000	5,000	0,063	2,499	0,001	-0,043

In X-axis, steady error is observed due to friction. In Y-axis minimum error is occurred. In parabolic trajectory synchronization error is increased continuously as

time passed.

Time	X Command	X Error	Y Command	Y Error	Syn. Error
	Table 3.8: Drawing Parabola under Friction with Coupling.				
0,000	0,000	0,000	0,000	0,000	0,000
0,251	0,251	0,058	0,004	0,003	0,000
0,501	0,501	0,061	0,020	0,005	0,000
0,751	0,751	0,061	0,048	0,008	-0,001
1,001	1,001	0,058	0,090	0,010	-0,001
1,251	1,251	0,054	0,145	0,011	-0,002
1,501	1,501	0,048	0,214	0,011	-0,003
1,751	1,751	0,039	0,297	0,009	-0,004
2,001	2,001	0,028	0,395	0,005	-0,006
2,251	2,251	0,015	0,508	-0,002	-0,007
2,501	2,501	0,004	0,633	-0,008	-0,009
2,751	2,751	0,002	0,768	-0,012	-0,011
3,001	3,001	0,005	0,912	-0,012	-0,012
3,251	3,251	0,009	1,067	-0,010	-0,014
3,501	3,501	0,014	1,234	-0,009	-0,015
3,751	3,751	0,018	1,414	-0,007	-0,016
4,001	4,001	0,022	1,606	-0,005	-0,017
4,251	4,251	0,025	1,810	-0,003	-0,019
4,501	4,501	0,027	2,028	-0,002	-0,020
4,751	4,751	0,029	2,258	-0,001	-0,021
5,000	5,000	0,031	2,500	0,000	-0,022

CCC decreases contour error under friction. But compared to linear, circular and elliptic contours, the least successful performance is occurred with parabolic contour. Since command value is increased, effectivity of proposed structure is decreased.

3.2   CCC STRUCTURE UNDER INNER DISTURBANCE

Inner disturbance is only applied to X-Axis and it is a sin wave.

$$d_i = A \sin(t) \tag{III.2}$$

3.2.1   Drawing Line under Inner Disturbance

Block diagram of the simulation structure is given in Figure 3.21. Inner disturbance is only applied to the X-Axis and CCC is P type with magnitude of 10000.
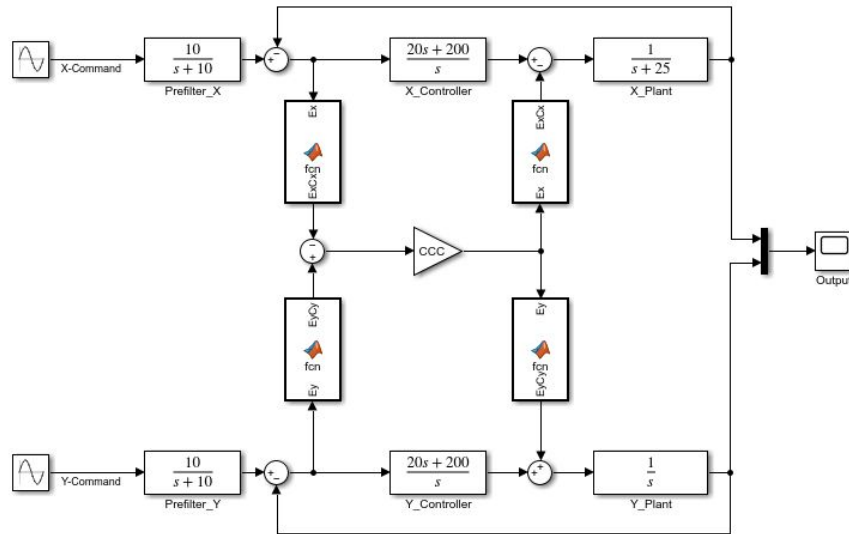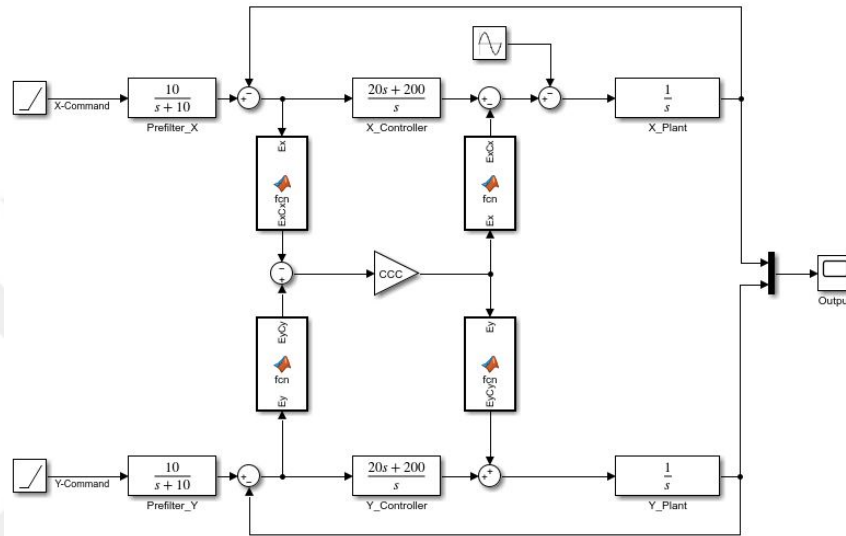

Figure 3.21: Block Diagram of Line Drawing under Inner Disturbance.

Comparison of the reference line and simulation results are given in Figure 3.22 and Figure 3.23.
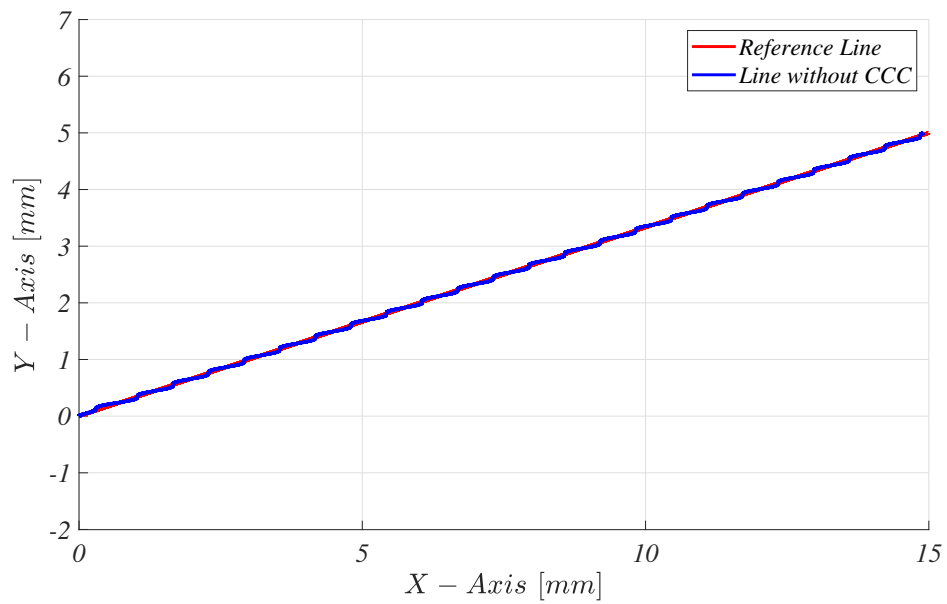
Figure 3.22: Drawing Line under Inner Disturbance without CCC.

Effect of inner disturbance can be seen in Figure 3.22. Duration of this simulation is 5 seconds.
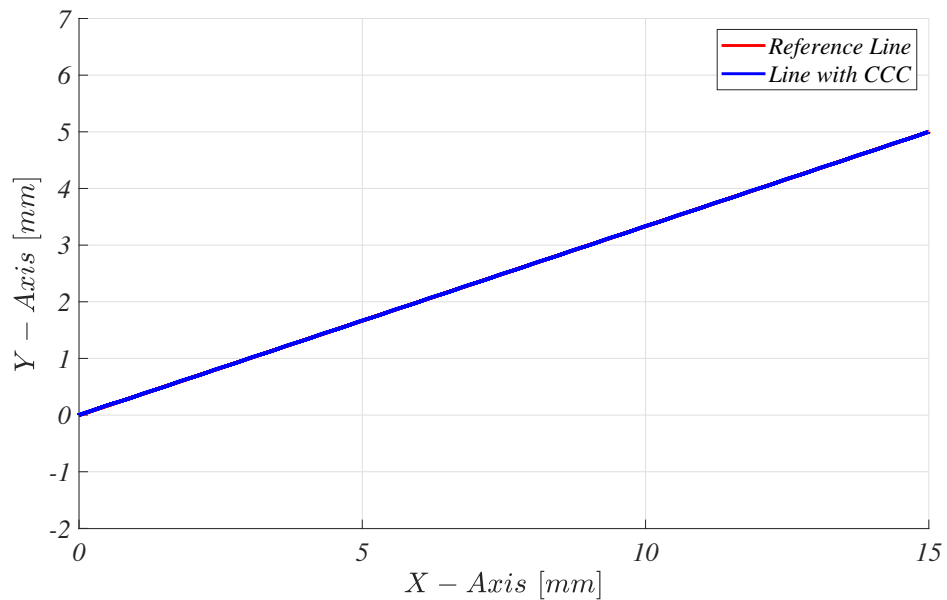
Figure 3.23: Drawing Line under Inner Disturbance with CCC.

Excellent performance is obtained for linear trajectory under inner disturbance. Almost zero synchronization error obtained in spite of unrealistically high disturbance.
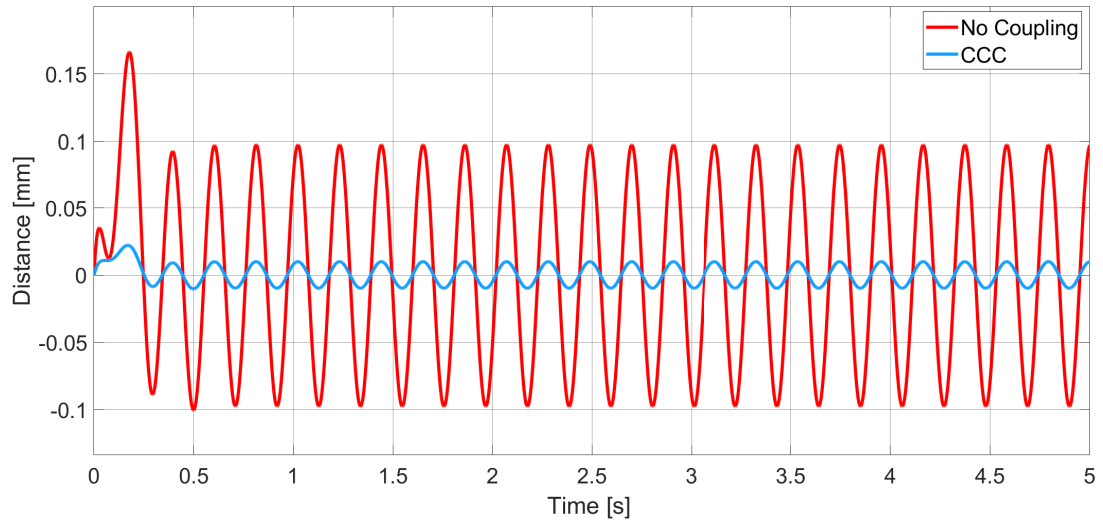
Figure 3.24: Drawing Line under Inner Disturbance - Error of X-Axis.

Due to the inner disturbance, oscillating error is observed in X and Y-Axis. But error of X-Axis is much smaller with CCC compared to no-coupling version which can be seen in Figure 3.24.
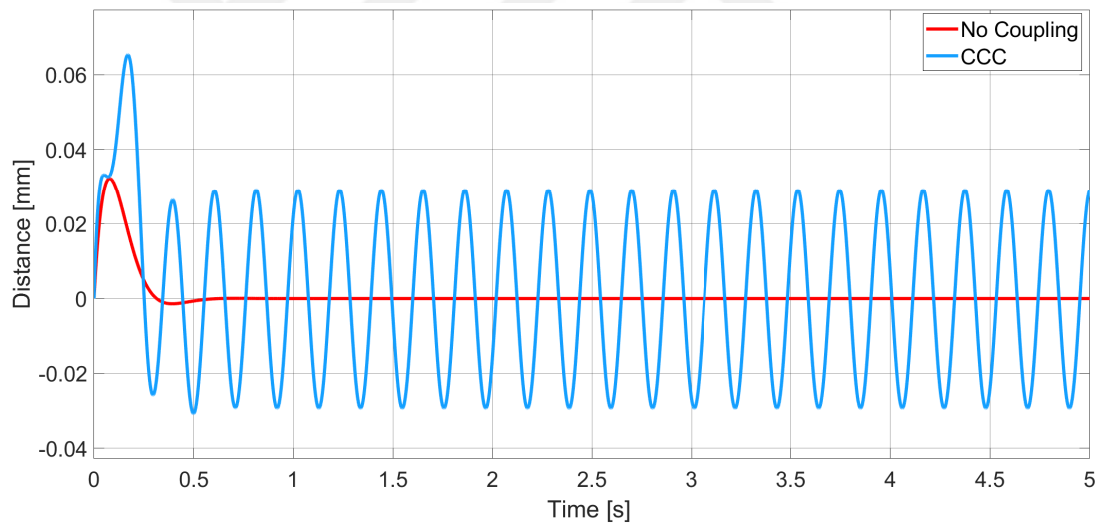
Figure 3.25: Drawing Line under Inner Disturbance - Error of Y-Axis.

In Y-Axis, error is converted to oscillating error after CCC's compensation. But magnitude of Y-Axis' error with CCC is smaller than no-coupling X-Axis error which is obvious in Figure 3.25.

Table 3.9: Drawing Line under Inner Disturbance without Coupling.

Time	X Command	X Error	Y Command	Y Error	Syn. Error
0,000	0,000	0,000	0,000	0,000	0,000
0,250	0,750	-0,009	0,245	0,005	0,010
0,500	1,500	-0,100	0,501	-0,001	0,095
0,750	2,250	-0,034	0,750	0,000	0,032
1,000	3,000	0,074	1,000	0,000	-0,070
1,250	3,750	0,085	1,250	0,000	-0,081
1,500	4,500	-0,015	1,500	0,000	0,014
1,750	5,250	-0,096	1,750	0,000	0,091
2,000	6,000	-0,051	2,000	0,000	0,049
2,250	6,750	0,060	2,250	0,000	-0,057
2,500	7,500	0,093	2,500	0,000	-0,088
2,750	8,250	0,004	2,750	0,000	-0,004
3,000	9,000	-0,090	3,000	0,000	0,085
3,250	9,750	-0,067	3,250	0,000	0,063
3,500	10,500	0,044	3,500	0,000	-0,042
3,750	11,250	0,097	3,750	0,000	-0,092
4,000	12,000	0,023	4,000	0,000	-0,022
4,250	12,750	-0,081	4,250	0,000	0,077
4,500	13,500	-0,079	4,500	0,000	0,075
4,750	14,250	0,026	4,750	0,000	-0,024
5,000	15,000	0,097	5,000	0,000	-0,092

Due to inner disturbance, error in X-Axis is observed. But in Y-axis no error is ocurred. Un-coordinated motion caused synchronization error which can be seen in table 3.9.

Table 3.10: Drawing Line under Inner Disturbance with Coupling.

Time	X Command	X Error	Y Command	Y Error	Syn. Error
0,000	0,000	0,000	0,000	0,000	0,000
0,251	0,752	0,000	0,250	0,001	0,000
0,501	1,502	-0,010	0,531	-0,031	0,000
0,751	2,252	-0,003	0,760	-0,010	0,000
1,001	3,002	0,008	0,978	0,022	-0,001
1,251	3,752	0,009	1,226	0,025	0,000
1,501	4,502	-0,002	1,506	-0,005	0,000
1,751	5,252	-0,010	1,780	-0,029	0,000
2,001	6,002	-0,005	2,016	-0,015	0,000
2,251	6,752	0,007	2,232	0,018	-0,001
2,501	7,502	0,010	2,473	0,028	0,000
2,751	8,252	0,000	2,750	0,001	0,000
3,001	9,002	-0,009	3,028	-0,027	0,000
3,251	9,752	-0,006	3,270	-0,020	0,000
3,501	10,502	0,005	3,487	0,014	-0,001
3,751	11,252	0,010	3,722	0,029	0,000
4,001	12,002	0,002	3,994	0,006	0,000
4,251	12,752	-0,008	4,275	-0,025	0,000
4,501	13,502	-0,008	4,524	-0,024	0,000
4,751	14,252	0,003	4,743	0,008	0,000
5,000	15,000	0,010	4,971	0,029	0,000

Good results are obtained for linear trajectory with inner disturbance. In spite of the extremely high inner disturbance, almost zero synchronization error is achieved.

3.2.2 Drawing Circle under Inner Disturbance

Block diagram of the simulation structure is given in Figure 3.26. Inner disturbance is only applied to the X-Axis and CCC is P type with magnitude of 10000.
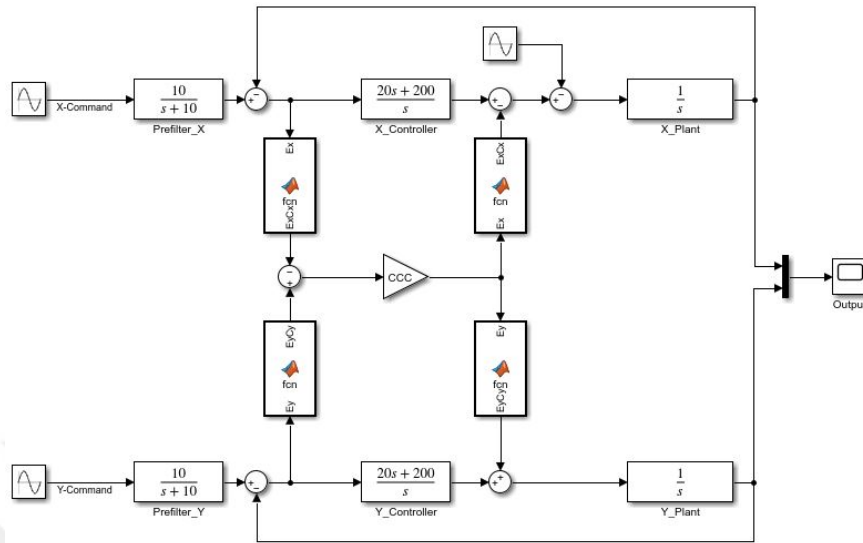
Figure 3.26: Block Diagram of Circle Drawing under Inner Disturbance.

Comparison of the reference circle and simulation results are given in Figure 3.27 and Figure 3.28.
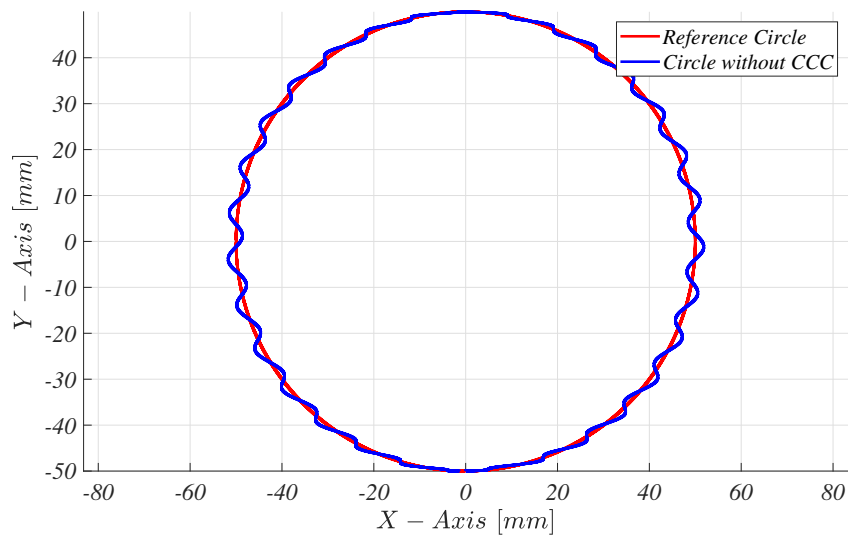
Figure 3.27: Drawing Circle under Inner Disturbance without CCC.

Inner disturbance deteriorate circular trajectory which can be seen in Figure 3.27. Duration of this simulation is 2π seconds.
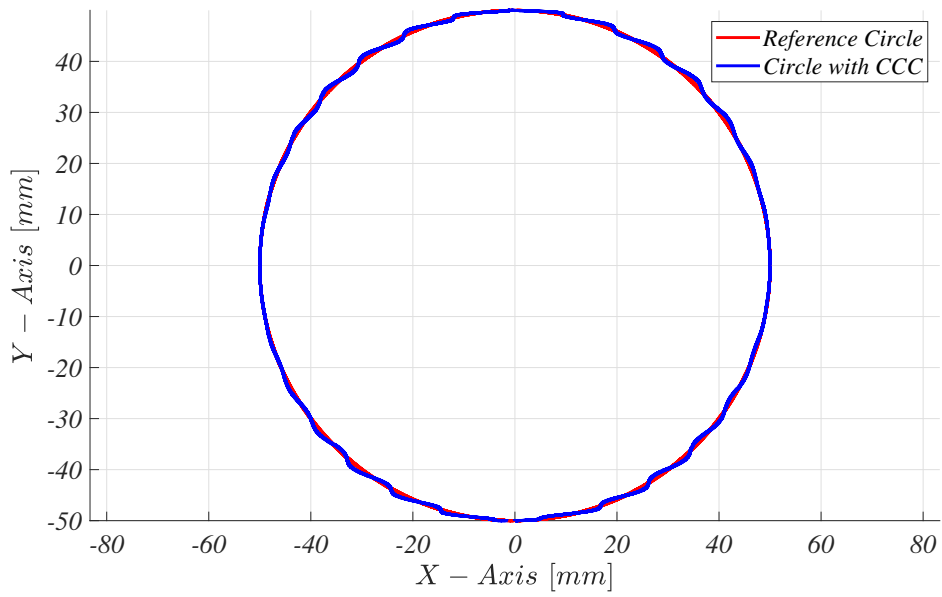
Figure 3.28: Drawing Circle under Inner Disturbance with CCC.

CCC compensation can be seen in Figure 3.30 clearly. Despite of the extreme inner disturbance, much circular contour is obtained compared to no-coupling version.
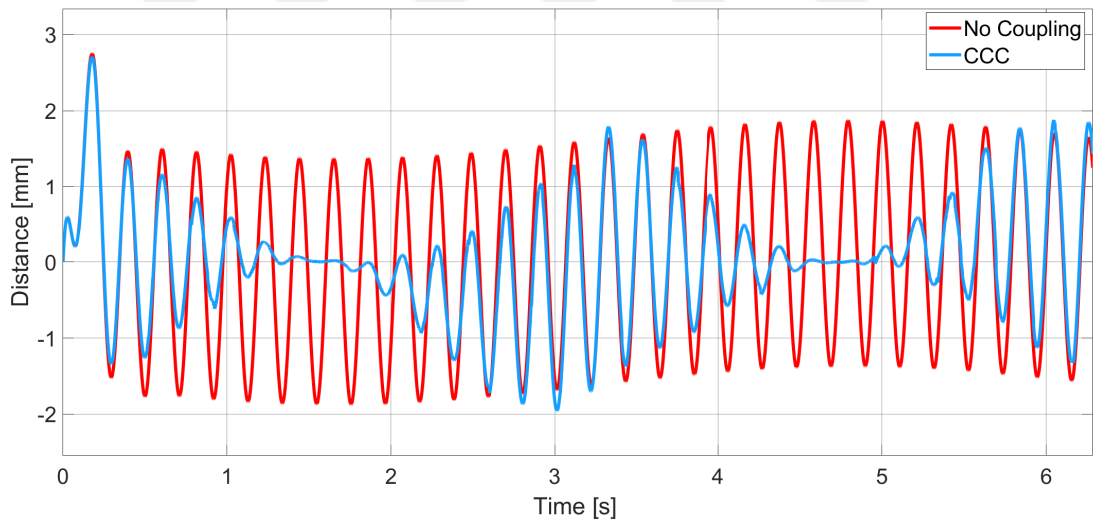
Figure 3.29: Drawing Circle under Inner Disturbance - Error of X-Axis.

X-Axis' error is decreased significantly which can be seen in Figure 3.30.
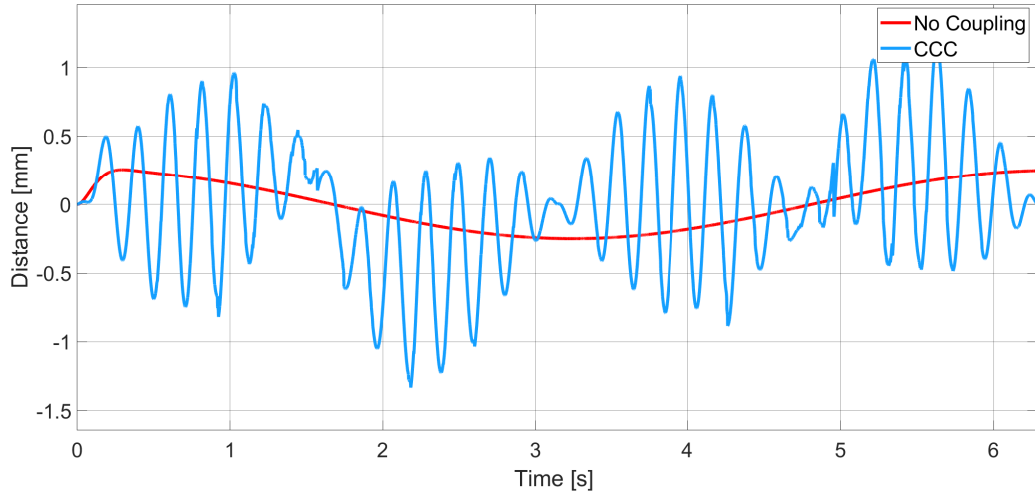
Figure 3.30: Drawing Circle under Inner Disturbance - Error of Y-Axis.

Error of Y-Axis is in Figure 3.30. Magnitude of Y-Axis error with CCC is smaller than no-coupling X-Axis error.

Table 3.11: Drawing Circle under Inner Disturbance without Coupling.

Time	X Command	X Error	Y Command	Y Error	Syn. Error
0,000	0,000	0,000	-50,000	0,000	0,000
$\pi/8$	19,148	1,472	-46,435	0,246	-16,784
$\pi/4$	35,341	0,889	-35,563	0,194	-24,550
$3\pi/8$	46,192	-0,350	-19,257	0,118	18,423
$\pi/2$	50,000	-1,478	-0,015	0,025	73,900
$5\pi/8$	46,203	-1,860	19,183	-0,072	84,577
$3\pi/4$	35,362	-1,245	35,507	-0,158	38,457
$7\pi/8$	19,129	0,001	46,416	-0,220	-10,200
π	-0,020	1,197	50,249	-0,249	-12,447
$9\pi/8$	-19,121	1,693	46,439	-0,239	-43,403
$5\pi/4$	-35,356	1,217	35,549	-0,194	-49,869
$11\pi/8$	-46,200	0,111	19,238	-0,118	-7,369
$3\pi/2$	-50,000	-0,999	0,045	-0,025	49,951
$13\pi/8$	-46,196	-1,382	-19,202	0,072	65,262
$7\pi/4$	-35,348	-0,873	-35,521	0,158	36,468
$15\pi/8$	-19,157	0,267	-46,405	0,220	5,059
2π	0,000	1,260	-50,249	0,249	12,454

Inner disturbance is disrupted circular contour significantly. Serious synchronization error can be seen in Table 3.11.

49

Table 3.12: Drawing Circle under Inner Disturbance with Coupling.

Time	X Command	X Error	Y Command	Y Error	Syn. Error
0,000	0,000	0,000	-50,000	0,000	0,000
$\pi/8$	19,186	1,353	-46,734	0,562	0,000
$\pi/4$	35,366	0,637	-35,982	0,637	0,000
$3\pi/8$	46,194	0,063	-19,287	0,153	0,000
$\pi/2$	50,000	0,000	-0,226	0,239	0,000
$5\pi/8$	46,200	-0,436	20,173	-1,054	0,000
$3\pi/4$	35,356	-1,052	36,408	-1,053	-0,001
$7\pi/8$	19,124	-0,480	46,397	-0,199	0,000
π	-0,054	0,836	49,999	0,001	0,000
$9\pi/8$	-19,123	1,625	45,527	0,672	0,000
$5\pi/4$	-35,366	0,602	34,743	0,602	0,000
$11\pi/8$	-46,201	-0,034	19,200	-0,083	0,000
$3\pi/2$	-50,000	0,000	0,199	-0,185	0,000
$13\pi/8$	-46,194	-0,079	-18,942	-0,191	0,000
$7\pi/4$	-35,318	-0,229	-35,163	-0,229	0,000
$15\pi/8$	-19,141	0,386	-46,352	0,160	0,003
2π	0,000	1,383	-50,000	0,000	0,000

CCC is compensated synchronization error and almost zero contour error is achieved which is obvious in Table 3.12.

3.2.3 Drawing Ellipse under Inner Disturbance

Block diagram of the simulation structure is given in Figure 3.31.Inner disturbance is only applied to the X-Axis and CCC is P type with magnitude of 10000.
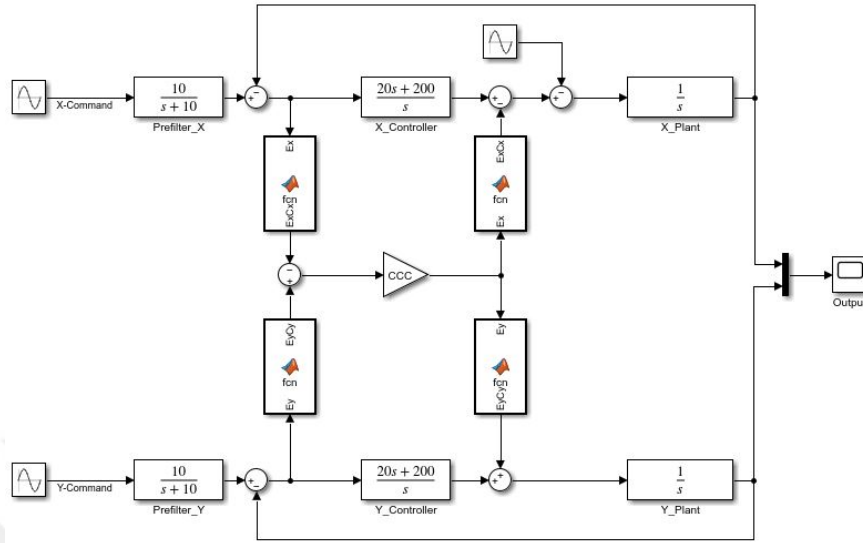
Figure 3.31: Block Diagram of Ellipse Drawing under Inner Disturbance.

Comparison of the reference ellipse and simulation results are given in Figure 3.32 and Figure 3.33.
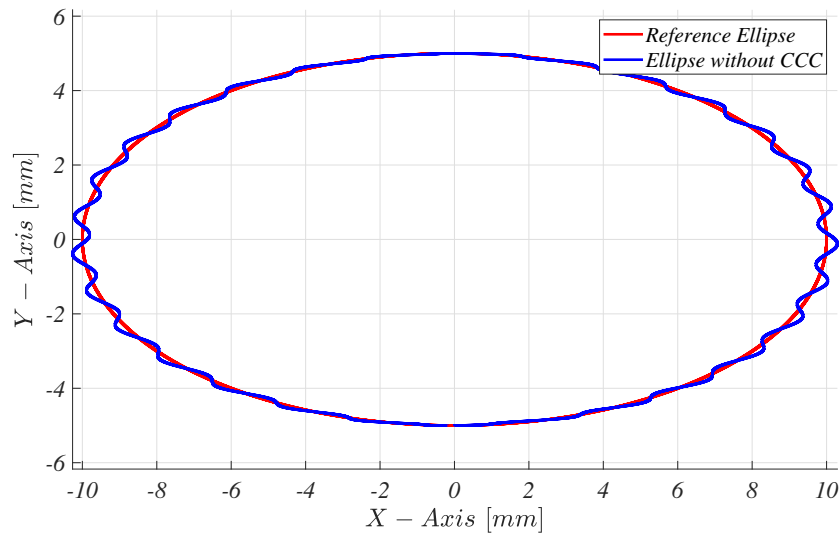
Figure 3.32: Drawing Ellipse under Inner Disturbance without CCC.

Without CCC at $\pi/2$ and $3\pi/2$, less contour error is occurred compared to π and 2π.

51
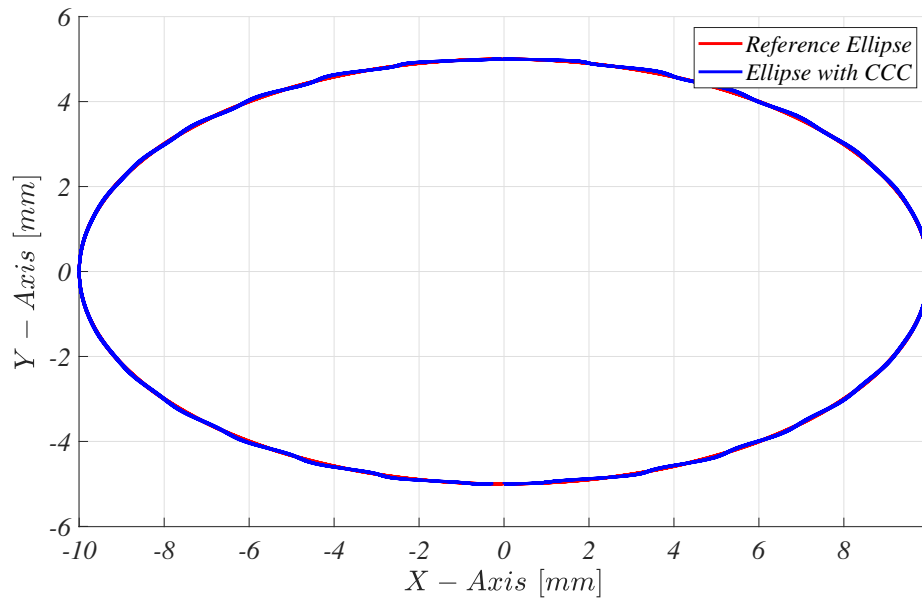
Figure 3.33: Drawing Ellipse under Inner Disturbance with CCC.

After CCC compensation, almost no contour error is achieved even at $\pi/2$ and $3\pi/2$. Duration of this simulation is 2π seconds.
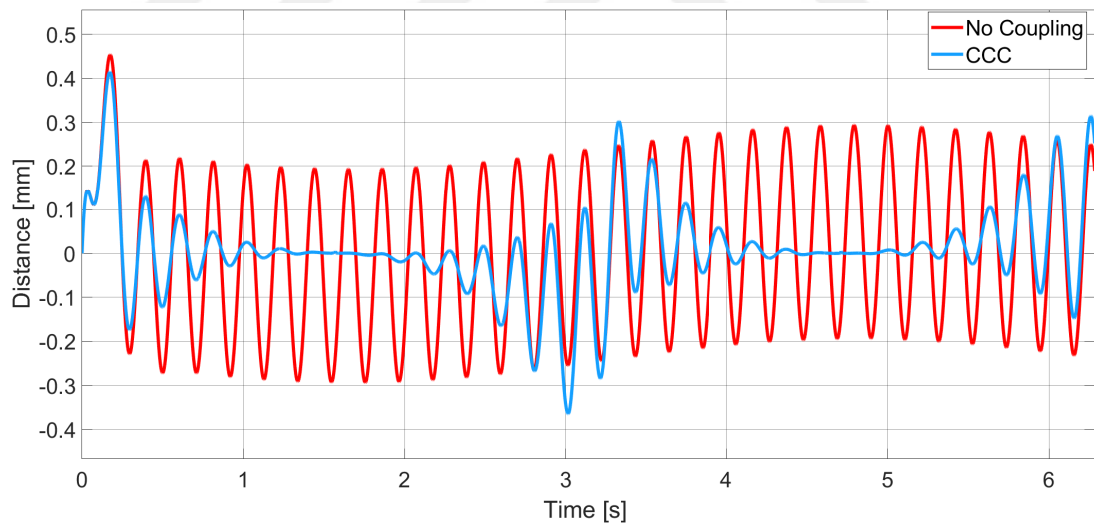
Figure 3.34: Drawing Ellipse under Inner Disturbance - Error of X-Axis.

Error of X-Axis is reduced greatly compared to no-coupling version which can be seen in Figure 3.34.
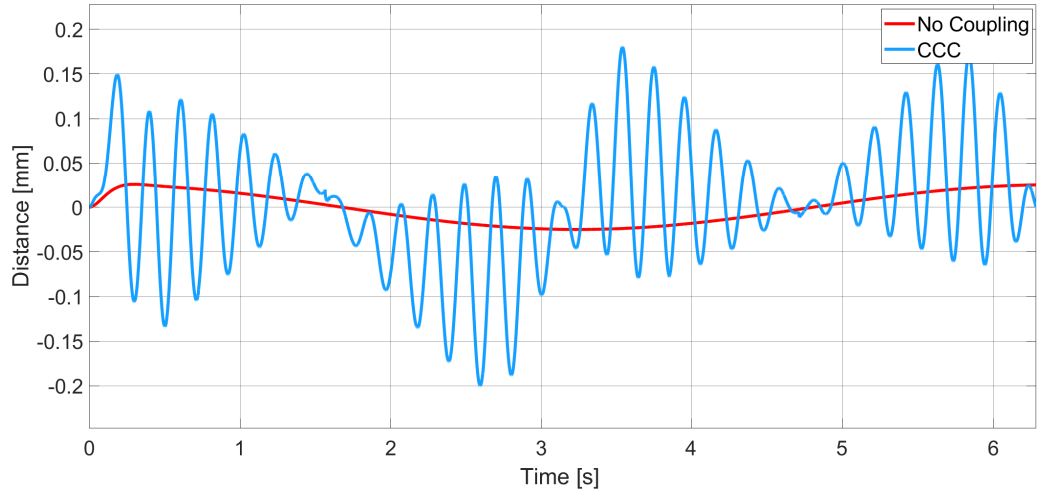
Figure 3.35: Drawing Ellipse under Inner Disturbance - Error of Y-Axis.

In Y-Axis' error, there are sinusoidal elements. CCC's output is the reason of these elements.

Table 3.13: Drawing Ellipse under Inner Disturbance without Coupling.

Time	X Command	X Error	Y Command	Y Error	Syn. Error
0,000	0,000	0,000	-5,000	0,000	0,000
$\pi/8$	3,830	0,214	-4,643	0,025	-0,705
$\pi/4$	7,068	0,125	-3,556	0,019	-0,818
$3\pi/8$	9,238	-0,063	-1,926	0,012	0,609
$\pi/2$	10,000	-0,234	-0,001	0,002	2,387
$5\pi/8$	9,241	-0,291	1,918	-0,007	2,674
$3\pi/4$	7,072	-0,196	3,551	-0,016	1,334
$7\pi/8$	3,826	-0,006	4,642	-0,022	-0,080
π	-0,004	0,178	5,025	-0,025	-0,125
$9\pi/8$	-3,824	0,258	4,644	-0,024	-1,095
$5\pi/4$	-7,071	0,191	3,555	-0,019	-1,416
$11\pi/8$	-9,240	0,028	1,924	-0,012	-0,278
$3\pi/2$	-10,000	-0,137	0,004	-0,003	1,412
$13\pi/8$	-9,239	-0,195	-1,920	0,007	1,819
$7\pi/4$	-7,070	-0,121	-3,552	0,016	0,913
$15\pi/8$	-3,831	0,046	-4,640	0,022	-0,074
2π	0,000	0,190	-5,025	0,025	0,125

Inner disturbance is deteriorated the trajectory. Maximum error in X-Axis is -0.291 and in Y-Axis 0,025 is observed.

Table 3.14: Drawing Ellipse under Inner Disturbance with Coupling.

Time	X Command	X Error	Y Command	Y Error	Syn. Error
0,000	0,000	0,000	-5,000	0,000	0,000
$\pi/8$	3,833	0,130	-4,726	0,108	0,000
$\pi/4$	7,070	0,035	-3,607	0,071	0,000
$3\pi/8$	9,239	0,001	-1,919	0,007	0,000
$\pi/2$	10,000	0,005	-0,018	0,023	0,000
$5\pi/8$	9,237	-0,019	2,005	-0,090	0,000
$3\pi/4$	7,067	-0,071	3,679	-0,142	0,000
$7\pi/8$	3,818	-0,096	4,700	-0,079	0,000
π	-0,010	0,042	5,000	0,000	0,000
$9\pi/8$	-3,828	0,216	4,440	0,179	0,000
$5\pi/4$	-7,074	0,045	3,443	0,091	0,000
$11\pi/8$	-9,241	0,000	1,912	-0,001	0,000
$3\pi/2$	-10,000	0,001	0,002	0,000	0,000
$13\pi/8$	-9,238	-0,004	-1,893	-0,021	0,000
$7\pi/4$	-7,068	-0,008	-3,520	-0,017	0,000
$15\pi/8$	-3,822	0,065	-4,674	0,053	0,000
2π	0,000	0,254	-5,000	0,000	0,000

CCC have better performance in compensating synchronization error compared to circular contour. Magnitude of Y-Axis error with CCC is smaller than no-couupling X-Axis error.

3.2.4 Drawing Parabola under Inner Disturbance

Block diagram of the simulation structure is given in Figure 3.36. Inner disturbance is only applied to the X-Axis and CCC is P type with magnitude of 1000.
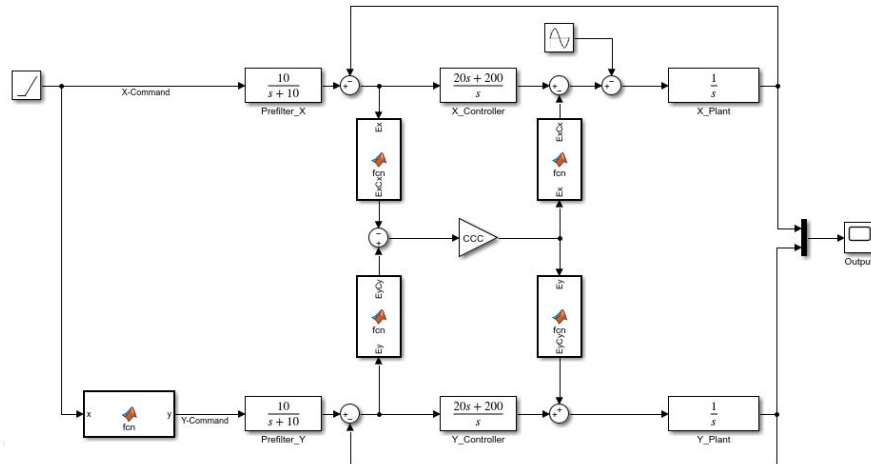
Figure 3.36: Block Diagram of Parabola Drawing under Inner Disturbance.

Comparison of the reference parabola and simulation results are given in Figure 3.37 and Figure 3.38.
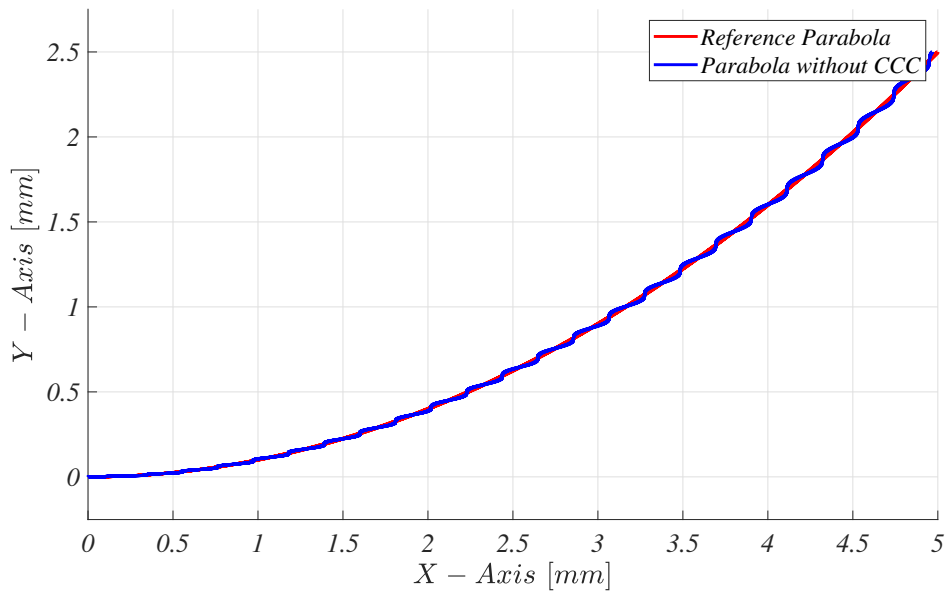

Figure 3.37: Drawing Parabola under Inner Disturbance without CCC.

Sinusoidal inner disturbance is deteorited the trajectory which can be seen in Figure 3.37.
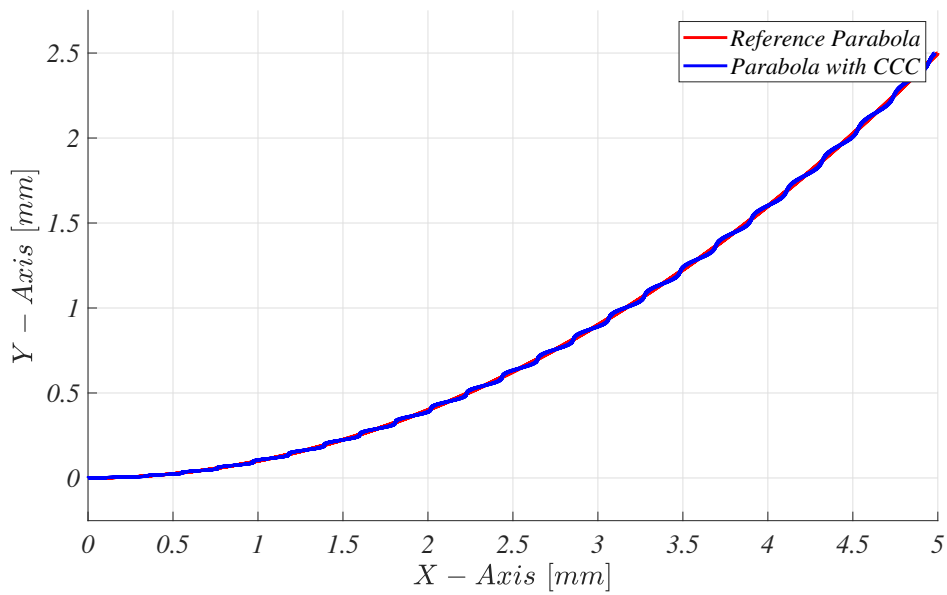
Figure 3.38: Drawing Parabola under Inner Disturbance with CCC.

Comparing Figure 3.37 and Figure 3.38 indicates that contour error is reduced with CCC structure. But still sinusoidal disturbance is visible at the last half of the simulation. Duration of this simulation is 5 seconds.
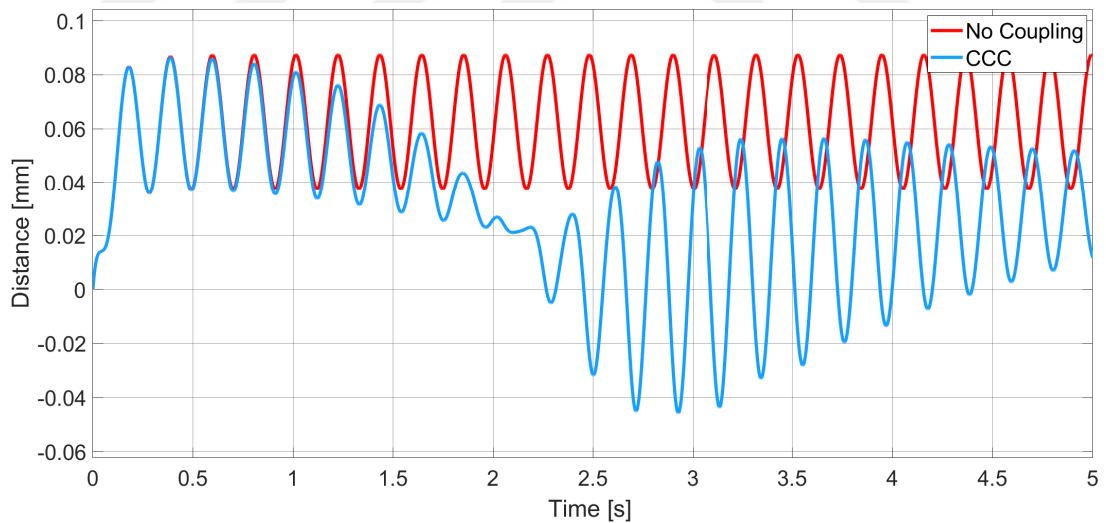
Figure 3.39: Drawing Parabola under Inner Disturbance - Error of X-Axis.

In Figure 3.39 error in X-Axis is visible. Magnitude of this error is between -0.05 and 0.08.
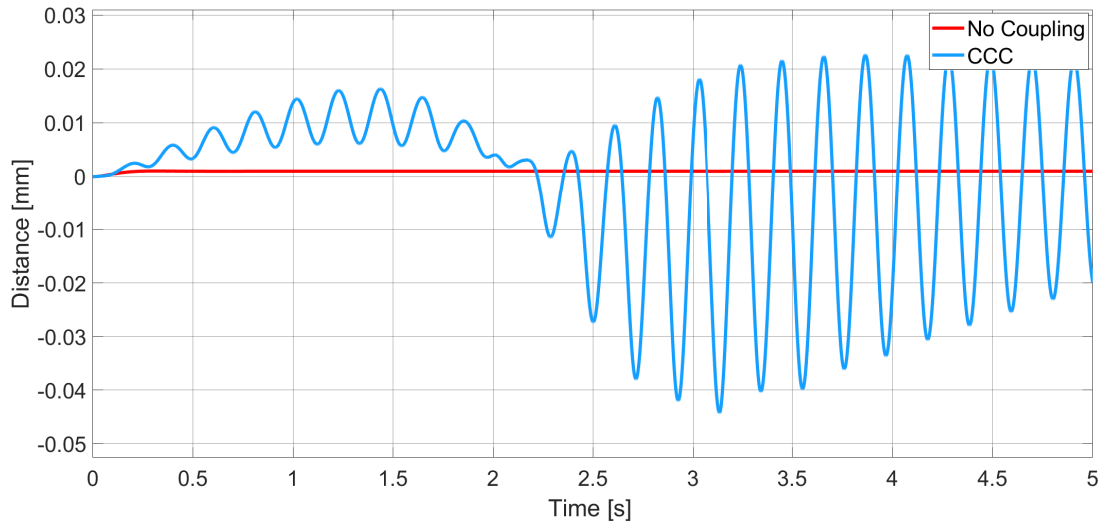
Figure 3.40: Drawing Parabola under Inner Disturbance - Error of Y-Axis.

In Y-Axis, sinusoidal error is occurred due to CCC compensation. Also magnitude of Y-Axis error with CCC is smaller than no-coupling X-Axis error.

Table 3.15: Drawing Parabola under Inner Disturbance without Coupling.

Time	X Command	X Error	Y Command	Y Error	Syn. Error
0,000	0,000	0,000	0,000	0,000	0,000
0,250	0,250	0,046	0,005	0,001	-0,001
0,500	0,500	0,038	0,024	0,001	-0,003
0,750	0,750	0,060	0,055	0,001	-0,008
1,000	1,000	0,085	0,099	0,001	-0,015
1,250	1,250	0,081	0,155	0,001	-0,018
1,500	1,500	0,053	0,224	0,001	-0,014
1,750	1,750	0,038	0,305	0,001	-0,011
2,000	2,000	0,055	0,399	0,001	-0,019
2,250	2,250	0,082	0,505	0,001	-0,032
2,500	2,500	0,084	0,624	0,001	-0,036
2,750	2,750	0,058	0,755	0,001	-0,027
3,000	3,000	0,038	0,899	0,001	-0,019
3,250	3,250	0,050	1,055	0,001	-0,026
3,500	3,500	0,079	1,224	0,001	-0,044
3,750	3,750	0,086	1,405	0,001	-0,050
4,000	4,000	0,063	1,599	0,001	-0,038
4,250	4,250	0,039	1,805	0,001	-0,024
4,500	4,500	0,046	2,024	0,001	-0,030
4,750	4,750	0,075	2,255	0,001	-0,050
5,000	5,000	0,087	2,499	0,001	-0,061

In the first half of the simulation, one third of the synchronization error is observed compared to no-coupling alternative. But in the last half of the simulation,

synchronization error is increased to the half of the initial contour error.

Table 3.16: Drawing Parabola under Inner Disturbance with Coupling.

Time	X Command	X Error	Y Command	Y Error	Syn. Error
0,000	0,000	0,000	0,000	0,000	0,000
0,251	0,251	0,046	0,004	0,002	0,000
0,501	0,501	0,038	0,022	0,003	0,000
0,751	0,751	0,058	0,049	0,008	-0,001
1,001	1,001	0,079	0,086	0,014	-0,001
1,251	1,251	0,070	0,141	0,015	-0,002
1,501	1,501	0,041	0,216	0,010	-0,003
1,751	1,751	0,026	0,302	0,005	-0,004
2,001	2,001	0,026	0,396	0,004	-0,006
2,251	2,251	0,007	0,512	-0,006	-0,008
2,501	2,501	-0,032	0,653	-0,027	-0,010
2,751	2,751	-0,019	0,779	-0,023	-0,010
3,001	3,001	0,034	0,893	0,007	-0,011
3,251	3,251	0,055	1,037	0,020	-0,013
3,501	3,501	0,016	1,233	-0,008	-0,016
3,751	3,751	-0,018	1,441	-0,035	-0,017
4,001	4,001	0,002	1,621	-0,021	-0,017
4,251	4,251	0,042	1,794	0,012	-0,018
4,501	4,501	0,052	2,005	0,021	-0,019
4,751	4,751	0,030	2,258	-0,001	-0,021
5,000	5,000	0,012	2,520	-0,020	-0,022

Although synchronization error is reduced compared to no-coupling structure, contour error is increased parallel to the X-Axis command value.

3.3   CCC STRUCTURE UNDER FRICTION AND INNER DISTURBANCE

Friction is only applied to X-Axis. Plant of X-Axis is:

$$P = \frac{1}{s + 25} \tag{III.3}$$

And inner disturbance is only applied to X-Axis and it is a sin wave.

$$d_i = A\,sin(t) \tag{III.4}$$

3.3.1   Drawing Line under Friction and Inner Disturbance

Block diagram of the simulation structure is given in Figure 3.41. Friction and inner disturbance is only applied to the X-Axis and CCC is P type with magnitude of 10000.

Figure 3.41: Block Diagram of Line Drawing under Friction and Inner Disturbance.

Comparison of the reference line and simulation results are given in Figure 3.42 and Figure 3.43.
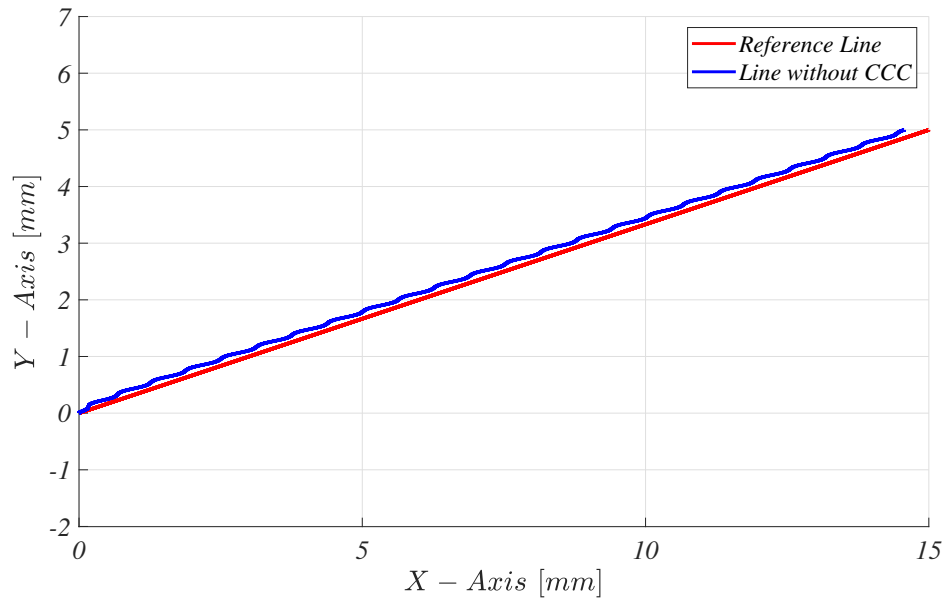
Figure 3.42: Drawing Line under Friction and Inner Disturbance without CCC.

Effects of friction and inner disturbance are obvious in Figure 3.42. In X-Axis slower and deteriorated motion is occurred. But in Y-Axis no error is observed.
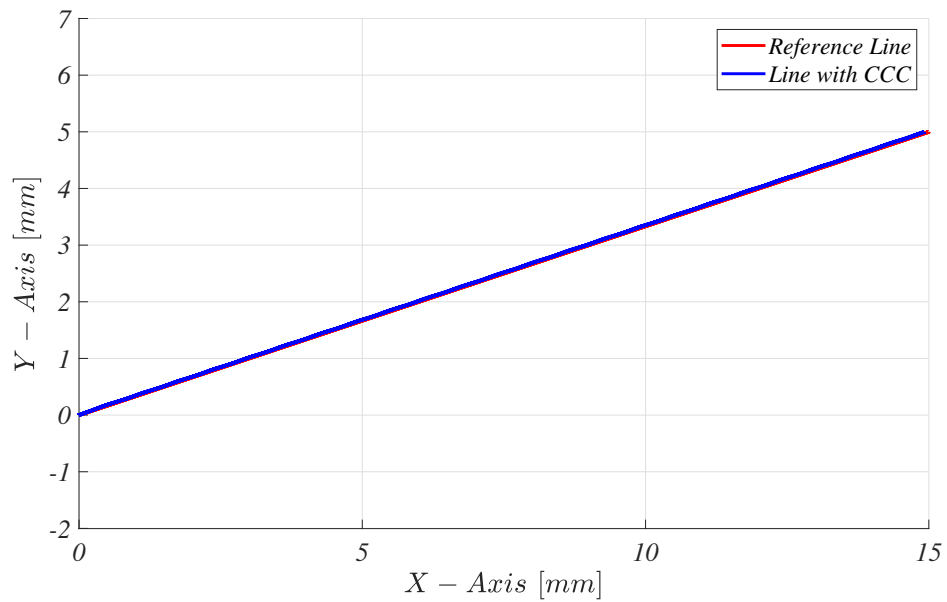
Figure 3.43: Drawing Line under Friction and Inner Disturbance with CCC.

Both friction and the inner disturbance are fully compensated by proposed CCC structure. Sinusoidal deviation from reference line and X-Axis' slower motion can be

seen in Figure 3.42. After application of CCC, reference linear trajectory is obtained. Duration of this simulation is 5 seconds.
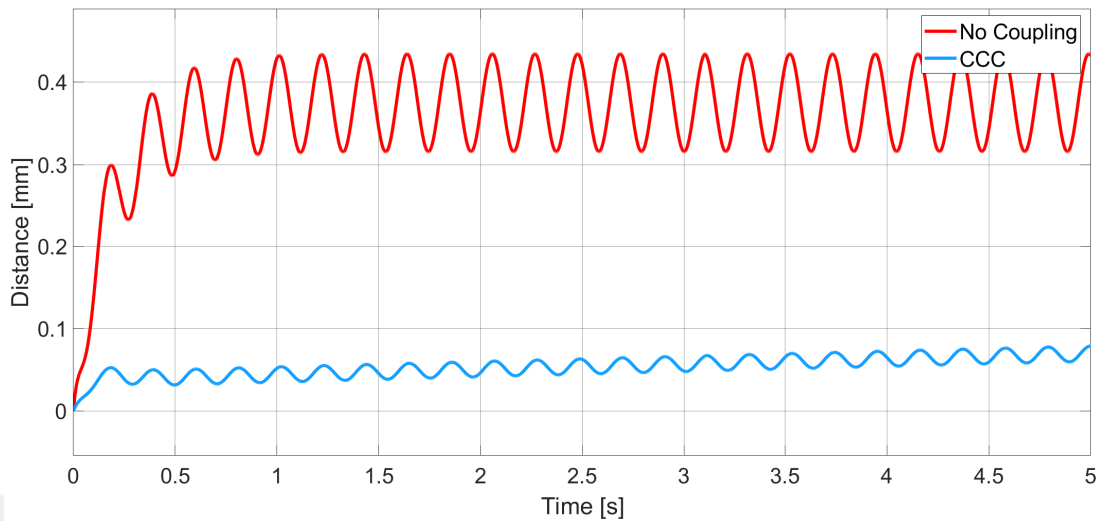
Figure 3.44: Drawing Line under Friction and Inner Disturbance - Error of X-Axis.

Due the friction and the inner disturbance high error in X-Axis is occurred which is obvious in Figure 3.44. But, this unwanted effects are neutralized with CCC and less error is occurred in X-Axis.
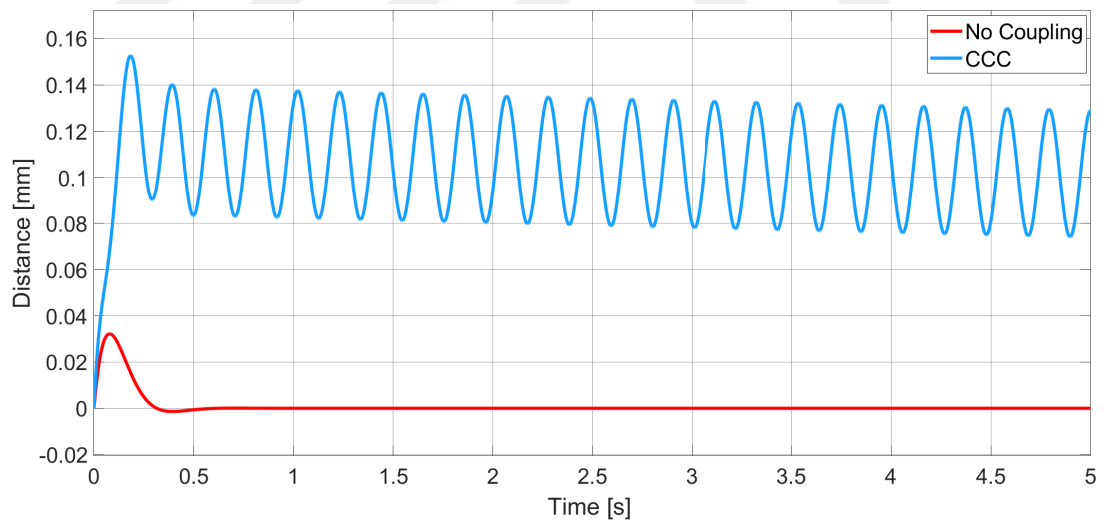
Figure 3.45: Drawing Line under Friction and Inner Disturbance - Error of Y-Axis.

To compensate X-Axis motion, CCC manipulates Y-Axis and this axis' error is increased. But magnitude of Y-Axis error with CCC is smaller than no-coupling X-Axis error.

Table 3.17: Drawing Line under Friction and Inner Disturbance without Coupling.

Time	X Command	X Error	Y Command	Y Error	Syn. Error
0,000	0,000	0,000	0,000	0,000	0,000
0,250	0,750	0,241	0,245	0,005	-0,227
0,500	1,500	0,293	0,501	-0,001	-0,278
0,750	2,250	0,369	0,750	0,000	-0,350
1,000	3,000	0,429	1,000	0,000	-0,407
1,250	3,750	0,411	1,250	0,000	-0,390
1,500	4,500	0,344	1,500	0,000	-0,327
1,750	5,250	0,317	1,750	0,000	-0,301
2,000	6,000	0,365	2,000	0,000	-0,346
2,250	6,750	0,426	2,250	0,000	-0,404
2,500	7,500	0,420	2,500	0,000	-0,399
2,750	8,250	0,355	2,750	0,000	-0,337
3,000	9,000	0,316	3,000	0,000	-0,300
3,250	9,750	0,354	3,250	0,000	-0,336
3,500	10,500	0,419	3,500	0,000	-0,398
3,750	11,250	0,427	3,750	0,000	-0,405
4,000	12,000	0,367	4,000	0,000	-0,348
4,250	12,750	0,317	4,250	0,000	-0,301
4,500	13,500	0,343	4,500	0,000	-0,326
4,750	14,250	0,411	4,750	0,000	-0,390
5,000	15,000	0,432	5,000	0,000	-0,409

Due to friction and inner disturbance, error in X-Axis is observed. Motion in Y-Axis is error-less. Synchronization error is between -0.227 and -0.409.

Table 3.18: Drawing Line under Friction and Inner Disturbance with Coupling.

Time	X Command	X Error	Y Command	Y Error	Syn. Error
0,000	0,000	0,000	0,000	0,000	0,000
0,251	0,752	0,038	0,141	0,110	-0,002
0,501	1,502	0,032	0,417	0,083	-0,004
0,751	2,252	0,040	0,648	0,103	-0,006
1,001	3,002	0,052	0,868	0,132	-0,007
1,251	3,752	0,054	1,118	0,132	-0,009
1,501	4,502	0,045	1,398	0,103	-0,010
1,751	5,252	0,040	1,670	0,081	-0,012
2,001	6,002	0,047	1,906	0,095	-0,014
2,251	6,752	0,059	2,125	0,126	-0,016
2,501	7,502	0,063	2,368	0,132	-0,018
2,751	8,252	0,055	2,645	0,105	-0,019
3,001	9,002	0,048	2,921	0,079	-0,021
3,251	9,752	0,053	3,163	0,088	-0,023
3,501	10,502	0,065	3,382	0,119	-0,024
3,751	11,252	0,071	3,619	0,131	-0,026
4,001	12,002	0,065	3,893	0,108	-0,027
4,251	12,752	0,057	4,172	0,079	-0,029
4,501	13,502	0,059	4,419	0,081	-0,031
4,751	14,252	0,071	4,639	0,111	-0,033
5,000	15,000	0,079	4,871	0,129	-0,034

Good compensating performance is achieved with CCC. Comparing Table 3.17 and Table 3.18 indicates the decrease in X-Axis error and synchronization error and increase in Y-Axis error. More than 90% contour error reduction is achieved for linear contour.

3.3.2 Drawing Circle under Friction and Inner Disturbance

Block diagram of the simulation structure is given in Figure 3.46. Friction and the inner disturbance are only applied to the X-Axis and CCC is P type with magnitude of 10000.
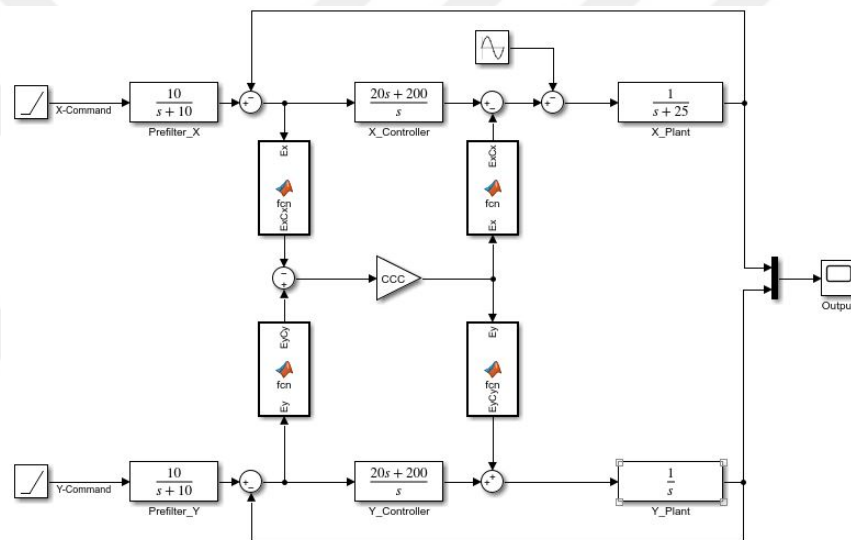

Figure 3.46: Block Diagram of Circle Drawing under Friction and Inner Disturbance.

Comparison of the reference circle and simulation results are given in Figure 3.47 and Figure 3.48.

Figure 3.47: Drawing Circle under Friction and Inner Disturbance without CCC.

Effects of the friction and the inner disturbance are obvious in Figure 3.47.

64
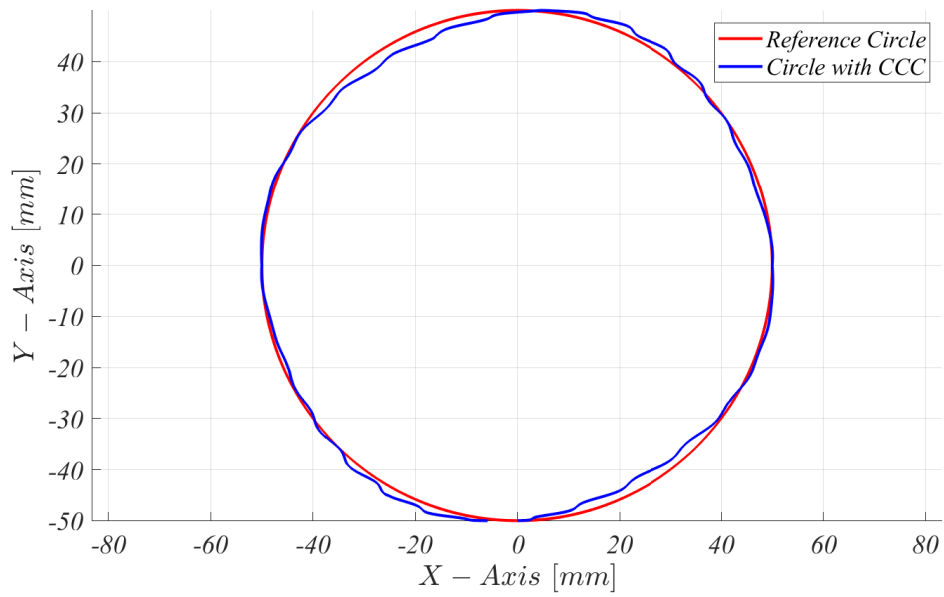
Figure 3.48: Drawing Circle under Friction and Inner Disturbance with CCC.

After CCC's compensation, more circular contour is established which can be seen in 3.48. Duration of this simulation is 2π seconds.
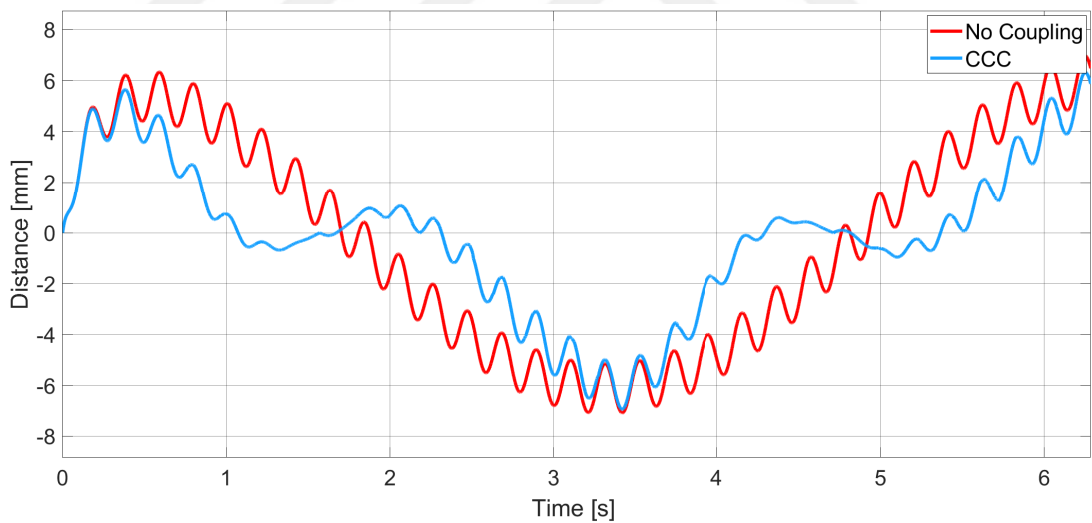
Figure 3.49: Drawing Circle under Friction and Inner Disturbance - Error of X-Axis.

In Figure 3.49 reduction in error of X-Axis can be observed. In some regions error is completely eliminated by CCC structure.
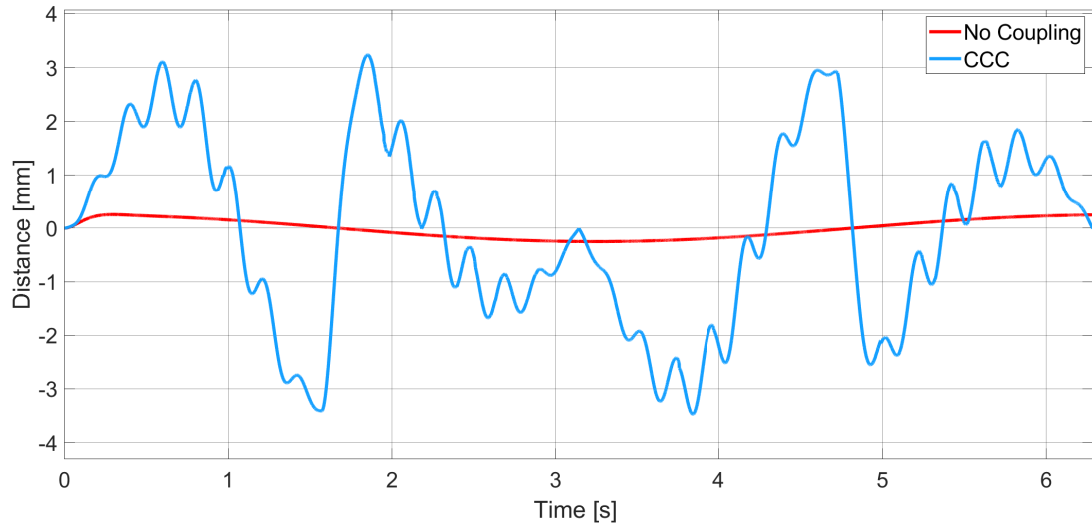
Figure 3.50: Drawing Circle under Friction and Inner Disturbance - Error of Y-Axis.

Without coupling, much less error is occurred in Y-Axis. But, CCC increases error in order to achieve less synchronization error. Also magnitude of Y-Axis error with CCC is smaller than no-coupling X-Axis error.

Table 3.19: Drawing Circle under Friction and Inner Disturbance without Coupling.

Time	X Command	X Error	Y Command	Y Error	Syn. Error
0,000	0,000	0,000	-50,000	0,000	0,000
$\pi/8$	19,148	6,196	-46,435	0,246	-106,882
$\pi/4$	35,341	5,818	-35,563	0,194	-198,430
$3\pi/8$	46,192	3,616	-19,257	0,118	-164,658
$\pi/2$	50,000	0,660	-0,015	0,025	-33,011
$5\pi/8$	46,203	-2,222	19,183	-0,072	101,330
$3\pi/4$	35,362	-4,349	35,507	-0,158	148,400
$7\pi/8$	19,129	-5,447	46,416	-0,220	94,314
π	-0,020	-5,587	50,249	-0,249	-12,011
$9\pi/8$	-19,121	-5,054	46,439	-0,239	85,833
$5\pi/4$	-35,356	-4,174	35,549	-0,194	140,921
$11\pi/8$	-46,200	-3,027	19,238	-0,118	137,664
$3\pi/2$	-50,000	-1,579	0,045	-0,025	78,968
$13\pi/8$	-46,196	0,338	-19,202	0,072	-14,250
$7\pi/4$	-35,348	2,600	-35,521	0,158	-86,233
$15\pi/8$	-19,157	4,859	-46,405	0,220	-82,681
2π	0,000	6,484	-50,249	0,249	12,858

Without CCC high error in X-Axis is occurred. But in Y-axis relatively less error is occurred. Quite high synchronization error can be observed in Table 3.19.

Table 3.20: Drawing Circle under Friction and Inner Disturbance with Coupling.

Time	X Command	X Error	Y Command	Y Error	Syn. Error
0,000	0,000	0,000	-50,000	0,000	0,000
$\pi/8$	19,154	5,591	-48,497	2,311	0,000
$\pi/4$	35,363	2,664	-38,009	2,661	-0,001
$3\pi/8$	46,195	-0,450	-18,045	-1,086	-0,001
$\pi/2$	50,000	0,001	3,511	-3,495	-0,001
$5\pi/8$	46,203	0,663	17,513	1,600	-0,001
$3\pi/4$	35,360	-0,884	36,235	-0,884	-0,001
$7\pi/8$	19,128	-3,318	47,573	-1,377	0,000
π	-0,048	-4,708	50,009	-0,009	0,000
$9\pi/8$	-19,138	-4,814	48,193	-2,000	0,000
$5\pi/4$	-35,358	-2,059	37,414	-2,061	0,001
$11\pi/8$	-46,203	0,274	18,450	0,663	0,001
$3\pi/2$	-50,000	0,003	-2,911	2,929	0,001
$13\pi/8$	-46,188	-0,959	-16,832	-2,317	0,001
$7\pi/4$	-35,345	0,133	-35,499	0,132	0,001
$15\pi/8$	-19,117	3,084	-47,475	1,274	0,000
2π	0,000	5,870	-49,993	-0,007	0,000

Significant synchronization error decrease is obtained by proposed structure which can be seen in Table 3.4. In this table less X-Axis error and more Y-Axis error can be observed.

67

3.3.3 Drawing Ellipse under Friction and Inner Disturbance

Block diagram of the simulation structure is given in Figure 3.51. Friction and the inner disturbance are only applied to the X-Axis and CCC is P type with magnitude of 10000.
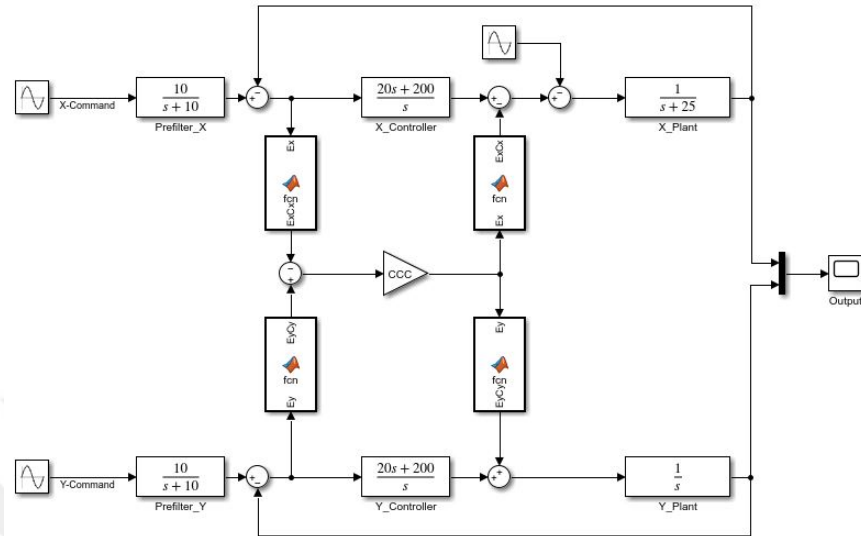

Figure 3.51: Block Diagram of Ellipse Drawing under Friction and Inner Disturbance.

Comparison of the reference ellipse and simulation results are given in Figure 3.52 and Figure 3.53.
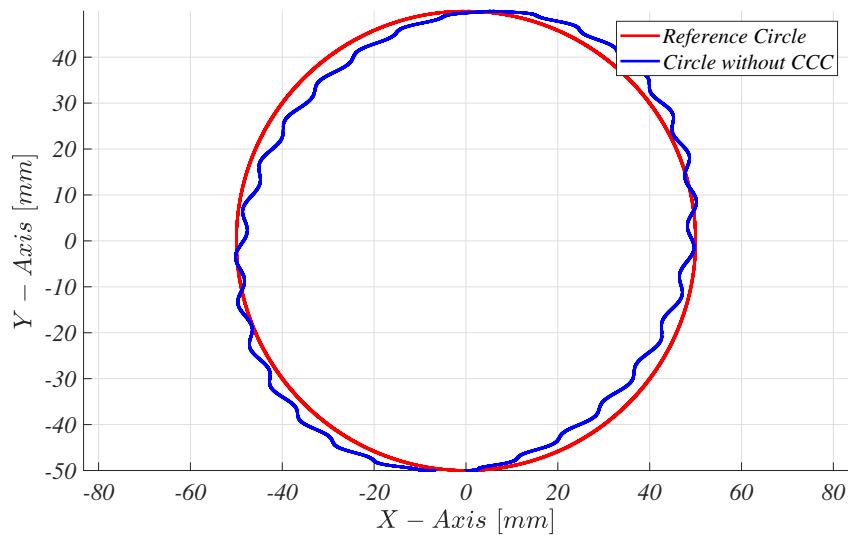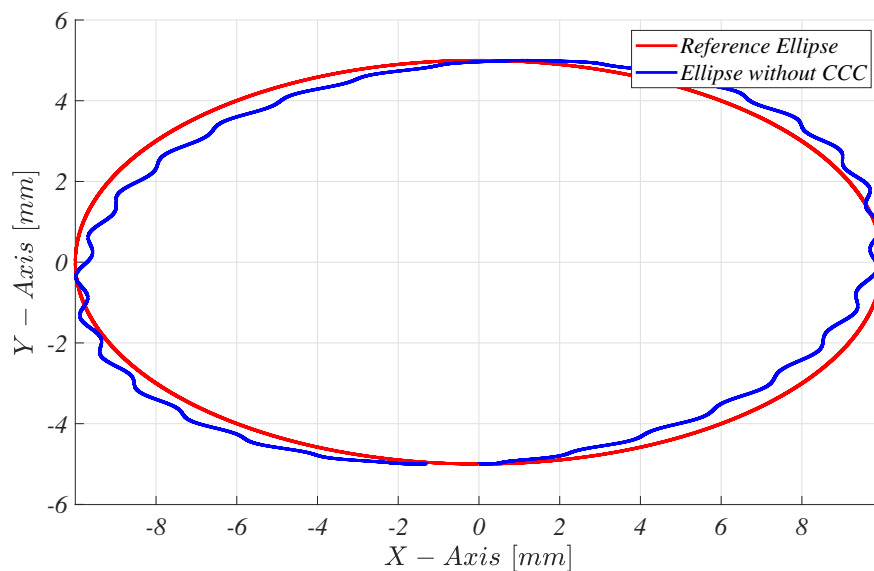

Figure 3.52: Drawing Ellipse under Friction and Inner Disturbance without CCC.

Double effect of the friction and the inner disturbance damaged elliptic contour which can be seen in Figure 3.52.
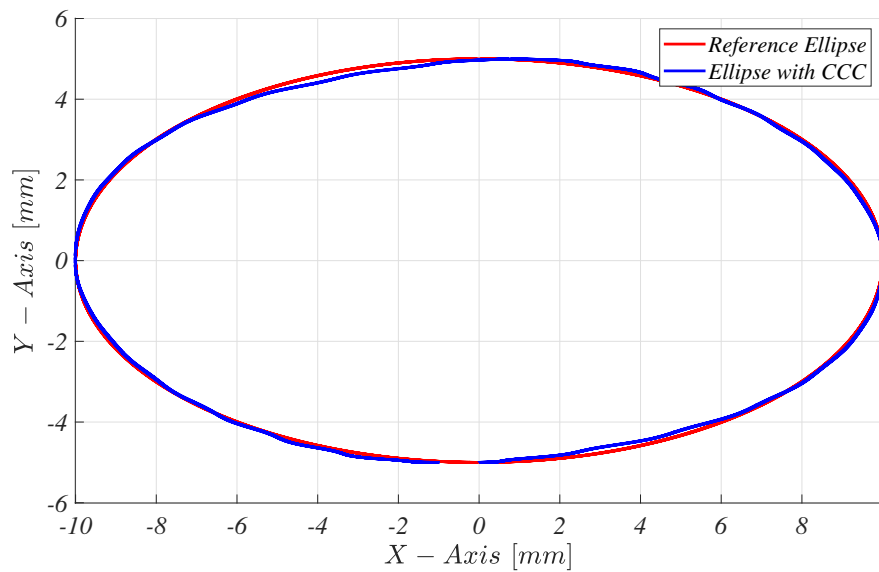
Figure 3.53: Drawing Ellipse under Friction and Inner Disturbance with CCC.

CCC decreases synchronization error and more elliptic trajectory can be followed. In the second and fourth quarter of the ellipse less performance is occurred which is observed in Figure 3.53. Duration of this simulation is 2π seconds.
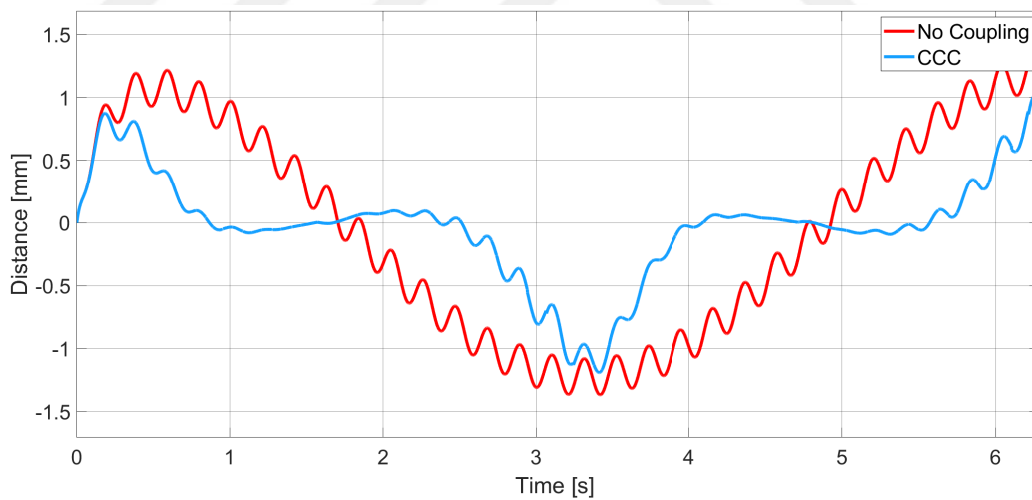
Figure 3.54: Drawing Ellipse under Friction and Inner Disturbance - Error of X-Axis.

In Figure 3.54 decrease in error of X-Axis can be observed. In one third of the simulation almost zero error is observed. In other regions error is reduced significantly.

69
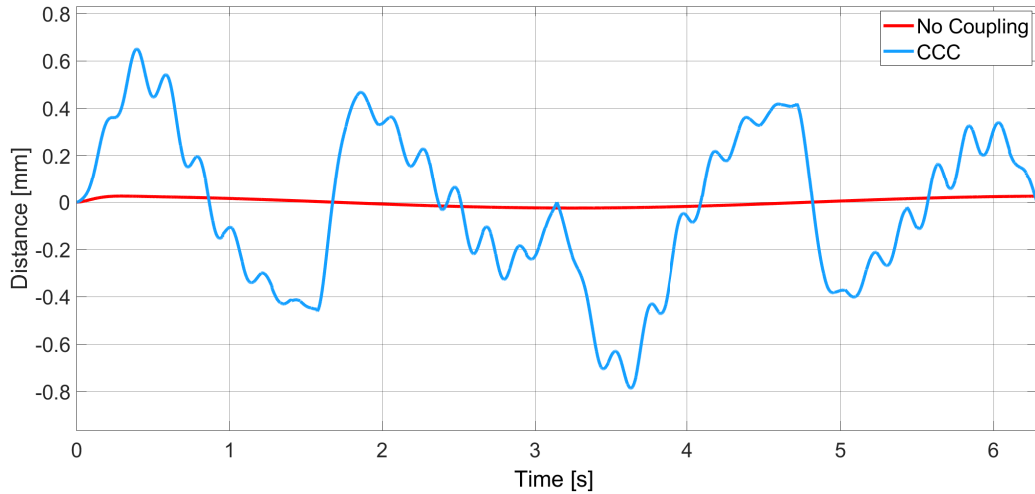
Figure 3.55: Drawing Ellipse under Friction and Inner Disturbance - Error of Y-Axis.

Decrease is transferred to Y-Axis for synchronization which can be seen in Figure 3.55. Without CCC, Y-Axis error is much more smaller than X-Axis'.

Table 3.21: Drawing Ellipse under Friction and Inner Disturbance without Coupling.

Time	X Command	X Error	Y Command	Y Error	Syn. Error
0,000	0,000	0,000	-5,000	0,000	0,000
$\pi/8$	3,830	1,191	-4,643	0,025	-4,443
$\pi/4$	7,068	1,120	-3,556	0,019	-7,846
$3\pi/8$	9,238	0,708	-1,926	0,012	-6,522
$\pi/2$	10,000	0,154	-0,001	0,002	-1,499
$5\pi/8$	9,241	-0,397	1,918	-0,007	3,656
$3\pi/4$	7,072	-0,826	3,551	-0,016	5,788
$7\pi/8$	3,826	-1,074	4,642	-0,022	4,011
π	-0,004	-1,140	5,025	-0,025	-0,115
$9\pi/8$	-3,824	-1,058	4,644	-0,024	3,937
$5\pi/4$	-7,071	-0,879	3,555	-0,019	6,146
$11\pi/8$	-9,240	-0,621	1,924	-0,012	5,713
$3\pi/2$	-10,000	-0,293	0,004	-0,003	2,964
$13\pi/8$	-9,239	0,115	-1,920	0,007	-1,046
$7\pi/4$	-7,070	0,564	-3,552	0,016	-3,930
$15\pi/8$	-3,831	0,986	-4,640	0,022	-3,674
2π	0,000	1,274	-5,025	0,025	0,131

Friction and inner disturbance are deteriorated the trajectory. Maximum error in X-Axis is 1.274 and in Y-Axis is 0.25.

Table 3.22: Drawing Ellipse under Friction and Inner Disturbance with Coupling.

Time	X Command	X Error	Y Command	Y Error	Syn. Error
0,000	0,000	0,000	-5,000	0,000	0,000
$\pi/8$	3,831	0,786	-5,270	0,651	-0,001
$\pi/4$	7,072	0,098	-3,730	0,195	-0,002
3$\pi/8$	9,240	-0,067	-1,584	-0,328	-0,002
$\pi/2$	10,000	0,005	0,454	-0,452	-0,002
5$\pi/8$	9,240	0,071	1,573	0,338	-0,002
3$\pi/4$	7,067	0,009	3,519	0,018	-0,001
7$\pi/8$	3,818	-0,296	4,866	-0,245	-0,001
π	-0,005	-0,762	5,001	-0,001	0,000
9$\pi/8$	-3,831	-0,765	5,254	-0,636	0,000
5$\pi/4$	-7,074	-0,073	3,680	-0,146	0,001
11$\pi/8$	-9,244	0,057	1,632	0,276	0,002
3$\pi/2$	-10,000	0,005	-0,409	0,410	0,002
13$\pi/8$	-9,237	-0,082	-1,520	-0,396	0,002
7$\pi/4$	-7,068	-0,056	-3,426	-0,111	0,001
15$\pi/8$	-3,826	0,305	-4,873	0,253	0,005
2π	0,000	0,973	-4,999	-0,001	0,000

Comparing Table 3.21 and Table 3.22 indicates almost zero contour error for elliptic trajectory, while error of X-Axis is decreasing, error of Y-Axis is increasing.

71

3.3.4 Drawing Parabola under Friction and Inner Disturbance

Block diagram of the simulation structure is given in Figure 3.56. Friction and the inner disturbance are only applied to the X-Axis and CCC is P type with magnitude of 1000.
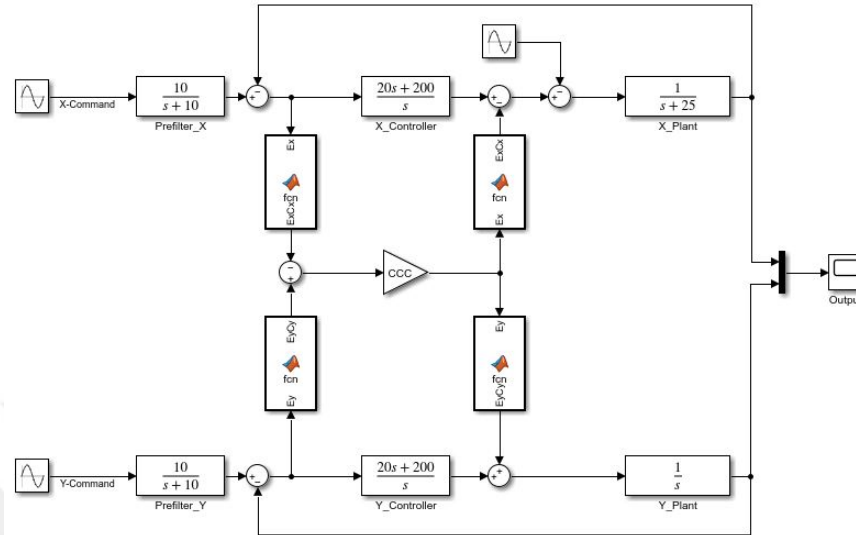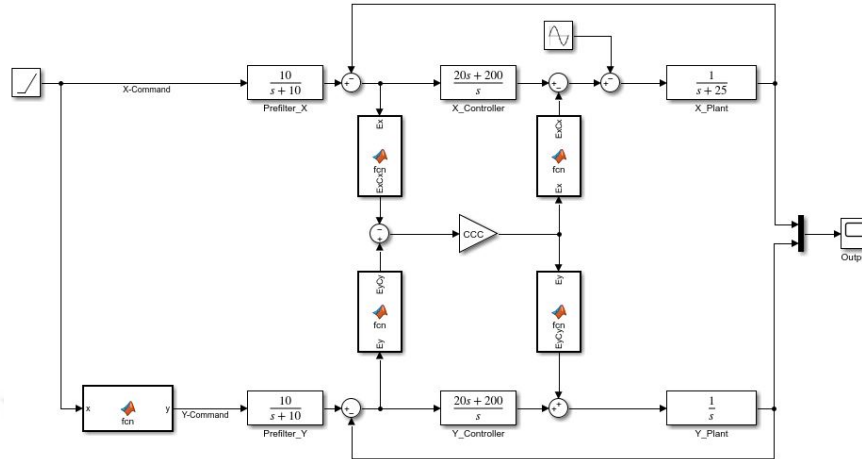

Figure 3.56: Block Diagram of Parabola Drawing under Friction and Inner Disturbance.

Comparison of the reference parabola and simulation results are given in Figure 3.57 and Figure 3.58.
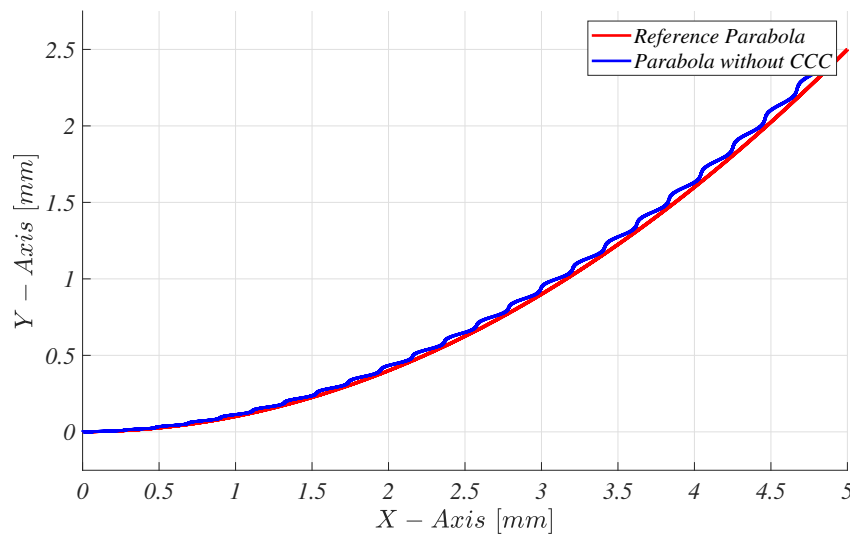
Figure 3.57: Drawing Parabola under Friction and Inner Disturbance without CCC.

Friction slowed down and inner disturbance is deteriorated the motion in X-Axis which can be seen in Figure 3.57. As time increased damage of unwanted effects are also increased.

72
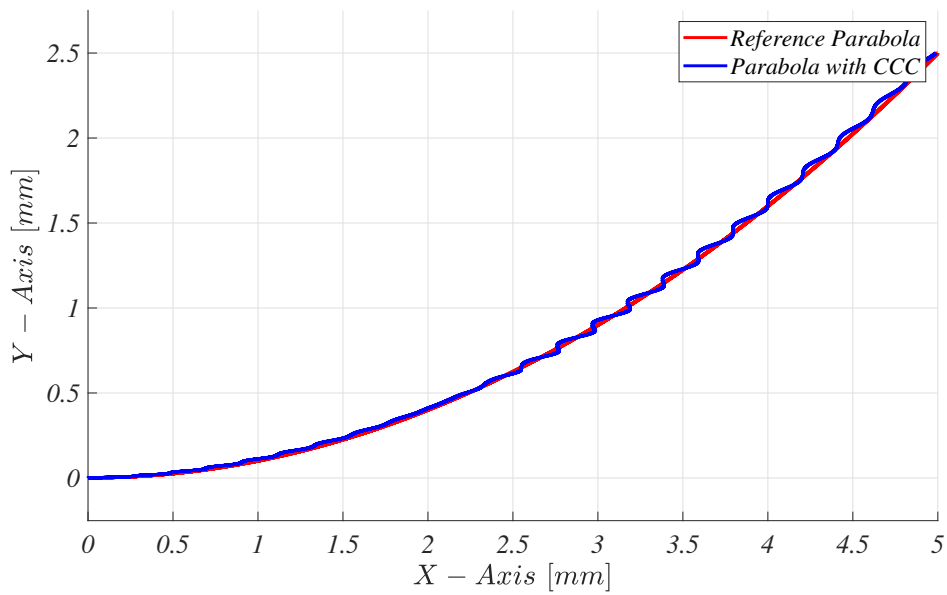
Figure 3.58: Drawing Parabola under Friction and Inner Disturbance with CCC.

Despite of the high friction and the inner disturbance, satisfactory contour error compensation is obtained. Duration of this simulation is 5 seconds.
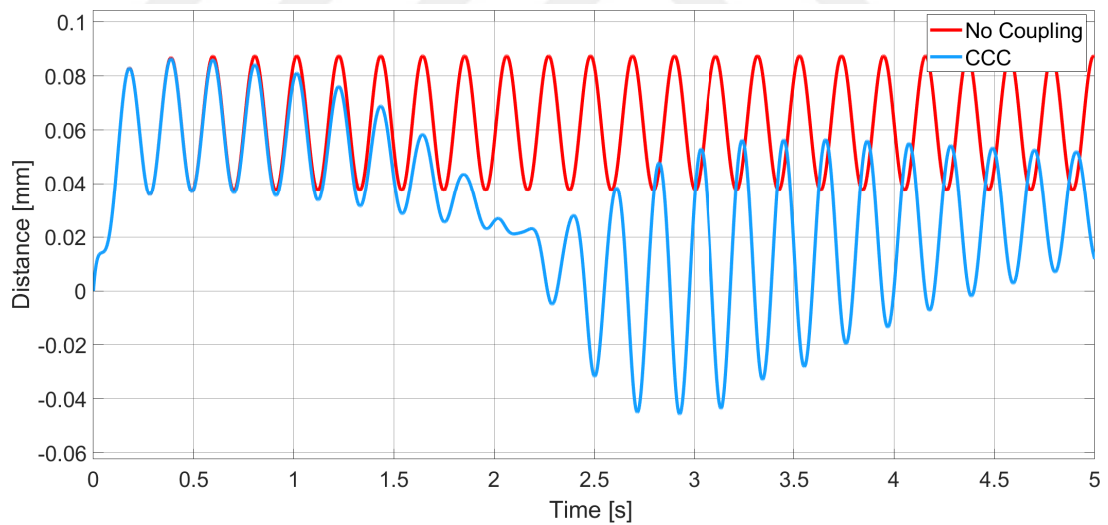
Figure 3.59: Drawing Parabola under Friction and Inner Disturbance - Error of X-Axis.

In Figure 3.59 error in X-Axis is visible. But magnitude of this error is between -0.05 and 0.08 which is less than no-coupling version.
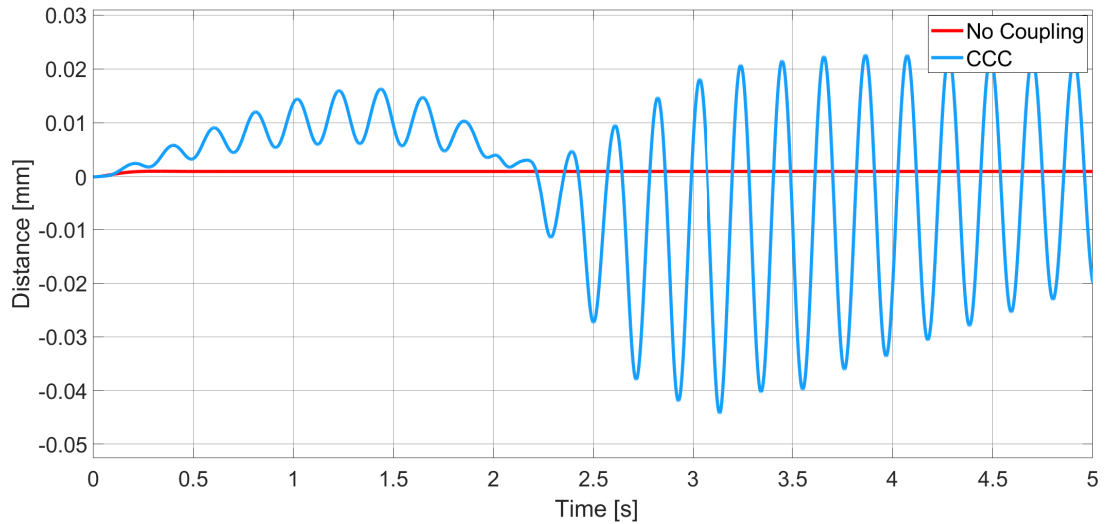
Figure 3.60: Drawing Parabola under Friction and Inner Disturbance - Error of Y-Axis.

In Y-Axis sinusoidal error is occurred due to CCC compensation. Also magnitude of Y-Axis error with CCC is smaller than no-coupling X-Axis error.

Table 3.23: Drawing Parabola under Friction and Inner Disturbance without Coupling.

Time	X Command	X Error	Y Command	Y Error	Syn. Error
0,000	0,000	0,000	0,000	0,000	0,000
0,250	0,250	0,046	0,005	0,001	-0,001
0,500	0,500	0,038	0,024	0,001	-0,003
0,750	0,750	0,060	0,055	0,001	-0,008
1,000	1,000	0,085	0,099	0,001	-0,015
1,250	1,250	0,081	0,155	0,001	-0,018
1,500	1,500	0,053	0,224	0,001	-0,014
1,750	1,750	0,038	0,305	0,001	-0,011
2,000	2,000	0,055	0,399	0,001	-0,019
2,250	2,250	0,082	0,505	0,001	-0,032
2,500	2,500	0,084	0,624	0,001	-0,036
2,750	2,750	0,058	0,755	0,001	-0,027
3,000	3,000	0,038	0,899	0,001	-0,019
3,250	3,250	0,050	1,055	0,001	-0,026
3,500	3,500	0,079	1,224	0,001	-0,044
3,750	3,750	0,086	1,405	0,001	-0,050
4,000	4,000	0,063	1,599	0,001	-0,038
4,250	4,250	0,039	1,805	0,001	-0,024
4,500	4,500	0,046	2,024	0,001	-0,030
4,750	4,750	0,075	2,255	0,001	-0,050
5,000	5,000	0,087	2,499	0,001	-0,061

In X-axis error is fluctuating due to sinusoidal disturbance. But in Y-Axis steady error can be observed in Table 3.23. Synchronization error is increased continuously.

Table 3.24: Drawing Parabola under Friction and Inner Disturbance with Coupling.

Time	X Command	X Error	Y Command	Y Error	Syn. Error
0,000	0,000	0,000	0,000	0,000	0,000
0,251	0,251	0,046	0,004	0,002	0,000
0,501	0,501	0,038	0,022	0,003	0,000
0,751	0,751	0,058	0,049	0,008	-0,001
1,001	1,001	0,079	0,086	0,014	-0,001
1,251	1,251	0,070	0,141	0,015	-0,002
1,501	1,501	0,041	0,216	0,010	-0,003
1,751	1,751	0,026	0,302	0,005	-0,004
2,001	2,001	0,026	0,396	0,004	-0,006
2,251	2,251	0,007	0,512	-0,006	-0,008
2,501	2,501	-0,032	0,653	-0,027	-0,010
2,751	2,751	-0,019	0,779	-0,023	-0,010
3,001	3,001	0,034	0,893	0,007	-0,011
3,251	3,251	0,055	1,037	0,020	-0,013
3,501	3,501	0,016	1,233	-0,008	-0,016
3,751	3,751	-0,018	1,441	-0,035	-0,017
4,001	4,001	0,002	1,621	-0,021	-0,017
4,251	4,251	0,042	1,794	0,012	-0,018
4,501	4,501	0,052	2,005	0,021	-0,019
4,751	4,751	0,030	2,258	-0,001	-0,021
5,000	5,000	0,012	2,520	-0,020	-0,022

CCC decreases contour error under friction and the inner disturbance. But compared to linear, circular and elliptic contours, the least successful performance is occurred with parabolic contour. Since command value is increased, effectivity of proposed structure is decreased.

3.4   SUMMARY OF THE SIMULATION RESULTS

Brief summary of the simulation results are given in this chapter. Common point of the simulations are decreasing error in X-Axis and increasing error in Y-Axis. With CCC, decrease in synchronization error is always obtained.

For linear trajectories, results are satisfactory which can be seen in Table 3.25. Friction and the inner disturbance are deteriorated X-Axis output but CCC does its duty. Synchronization error is reduced to 9.5% under friction and 2% under the inner disturbance. For under both friction and inner disturbance, reduction to 9.6% is achieved.

For circular and elliptic trajectories successful results are established. Table 3.26 and Table 3.27 summarize the results. Almost zero synchronization error is achieved for circle under friction, inner disturbance and both. In elliptic trajectory, maximum 0.3% synchronization error is observed under friction and inner disturbance.

For parabolic trajectory, reasonable results are achieved and given in Table 3.28. Under friction, half of the synchronization error and under inner disturbance two third of the synchronization error are eliminated. While following parabolic trajectory under both friction and the inner disturbance, simulation results are identical with inner disturbance which can be seen in Table 3.28. This situation indicates that inner disturbance is more dominant than friction when it comes to synchronization for parabolic trajectories.

Table 3.25: Simulation Results of Linear Trajectory.

Time	Friction			Disturbance			Friction + Disturbance		
	Contour Error		Remaining	Contour Error		Remaining	Contour Error		Remaining
	No Coupling	CCC	Syn. Error	No Coupling	CCC	Syn. Error	No Coupling	CCC	Syn. Error
0,000	0,000	0,000	-	0,000	0,000	-	0,000	0,000	-
0,250	-0,261	-0,002	0,7%	0,010	0,000	0,2%	-0,227	-0,002	0,7%
0,500	-0,329	-0,004	1,1%	0,095	0,000	0,1%	-0,278	-0,004	1,3%
0,750	-0,348	-0,005	1,6%	0,032	0,000	1,2%	-0,350	-0,006	1,6%
1,000	-0,354	-0,007	2,0%	-0,070	-0,001	0,7%	-0,407	-0,007	1,8%
1,250	-0,355	-0,009	2,5%	-0,081	0,000	0,4%	-0,390	-0,009	2,3%
1,500	-0,356	-0,011	3,0%	0,014	0,000	0,0%	-0,327	-0,010	3,2%
1,750	-0,356	-0,012	3,5%	0,091	0,000	0,0%	-0,301	-0,012	4,0%
2,000	-0,356	-0,014	4,0%	0,049	0,000	0,7%	-0,346	-0,014	4,1%
2,250	-0,356	-0,016	4,4%	-0,057	-0,001	0,9%	-0,404	-0,016	4,0%
2,500	-0,356	-0,017	4,9%	-0,088	0,000	0,4%	-0,399	-0,018	4,4%
2,750	-0,356	-0,019	5,4%	-0,004	0,000	0,7%	-0,337	-0,019	5,6%
3,000	-0,356	-0,021	5,8%	0,085	0,000	0,0%	-0,300	-0,021	6,9%
3,250	-0,356	-0,022	6,3%	0,063	0,000	0,4%	-0,336	-0,023	6,7%
3,500	-0,356	-0,024	6,8%	-0,042	-0,001	1,2%	-0,398	-0,024	6,1%
3,750	-0,356	-0,026	7,2%	-0,092	0,000	0,4%	-0,405	-0,026	6,4%
4,000	-0,356	-0,027	7,7%	-0,022	0,000	0,3%	-0,348	-0,027	7,8%
4,250	-0,356	-0,029	8,2%	0,077	0,000	0,1%	-0,301	-0,029	9,6%
4,500	-0,356	-0,031	8,6%	0,075	0,000	0,3%	-0,326	-0,031	9,4%
4,750	-0,356	-0,032	9,1%	-0,024	0,000	2,0%	-0,390	-0,033	8,3%
5,000	-0,356	-0,034	9,5%	-0,092	0,000	0,5%	-0,409	-0,034	8,3%

Table 3.26: Simulation Results of Circular Trajectory.

Time	Friction			Disturbance			Friction + Disturbance		
	Contour Error		Remaining	Contour Error		Remaining	Contour Error		Remaining
	No Coupling	CCC	Syn. Error	No Coupling	CCC	Syn. Error	No Coupling	CCC	Syn. Error
0,000	0,000	0,000	-	0,000	0,000	-	0,000	0,000	-
π/8	-88,419	0,000	0,0%	-16,784	0,000	0,0%	-106,882	0,000	0,0%
π/4	-167,609	-0,001	0,0%	-24,550	0,000	0,0%	-198,430	-0,001	0,0%
3π/8	-151,004	-0,001	0,0%	18,423	0,000	0,0%	-164,658	-0,001	0,0%
π/2	-55,434	-0,001	0,0%	73,900	0,000	0,0%	-33,011	-0,001	0,0%
5π/8	57,654	-0,001	0,0%	84,577	0,000	0,0%	101,330	-0,001	0,0%
3π/4	117,461	-0,002	0,0%	38,457	-0,001	0,0%	148,400	-0,001	0,0%
7π/8	88,522	0,000	0,0%	-10,200	0,000	0,0%	94,314	0,000	0,0%
π	-11,951	0,000	0,0%	-12,447	0,000	0,0%	-12,011	0,000	0,0%
9π/8	106,038	0,000	0,0%	-43,403	0,000	0,0%	85,833	0,000	0,0%
5π/4	171,967	0,001	0,0%	-49,869	0,000	0,0%	140,921	0,001	0,0%
11π/8	151,861	0,001	0,0%	-7,369	0,000	0,0%	137,664	0,001	0,0%
3π/2	55,743	0,001	0,0%	49,951	0,000	0,0%	78,968	0,001	0,0%
13π/8	-57,707	0,001	0,0%	65,262	0,000	0,0%	-14,250	0,001	0,0%
7π/4	-117,234	0,001	0,0%	36,468	0,000	0,0%	-86,233	0,001	0,0%
15π/8	-88,100	0,000	0,0%	5,059	0,003	0,1%	-82,681	0,000	0,0%
2π	12,801	0,000	0,0%	12,454	0,000	0,0%	12,858	0,000	0,0%

Table 3.27: Simulation Results of Elliptic Trajectory.

Time	Friction			Disturbance			Friction + Disturbance		
	Contour Error		Remaining	Contour Error		Remaining	Contour Error		Remaining
	No Coupling	CCC	Syn. Error	No Coupling	CCC	Syn. Error	No Coupling	CCC	Syn. Error
0,000	0,000	0,000	-	0,000	0,000	-	0,000	0,000	-
$\pi/8$	-3,887	-0,001	0,0%	-0,705	0,000	0,0%	-4,443	-0,001	0,0%
$\pi/4$	-6,919	-0,001	0,0%	-0,818	0,000	0,0%	-7,846	-0,002	0,0%
$3\pi/8$	-6,112	-0,002	0,0%	0,609	0,000	0,0%	-6,522	-0,002	0,0%
$\pi/2$	-2,172	-0,002	0,1%	2,387	0,000	0,0%	-1,499	-0,002	0,1%
$5\pi/8$	2,347	-0,002	0,1%	2,674	0,000	0,0%	3,656	-0,002	0,0%
$3\pi/4$	4,862	-0,001	0,0%	1,334	0,000	0,0%	5,788	-0,001	0,0%
$7\pi/8$	3,838	-0,001	0,0%	-0,080	0,000	0,4%	4,011	-0,001	0,0%
π	-0,114	0,000	0,4%	-0,125	0,000	0,2%	-0,115	0,000	0,4%
$9\pi/8$	4,479	0,000	0,0%	-1,095	0,000	0,0%	3,937	0,000	0,0%
$5\pi/4$	7,075	0,001	0,0%	-1,416	0,000	0,0%	6,146	0,001	0,0%
$11\pi/8$	6,138	0,002	0,0%	-0,278	0,000	0,0%	5,713	0,002	0,0%
$3\pi/2$	2,268	0,002	0,1%	1,412	0,000	0,0%	2,964	0,002	0,1%
$13\pi/8$	-2,350	0,002	0,1%	1,819	0,000	0,0%	-1,046	0,002	0,1%
$7\pi/4$	-4,862	0,001	0,0%	0,913	0,000	0,0%	-3,930	0,001	0,0%
$15\pi/8$	-3,838	0,001	0,0%	-0,074	0,000	0,1%	-3,674	0,005	0,1%
2π	0,130	0,000	0,3%	0,125	0,000	0,1%	0,131	0,000	0,3%

Table 3.28: Simulation Results of Parabolic Trajectory.

Time	Friction			Disturbance			Friction + Disturbance		
	Contour Error		Remaining	Contour Error		Remaining	Contour Error		Remaining
	No Coupling	CCC	Syn. Error	No Coupling	CCC	Syn. Error	No Coupling	CCC	Syn. Error
0,000	0,000	0,000	-	0,000	0,000	-	0,000	0,000	-
0,250	-0,002	0,000	4,3%	-0,001	0,000	3,2%	-0,001	0,000	3,2%
0,500	-0,005	0,000	5,9%	-0,003	0,000	9,4%	-0,003	0,000	9,4%
0,750	-0,008	-0,001	8,4%	-0,008	-0,001	9,9%	-0,008	-0,001	9,9%
1,000	-0,011	-0,001	11,2%	-0,015	-0,001	9,3%	-0,015	-0,001	9,3%
1,250	-0,014	-0,002	14,3%	-0,018	-0,002	11,0%	-0,018	-0,002	11,0%
1,500	-0,017	-0,003	17,8%	-0,014	-0,003	18,8%	-0,014	-0,003	18,8%
1,750	-0,019	-0,004	21,6%	-0,011	-0,004	33,8%	-0,011	-0,004	33,8%
2,000	-0,022	-0,006	25,8%	-0,019	-0,006	30,7%	-0,019	-0,006	30,7%
2,250	-0,024	-0,007	30,3%	-0,032	-0,008	26,1%	-0,032	-0,008	26,1%
2,500	-0,027	-0,009	34,3%	-0,036	-0,010	28,1%	-0,036	-0,010	28,1%
2,750	-0,029	-0,011	37,6%	-0,027	-0,010	39,1%	-0,027	-0,010	39,1%
3,000	-0,031	-0,012	40,0%	-0,019	-0,011	60,2%	-0,019	-0,011	60,2%
3,250	-0,033	-0,014	41,8%	-0,026	-0,013	50,4%	-0,026	-0,013	50,4%
3,500	-0,035	-0,015	43,3%	-0,044	-0,016	36,2%	-0,044	-0,016	36,2%
3,750	-0,036	-0,016	44,6%	-0,050	-0,017	34,0%	-0,050	-0,017	34,0%
4,000	-0,038	-0,017	45,7%	-0,038	-0,017	45,0%	-0,038	-0,017	45,0%
4,250	-0,040	-0,019	46,9%	-0,024	-0,018	71,9%	-0,024	-0,018	71,9%
4,500	-0,041	-0,020	48,0%	-0,030	-0,019	64,2%	-0,030	-0,019	64,2%
4,750	-0,042	-0,021	49,1%	-0,050	-0,021	42,3%	-0,050	-0,021	42,3%
5,000	-0,043	-0,022	50,2%	-0,061	-0,022	36,9%	-0,061	-0,022	36,9%

CHAPTER IV

CONCLUSION AND FUTURE WORKS

In this thesis, nature and forming causes of contour error is explained. In one axis, root cause of error can be varying. Axial and contour errors have different cause and results. In order to accomplish coordinated movement, not only error free motion but also minimum relative deviation is required. Because, only one axis' inaccurate movement will lead unwanted error in desired contour. To achieve high precision and improve immunity to system uncertainties and disturbances, Cross-Coupled Controller (CCC) is considered in this thesis.

In principle, CCC calculates contour error instantaneously and feeds it into a controller and decompose the output of CCC into plant's input at a specific proportion. In this thesis, variable gain version of CCC is proposed. In conventional CCC, contour error is injected to each axis at equal amount. But, variable gain CCC injects contour error proportional to related axis' axial error. CCC structure and mathematical model of variable gains are explained comprehensively.

Linear, circular, elliptic and parabolic trajectories are chosen to test proposed structure. With different combinations of the trajectories, any contour needed can be achieved. For each different motion condition, variable gains are developed. Extra-large friction and disturbance are applied to only one of the axes. When an extra-large disruptive element is existed, effect of CCC is more obvious.

In the concluding part of the simulation, the performance of proposed CCC structure is examined for each trajectory under both friction and the inner disturbance and for the case where both are applied. In simulations, high precise synchronization control is obtained by CCC structure. Under friction, CCC structure reduces synchronization error significantly for circular and elliptic contours. For linear contour more than ninety and parabolic contours more than sixty-five percent improvement are achieved compared to un-coupled systems. Under the inner disturbance, CCC structure lowered the contour error to zero for linear, circular and elliptic and decrease more than sixty percent for parabolic trajectories. Similar results are achieved for simultaneous effects of friction and disturbances which indicate robustness of the proposed control scheme.

Proposed structure can be applied into various multi-axis systems such as CNC machines, gantries and path-follower devices. Converting the controller from

un-coupling controller to CCC requires no hardware. Existing systems can be upgraded by just reprogramming the controller.

In this thesis, a simple proportional controller is used as a CCC. If a more complex controller is used (PI, PID, sliding mode controller, H_∞), more robust and effective controller can be obtained.

Suggested variable gain is calculated for four different trajectories (linear, circular, elliptic and parabolic). But a common variable gain and CCC can be designed for all different trajectories.

REFERENCES

[1] SARACHIK Philip and RAGAZZINI John Ralph (1957), "A 2-dimensional feedback control system", *Transactions of the American Institute of Electrical Engineers*, Vol. 76, No. 2, pp. 55-61.

[2] KOREN Yoram (1980), "Cross-Coupled Biaxial Computer Control for Manufacturing Systems", *Journal of Dynamic Systems, Measurement and Control, Transactions of the ASME*, Vol. 102, No. 4, pp. 265–272.

[3] KOREN Yoram and LO Ch-Ch (1991), "Variable-gain cross-coupling controller for contouring", *CIRP annals*, Vol. 40, No. 1, pp. 371-374.

[4] YEH Syh-Shiuh and HSU Pau-Lo (1999), "Theory and applications of the robust cross-coupled control design", *Journal of Dynamic Systems, Measurement and Control, Transactions of the ASME*, Vol. 121, No. 3, pp. 524-530.

[5] SHIH Yi-Ti, CHEN Chin-Sheng and LEE An-Chen (2002), "A novel cross-coupling control design for bi-axis motion", *International Journal of machine tools and manufacture*, Vol. 42, No. 14, pp. 1539-1548.

[6] LIU Hugh and SUN Dong (2005), "Uniform synchronization in multi-axis motion control", *Proceedings of the 2005, American Control Conference*, pp. 4537-4542, Portland.

[7] TSAI Mi-Ching, HSIEH Min-Fu and YAO Wu-Sung (2003), "Synchronous control of linear servo systems for CNC machine tools", *European Control Conference*, pp. 2339-2344, Cambridge.

[8] XIAO Yong, ZHU Kuanyi, and LIAW Hwee Choo (2005), "Generalized synchronization control of multi-axis motion systems", *Control engineering practice*, Vol. 13, No. 7, pp. 809-819.

[9] SUN Dong, SHAO Xiaoyin and FENG Gang (2007), "A model-free cross-coupled control for position synchronization of multi-axis motions: theory and experiments", *IEEE Transactions on Control Systems Technology*, Vol. 15, No. 2, pp. 306-314.

[10] SUN Dong and TONG Ming-Chau (2009), "A synchronization approach for the minimization of contouring errors of CNC machine tools", *IEEE transactions on automation science and engineering*, Vol. 6, No. 4, pp. 720-729.

[11] BYUN Jung-Hwan and CHOI Myung-Soo (2012), "A method of synchronous control system for dual parallel motion stages", *International Journal of Precision Engineering and Manufacturing*, Vol. 13, pp. 883-889.

[12] XIAO Yong, PANG Yujun, GE Xiaoyu and SUN Jingna (2013), "Synchronous control for high-accuracy biaxial motion systems", *Journal of Control Theory and Applications*, Vol. 11, pp. 294-298.

[13] XIAO Yong and KIM Zhu (2006), "Optimal synchronization control of high-precision motion systems", *IEEE Transactions on Industrial Electronics*, Vol. 53, No. 4, pp. 1160-1169.

[14] TSAI Ming-Chau and SHEN Bian-Sen (2007), "Synchronisation control of parallel dual inverted pendulums driven by linear servomotors", *IET Control Theory and Applications*, Vol. 1, No. 1, pp. 320-327.

[15] LIN Faa-Jeng, CHOU Po-Huan, CHEN Chin-Sheng and LIN Yu-Sheng (2011), "DSP-based cross-coupled synchronous control for dual linear motors via intelligent complementary sliding mode control", *IEEE Transactions on Industrial Electronics*, Vol. 59, No. 2, pp. 1061-1073.

[16] WU Han, ZHANG Changfan, NIU Mangang and XIAO Yuanyuan (2013), "Leader-follower flocking for cooperative control of multiple motors", *Chinese Automation Congress*, pp. 820-825, Hunan.

[17] BLAHA Lukas (2014), "Multi-axis time synchronization for uncoordinated motion planning with hard constraints", *IFAC Proceedings Volumes*, Vol. 47, No. 3, pp. 3845-3850.

[18] CHEN Chin-Sheng and CHEN Li-Yeh (2012), "Robust cross-coupling synchronous control by shaping position commands in multiaxes system", *IEEE Transactions on Industrial Electronics*, Vol. 59, No. 12, pp. 4761-4773.

[19] HE Fang and WANG Chuang (2017), "Cross-coupling synchronous control of dual-motor networked motion control system", *36th Chinese Control Conference*, pp. 7628-7633, Dalian.

[20] ZHONG Guoliang, SHAO Zhizhongi, DENG Hua and REN Junli (2017), "Precise position synchronous control for multi-axis servo systems", *IEEE Transactions on Industrial Electronics*, Vol. 64, No. 5, pp. 3707-3717.

[21] LI Cong, ZHU Xiacong and WANG Qingfeng (2014), "Adaptive robust synchronous control with dynamic thrust allocation of dual drive gantry stage", *IEEE/ASME International Conference on Advanced Intelligent Mechatronics*, pp. 316-321, Besancon.

[22] YAO Suhua, GAO Guoqinand and GAO Zhiqiang (2021), "On multi-axis motion synchronization: The cascade control structure and integrated smc–adrc design", *ISA transactions*, Vol. 109, pp. 259-268.